Compressible five-equation two-phased flow models towards the computation of the water hammer phenomenon
approximate Riemann solvers

ten Eikelder, M.F.P.

Award date:
2015

Compressible five-equation two-phase flow models towards the computation of the water hammer phenomenon

Approximate Riemann solvers

M.F.P. ten Eikelder
August 2015

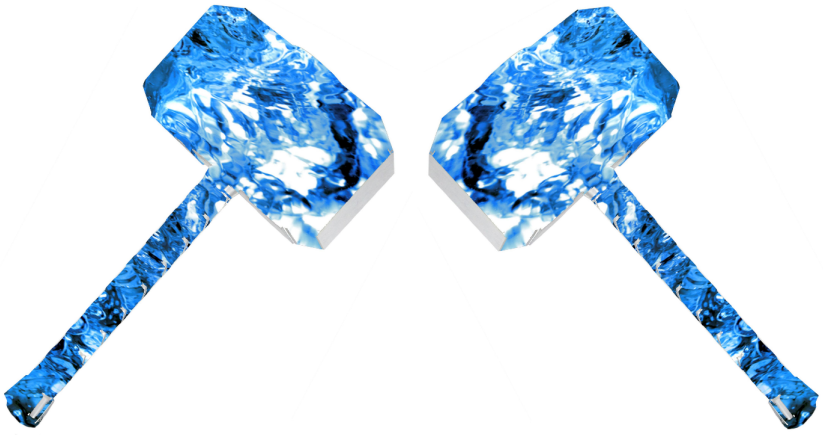

eDF

TU/e Technische Universiteit Eindhoven University of Technology

Compressible five-equation two-phase flow models towards the computation of the water hammer phenomenon

Approximate Riemann solvers

Master of Science Thesis

M.F.P. ten Eikelder
August 2015

Eindhoven University of Technology
Department of Mathematics & Computer Science
Industrial and Applied Mathematics

Supervisors:
dr. Frédéric Daude[1]
prof. dr. ir. Barry Koren[2]

[1] EDF R&D, AMA/T61
[2] Eindhoven University of Technology

Preface

This thesis is my final work of my study program Industrial and Applied Mathematics at the department of Mathematics and Computer Science of Eindhoven University of Technology. The work of six months has been conducted at the department of Analyses Mécaniques et Acoustique, Recherche et Développement at Électricité de France (EDF) in Clamart (a suburb of Paris), France.

After this second internship in my Master's (the first one was in Kanpur, India for three months) it is time to return to the Netherlands. I will continue in computational fluid dynamics research in a PhD-position under the supervision of Federico Toschi at the Eindhoven University of Technology.

My graduation period was without doubt the most instructive and productive period of my entire study. It would not have been a success with the support of many people, whom I would like to thank.

First of all I would like to thank my daily supervisor Frédéric Daude. Thank you for offering me this challenging project and thank you for the many useful discussions we had! Since your knowledge of the two-phase flow literature is truly amazing, you responded to many of my questions by providing several papers, from which I learned a lot.

Secondly, I am grateful to my graduation supervisor Barry Koren. His interest and enthusiasm has contributed a lot to the project. Thank you for making time to discuss during my visits to the Netherlands. Barry gave me a lot of freedom during my research, which I have considered as a privilege. Furthermore, I like to thank you for quickly responding to all of my emails, I really appreciate it. I know that this is something not all supervisors would do.

There are many others I would like to thank. Hippolyte Lochon, thank you for your very critical view on the modelling part and the treatment of the non-conservative products. Jasper Kreeft, thank you for showing interest in my work and for providing me the source code of the Osher solver of your model, this has saved me a lot of time. I appreciate it. Arris Tijsseling, thank you for introducing me to eDF and for the introductory visit to eDF!

Nicolas, Victor, Frédéric, Lotte, Romain, Frédéric Payet, Celia, thank you for the many hours of running in the woods during lunch time. Despite the fact that I could not always join due to injuries, I really enjoyed it! Merci beaucoup! Chau and Li, I enjoyed the many table tennis trainings we had: Merci! Amine, Bachir, Elodie, Victor, Frédéric Payet, Lotte, Celia, Jerome Delplace, Julie, Hippolyte and Olivier thank you very much for the great weekend trip to Madrid!

Last but not least, I would like to thank my friends, parents and (little ;-)) brothers in the Netherlands for the nice trips we made and for their endless support during my entire study. Bedankt!

Marco ten Eikelder,
Clamart, France, August 2015

Abstract

The purpose of this thesis is to develop a robust, efficient and accurate numerical method for the five-equation two-phase flow model. Among the various formulations of the five-equation models that exist, we identify two possible candidates: (i) The original formulation of Kapila et al. and (ii) a new, more physical, formulation proposed by Kreeft and Koren. To compare both models, HLLC-type solvers based on the integral formulation of the problem and Osher-type solvers based on the splitting of the flux and the integration path, are used. An HLLC-type solver for Kapila's model and an Osher-type solver for Kreeft and Koren's formulation already exist. For the comparison the new schemes are developed: An HLLC-type solver for Kreeft and Koren's model and an Osher-type solver for Kapila's model.

Furthermore, a novel Lagrange-projection like scheme for the five-equation two-phase flow model (Kapila's formulation) is developed. This method decouples the acoustic and transport phenomena leading to two submodels. For the acoustic part an HLLC-type solver and for the transport part an upwind scheme is used. Both submodels are solved without the use of Riemann invariants. The new numerical method lends itself perfectly for an analysis in the low Mach regime. An improvement of the scheme in the low Mach regime can be made and implemented easily.

A comparison (with first order spatial and temporal accuracy) of the various models and schemes on several shock tube test cases is made. This reveals that Kapila's model with the HLLC-type scheme is the best combination based on accuracy and computational efficiency. The new Lagrange-projection like scheme, which is designed for low Mach regime, also performs well for the shock tube test cases. It should be tested for the low Mach regime in a further research.

To use the model for water hammer computations, a new mass and heat flux extension of the model is derived. The formulation of the model of Kreeft and Koren is required here.

Nomenclature

Greek symbols

Γ	bulk Grüneisen coefficient
Π	surrogate pressure
Ω	finite volume cell
α	volume fraction
β	mass fraction
γ	adiabatic index = ratio of specific heats
δ	correction parameter lagrangian method
θ	relaxation parameter heat flux
λ	eigenvalue
ν	relaxation parameter mass flux
π	pressure variable
ρ	density
ρ_I	interfacial density
τ	specific volume
φ	flux limiter
ϕ	parameter volume fraction equation
$\boldsymbol{\phi}$	numerical flux

Operators

$\partial_y \cdot$	partial derivative with respect variable y
$\mathrm{D} \cdot / \mathrm{D}t$	material derivative
$\nabla \bullet \cdot$	divergence operator
$\nabla \cdot$	gradient operator
$\mathbf{a} \otimes \mathbf{b}$	dyadic product vectors $\mathbf{a}$ and $\mathbf{b}$
$\mathbf{a} \cdot \mathbf{b}$	inner product vectors $\mathbf{a}$ and $\mathbf{b}$

Roman symbols

A	Jacobian matrix
$\mathcal{C}$	CFL number
E	total energy
$\mathcal{F}$	flux
M	Mach number
Q	heat flux
$\mathbf{Q}$	vector of conservative variables
$\mathbf{Q}^{\text{LAG}}$	vector of lagrangian variables
$\mathbf{Q}_s^{\text{LAG}}$	vector of lagrangian variables in relaxed system
$\mathcal{S}$	signal speed
T	temperature
$\mathbf{W}$	vector of primitive variables
$\dot{W}$	total rate-of-work term
$\dot{W}_M$	mechanical rate-of-work term
$\dot{W}_T$	thermodynamical rate-of-work term

a	parameter in relaxed system
c	speed of sound
e	bulk specific internal energy
e_I	interfacial internal energy
g	gibbs free energy
h	enthalpy
$\mathbf{l}$	left eigenvector
$\dot{m}$	mass flux
$\mathbf{n}$	normal vector
p	pressure
q	characteristic variable equation of state
r	slope flux limiter
$\mathbf{r}$	right eigenvector
s	entropy
t	time
$\mathbf{u}$	velocity vector
u, v	velocity components in x, y direction
x, y	Cartesian coordinates

Abbreviations

CFD	Computational Fluid Dynamics
CFL	Courant-Friedrichs-Lewy
EOS	Equation of state
FV	Finite volume
GNL	Genuinely nonlinear
GRI	Generalized Riemann invariant
LD	Linearly degenerate
LP	Lagrange-Projection
ODE	Ordinary differential equation
PDE	Partial differential equation
PG	Perfect gas
SG	Stiffened gas

List of Figures

List of Tables

Contents

1 Introduction

In this introductory Chapter we introduce two-fluid flow modeling and its industrial relevance. Also we describe what has been done already, as well as our research objectives and our new contributions. Finally, we give an overview of this thesis.

1.1 Background

Multiphase flow modeling, the science of how fluids interact, is a research topic that has been studied extensively for the last few decades. The industry started to study this topic in the 1960s [15]. Before this time, the knowledge about this topic was limited to the observations of the engineers. Nowadays, multiphase flow modeling is used a lot in industry, examples include (this list is by far not complete) the conversion of crude oil to high-value petroleum products in a refinery, pollution control, fluidized beds, plasma spray coating, fire suppression and control, transport of fluids and many more. Apart from the industrial applications, it is scientifically very interesting and challenging.

In this thesis we focus on two-phase flow models, which is the most basic case of multiphase flow modeling. It is used in power industry, petroleum industry and aeronautic industry. In particular, it is used for the simulation of flows of fluids (water and gas, gas and gas, oil and gas, etc.) through pipelines. The application we focus on is the modeling of the water hammer flow phenomenon, which we introduce in the next Section.

1.2 The water hammer phenomenon

The water hammer phenomenon is a concussion or the sound of a concussion of a moving fluid (mostly water) against the side(s) of the containing pipe or vessel. A (high) pressure wave is caused by a rapid change of the fluid velocity. There are different causes for water hammer phenomena to happen. We briefly discuss two of them: (i) the classical water hammer phenomenon and (ii) the condensation induced water hammer phenomenon.

Classical water hammer

For the classical water hammer phenomenon we consider a pipe filled with (one) fluid, see Figure 1.1 part 1. When the valve on the right side of the pipe is opened, the fluid starts moving to the right, as we visualize in part 2. As the fluid flows, it has a positive momentum. When the valve on the right side closes rapidly (see part 3), a high pressure wave is generated as a result of the rapid change of the momentum. This pressure wave propagates (possibly in both directions) in the pipe.

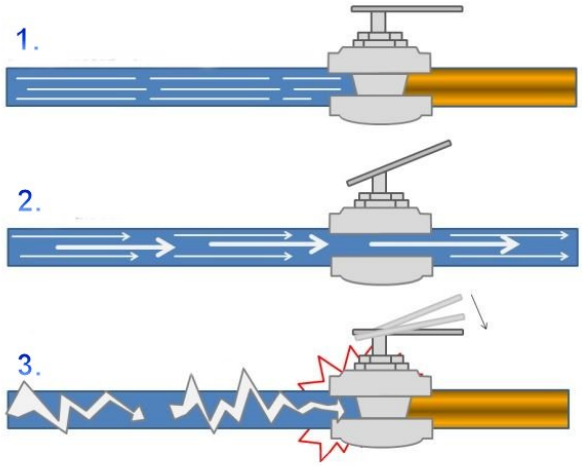

Figure 1.1: Classical Water Hammer

Condensation induced water hammer

This description is based on Kirsner [19]. The condensation induced water hammer is physically more difficult. As the name suggests, the water hammer phenomenon is caused by the rapid condensation of steam. Here, the pipe is filled with two fluids: water and steam. The steam has entered when water is drained from the formerly full pipe by opening a valve. The water has a (much) lower temperature than the steam as it cools due to the heat loss through the pipe wall. The steam in the line condenses due to the contact with both the water as well as the pipe walls, see Figure 1.2 part 1. This causes a pressure drop in the steam phase. As the steam condenses, it induces more steam to flow into the low pressure void. This flow of steam draws up waves (this is known as Kelvin Helmholtz instability). Since the rate of the heat transfer is rapid, the inflow of steam can draw up a wave that plugs the pipe, see part 2. We now have a pocket of steam which is isolated from the inflowing steam (slugflow). The pressure in this isolated pocket of steam decreases rapidly due to the continuation of the condensation. The pressure difference of the steam pocket and the inflowing steam causes the slug wave to rush into the void, see part 3. When the water slaps into itself, the sudden change in momentum is converted to overpressure waves: a water hammer phenomenon is caused. These high pressure waves travel in both directions of the pipe.

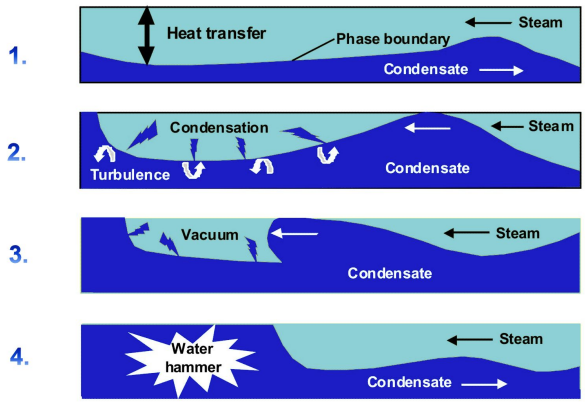

Figure 1.2: Condensation induced Water Hammer

1.3 Industrial context

Water hammer is a phenomenon that causes a lot of troubles. The collapsing overpressure waves can be sufficient to blow out several pipe elements or gaskets. Additionally, it is dangerous for people and can even result in death. One of the biggest accidents caused by the water hammer phenomenon happened at Russia's biggest hydroelectric power stations (Sayano-Shushenskaya) at August 17, 2009:

'*The Sayano-Shushenskaya hydro-electricity plant in Russia experienced large and rapid fluctuations in load and later a load rejection causing a catastrophic failure resulting in 75 fatalities, injuries, serious disruption to production at local industries, more than $1 billion damage to plant/equipment, expensive compensations, adverse environmental impact, and a 17% reduction in the company's share price.*'[2].

Water hammers also happen in the cooling systems of the nuclear power plants of Électricité de France (EDF). The cooling liquid gets in contact with steam causing a condensation induced water hammer. This is roughly visualized in Figure 1.3. The power plants of EDF are on average 30 to 50 days per year not available due to water hammer accidents which happen, on average, once or twice a year. Apart from the danger for the employees, the closing of a power plant costs around 1 million euro per day.

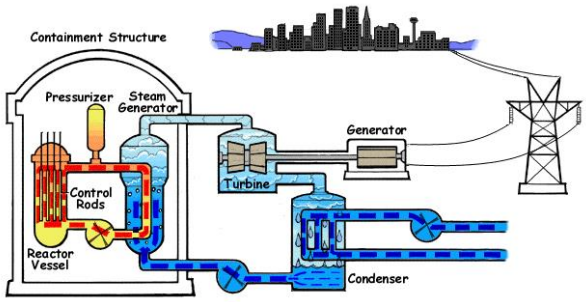

Figure 1.3: Schematic power plant

1.4 State of the art

For the modeling of two-phase flows two classes of models can be considered: (i) The most general two-fluid flow models and (ii) the smaller so-called homogeneous models. These homogeneous models are derived from the two-fluid flow models and form an alternative. In this thesis we focus on the *five-equation model*, which consists of five equations, from the homogeneous model class. There are two important five-equation models:

- The original five-equation model of Kapila et al. (2001) [18] derived from the two-fluid flow model of Baer and Nunziato (1986) [3].
- A new formulation of the model of Kapila et al. presented by Kreeft and Koren (2010) [22] in which the fifth equation, the topological equation, is replaced by an energy equation.

For the model of Kapila et al. an HLLC-type solver has been proposed by Daude et al. [11]. On the other hand, an Osher-type solver has been proposed by Kreeft and Koren [22] for their model.

1.5 Research objectives

The models of Kapila et al. and Kreeft and Koren have not been compared yet. This raises the question of which model to use in practice. This choice also depends on the corresponding numerical solver. In this thesis we would like to use the 'better' model, i.e. the model which performs the best at the test cases. It is difficult to compare the two different models (Kapila et al. and Kreeft and Koren) with different numerical methods (HLLC-type and Osher-type). Therefore one of our goals is to develop (i) an Osher-type solver for Kapila's model and (ii) an HLLC-type solver for the model of Kreeft and Koren. With these solvers at hand, we can compare the two different models (Kapila et al. and Kreeft and Koren) with different numerical methods (HLLC-type and Osher-type).

It is known that many Riemann solvers behave badly in the low Mach regime. In this regime water hammer phenomena can occur. Therefore, we are interested in a numerical scheme which behaves well in this regime. We choose to develop a Lagrange-Projection like scheme (for Kapila's model) for accessing the low Mach regime. It is not the goal of this scheme to behave better than HLLC-type and/or Osher-type schemes for the shock tube test cases: It is purpose is to behave well in the low Mach regime.

We will only consider (one-dimensional) shock tube test cases. This is the first step towards the simulation of water hammer phenomena with the five-equation model.

Furthermore, for the modeling of water hammer phenomena phase transition should be possible. The model of Kreeft and Koren does not have this possibility yet and has to be extended. On the other hand, in the model of Kapila et al. phase transitions terms can be taken into account.

1.6 Our contribution

Our new contributions in this thesis can be summarized as follows:

- Development of an Osher-type solver for Kapila's model,
- Development of an HLLC-type solver for the model of Kreeft and Koren,
- Development of a Lagrange-Projection like scheme for Kapila's model for accessing the low Mach regime,
- Comparison of the various models and schemes,
- A new extension of the five-equation model with mass and heat transfer.

1.7 Outline of this thesis

This thesis is divided into 2 main parts. In the first and largest part of the thesis, *Convective part*, we focus on the convective part of the five-equation model. This means that no source terms are taken into account here. This part consists of an introductory and modeling Chapter, three Chapters on various numerical methods (Osher-type scheme, HLLC-type scheme and a Lagrange-Projection like scheme) and a Chapter on the numerical results. Next, in part two, *Source terms*, we present our extension of phase transition of the five-equation model. In more detail:

In Chapter 2 we present the five-equation two-phase flow model, which is the central model in this thesis. We present both formulations: (i) the original one of Kapila et al. [18] and the one of

Kreeft and Koren [22]. Additionally, we discuss the mathematical properties of the model, give an introduction to Riemann problems and present the Finite Volume (FV) approximation of the model.

In Chapter 3 we present the first numerical method: An Osher-type solver. We derive an Osher-type solver for Kapila's model by applying the approach of Kreeft and Koren [22] for their model to the model of Kapila et al. [18].

In Chapter 4 we present the HLLC-type schemes of both models: (i) the original one of Kapila et al. [18] and the Kreeft and Koren [22] model. The aim of this Chapter is twofold: (i) It derives a new HLLC-type scheme for the model of Kreeft and Koren [22] and (ii) it serves as an introductory Chapter for the next Chapter: Chapter 5.

In Chapter 5 we propose a new all regime Lagrange-Projection like scheme. This is the main novelty of the thesis. We apply the idea of Chalons et al. [9] to split the Euler equations of gas dynamics into submodels (an acoustic and a transport part) to the five-equation model. For the acoustic system we propose an approximate HLLC-type scheme of a relaxed system and we use an upwind scheme for the transport system. A low Mach number correction is introduced to access the low Mach regime.

In Chapter 6 we compare the numerical schemes of the previous Chapters on five different shock tube test cases.

Chapter 7 is where we present our extension of the five-equation models with phase transition. This extension is partly based on Zein [37].

Finally, in Chapter 8 we draw the conclusions and summarize our work. Furthermore, we discuss the further work and open questions.

This thesis contains three appendices which access: (i) the implementation issues (ii) some derivations and (iii) some background on the derivation of the relaxed system which is used in Chapter 5.

1.8 Roadmap through the chapters

If the reader is familiar with the five-equation model and Riemann Problems, Chapter 2 can be skipped. If not, it is useful to read it first, since it is used in the Chapters 3 and 4-7. The Chapters 3 and 4 are not related, i.e. each one can be read separately. Next, we advice to read Chapter 4 before starting with Chapter 5 unless the reader is familiar with HLLC-type solvers.

Part I

Convective part

2
The five-equation model

In this Chapter we present the five-equation two-phase flow model. The five-equation model is the central model in this thesis. The original five-equation model of Kapila et al. (2001) [18] is derived from the two-fluid flow model of Baer and Nunziato (1986) [3]. The five-equation model models inviscid, non-heat-conducting, compressible two-fluid flow. It allows a mixture of the two fluids. Currently, there exist many different formulations of the same five-equation model. We consider the following two important five-equation models:

- *The original five-equation model of Kapila et al., referred to as Kapila's model*
- *A new formulation of the model of Kapila et al. presented by Kreeft and Koren (2010) [22] in which the fifth equation, the topological equation, is replaced by an energy equation. We refer to this model as the model of Kreeft & Koren*[1].

Furthermore, we present the mathematical properties of the model (which hold of course for both formulations). These properties are used in the development of the various numerical schemes.
The Chapter is organised as follows. We start off by presenting the original five-equation model of Kapila et al. [18] in Section 2.1. Next, in Section 2.2, we give the derivation of the model of Kreeft and Koren [22]. The mathematical properties of the model are discussed in Section 2.3. We present a brief introduction to Riemann problems in Section 2.4. Finally, we give the Finite volume (FV) approximation in Section 2.5.

2.1 Kapila's five-equation model

Kapila's model is derived from the general Baer Nunziato model by assuming both a single velocity and a single pressure at the two-fluid interface:

$$p_1 = p_2 \equiv p, \tag{2.1.1a}$$

$$\mathbf{u}_1 = \mathbf{u}_2 \equiv \mathbf{u}, \tag{2.1.1b}$$

[1] Keep in mind that this is actually the same model as the one of Kapila et al. in a new formulation

where p denotes pressure, $\mathbf{u}$ the velocity, and the superscripts refer to the two fluids. The complete derivation, presented in [18], is quite long and involved, which we will omit therefore here. The first three equations of the model are the Euler equations of gas dynamics, these read as:

$$\partial_t \rho + \nabla \cdot (\rho \mathbf{u}) = 0, \tag{2.1.2a}$$

$$\partial_t (\rho \mathbf{u}) + \nabla \cdot (\rho \mathbf{u} \otimes \mathbf{u}) + \nabla p = \mathbf{0}, \tag{2.1.2b}$$

$$\partial_t (\rho E) + \nabla \cdot (\rho E \mathbf{u}) + \nabla \cdot (p \mathbf{u}) = 0. \tag{2.1.2c}$$

Here, t denotes the time parameter, ρ denotes the bulk density and E the bulk energy density[2]. As there is no mass transfer in the model, the masses of the single fluids are conserved; the model consists of an equation describing the mass conservation of a single fluid (here fluid 1)[3]:

$$\partial_t (\alpha_1 \rho_1) + \nabla \cdot (\alpha_1 \rho_1 \mathbf{u}) = 0. \tag{2.1.3}$$

The variables α_k and ρ_k denote the volume fraction and the density of fluid k respectively, ($k = 1, 2$). The volume fraction α_k is defined as $\alpha_k = V_k/V$, where V is a control volume and V_k is volume of fluid k in V. The model allows a mixture of the two fluids, but no phase transition between the two fluids. In terms of single fluid variables, the bulk density and energy are given by

$$\rho = \alpha_1 \rho_1 + \alpha_2 \rho_2, \tag{2.1.4a}$$

$$\rho E = \alpha_1 \rho_1 E_1 + \alpha_2 \rho_2 E_2, \tag{2.1.4b}$$

where the energy densities of the fluids are

$$E_1 = e_1 + \frac{1}{2} \mathbf{u} \cdot \mathbf{u}, \tag{2.1.5a}$$

$$E_2 = e_2 + \frac{1}{2} \mathbf{u} \cdot \mathbf{u}, \tag{2.1.5b}$$

with e_1, e_2 the internal energy densities of the fluids 1 and 2, respectively. The bulk internal energy density is given by

$$\rho e = \alpha_1 \rho_1 e_1 + \alpha_2 \rho_2 e_2, \tag{2.1.6}$$

and hence,

$$E = e + \frac{1}{2} \mathbf{u} \cdot \mathbf{u}. \tag{2.1.7}$$

Furthermore, we mention that the *saturation constraint* should be fulfilled:

$$\alpha_1 + \alpha_2 = 1. \tag{2.1.8}$$

The fifth equation of the model is an equation for the volume fraction of fluid 1:

$$\partial_t \alpha_1 + \mathbf{u} \cdot \nabla \alpha_1 + \phi \nabla \cdot \mathbf{u} = 0, \tag{2.1.9}$$

[2] In this thesis sometimes we refer to this quantity with 'energy' where strictly speaking it is an 'energy density'.

[3] By substracting Eq. (2.1.3) from Eq. (2.1.2a) the mass conservation of fluid 2 is obtained.

where it can be shown that [22]

$$\phi = \alpha_1 \alpha_2 \frac{\mathfrak{z}_2 - \mathfrak{z}_1}{\mathfrak{z}}. \tag{2.1.10}$$

The parameters $\mathfrak{z}$ and $\mathfrak{z}_1, \mathfrak{z}_2$ are the (bulk) isentropic compressibilities of both fluids:

$$\mathfrak{z} = \alpha_1 \mathfrak{z}_1 + \alpha_2 \mathfrak{z}_2, \tag{2.1.11a}$$

$$\mathfrak{z}_1 = \frac{1}{\rho_1 c_1^2}, \tag{2.1.11b}$$

$$\mathfrak{z}_2 = \frac{1}{\rho_2 c_2^2}, \tag{2.1.11c}$$

with $c_1 = \left(\frac{\partial p}{\partial \rho_1}\right)_{s_1}, c_2 = \left(\frac{\partial p}{\partial \rho_2}\right)_{s_2}$ and s_1, s_2 the speed of sound and the entropy of both fluids, respectively. This fifth equation is a non-conservative equation. If the compressibilities of both fluids are equal, we obtain a transport equation for the volume fraction:

$$\partial_t \alpha_1 + \mathbf{u} \cdot \nabla \alpha_1 = 0. \tag{2.1.12}$$

Summarizing, Eq. (2.1.2a)-(2.1.2c), Eq. (2.1.3) and Eq. (2.1.9) form the five-equation model of Kapila et al. The model is completed with an equation of state. An equation of state describes a relation between some thermodynamical quantities, e.g. $e = e(p, \rho)$, see Appendix A.

2.2 Kreeft and Koren's five-equation model

A new formulation of Kapila's five-equation model has been derived by Kreeft and Koren in [22], which we will present briefly in this Section. The first four equations are the same as in Kapila's five-equation model. However the fifth equation of the model, replacing Eq. (2.1.9), which describes the energy of one of the two fluids, is new. The fifth equation of the model is a non-conservative equation which contains a term on the right-hand side which represents the energy exchange between two fluids due to work. The derivation is done from scratch, hence it is not based on Kapila's model or the model of Baer Nunziato. It is assumed that two fluids are mass conservative. Particles of the two fluids exert force on each other causing momentum exchange between two fluids. This results in an energy exchange. This exchange is due to the velocity and pressure relaxation.

Conservation laws

The conservation laws of mass, momentum and energy are given by

$$\frac{\partial}{\partial t} \int_V \rho \mathrm{d}V + \oint_S \rho \mathbf{u} \cdot \mathbf{n} \mathrm{d}S = 0, \tag{2.2.1a}$$

$$\frac{\partial}{\partial t} \int_V \rho \mathbf{u} \mathrm{d}V + \oint_S \rho \mathbf{u} \otimes \mathbf{u} \cdot \mathbf{n} \mathrm{d}S + \oint_S p \mathbf{n} \mathrm{d}S = \mathbf{0}, \tag{2.2.1b}$$

$$\frac{\partial}{\partial t} \int_V \rho E \mathrm{d}V + \oint_S \rho E \mathbf{u} \cdot \mathbf{n} \mathrm{d}S + \oint_S p \mathbf{u} \cdot \mathbf{n} \mathrm{d}S = 0, \tag{2.2.1c}$$

where V is a control volume, with boundary S, fixed in time and space. Here, ρ denotes the bulk density and E the bulk energy. There can be two fluids in one control volume. One can write down the conservation laws of each single fluid. Following Kreeft and Koren [22], the conservation laws of mass and momentum for fluid 1 read:

$$\partial_t \int_{V_1(t)} \rho_1 \mathrm{d}V_1 + \oint_{S_1(t)} \rho_1 \left(\mathbf{u} - \mathbf{u}_{S_1}\right) \cdot \mathbf{n} \mathrm{d}S_1 = 0, \tag{2.2.2a}$$

$$\partial_t \int_{V_1(t)} \rho_1 \mathbf{u} \mathrm{d}V_1 + \oint_{S_1(t)} \rho_1 \mathbf{u} \otimes \left(\mathbf{u} - \mathbf{u}_{S_1}\right) \cdot \mathbf{n} \mathrm{d}S_1 + \oint_{S_1(t)} p\mathbf{n} \mathrm{d}S_1 = \int_V \mathbf{F} \mathrm{d}V, \tag{2.2.2b}$$

where the volume $V_1(t)$ and surface $S_1(t)$ may now vary in time due to the motion of the interface with velocity $\mathbf{u}_{S_1}$. The integration of $\mathbf{F}$ is done over the total volume V since it is a result of both fluids. Note that the momentum of fluid 1 is not conserved; the force $\mathbf{F}$ represents the net force per unit of volume exerted on fluid 1. Furthermore, $\mathbf{F}$ contributes to the energy equation of fluid 1 in the form of rate of mechanical work performed per unit of volume: $\dot{W}_M = \mathbf{F} \cdot \mathbf{u}$. Apart from the mechanical work, the energy equation of fluid 1 is affected by the thermodynamical rate-of-work term $\dot{W}_T$. The equation reads

$$\begin{aligned} \partial_t \int_{V_1(t)} \rho_1 E_1 \mathrm{d}V_1 + \oint_{S_1(t)} \rho_1 E_1 \otimes \left(\mathbf{u} - \mathbf{u}_{S_1(t)}\right) \cdot \mathbf{n} \mathrm{d}S_1 \quad &+ \oint_{S_1(t)} p\mathbf{u} \cdot \mathbf{n} \mathrm{d}S_1 \\ &= \int_V \dot{W}_M + \dot{W}_T \mathrm{d}V. \end{aligned} \tag{2.2.3}$$

To eliminate the unknown surface $S_1(t)$ one can use the divergence theorem. Next, to eliminate the volume $V_1(t)$ we use the volume fraction of fluid 1: $\alpha_1 = V_1/V$. When changing from a moving domain to a fixed domain gives $\mathbf{u}_{S_1} = 0$. This simplifies the equations (2.2.2a) and (2.2.3) to

$$\partial_t \int_V \alpha_1 \rho_1 \mathrm{d}V + \int_V \nabla \cdot \alpha_1 \rho_1 \mathbf{u} \mathrm{d}V = 0, \tag{2.2.4a}$$

$$\begin{aligned} \partial_t \int_V \alpha_1 \rho_1 E_1 \mathrm{d}V + \int_V \nabla \cdot \alpha_1 \rho_1 E_1 \mathbf{u} \mathrm{d}V + \int_V \nabla \cdot \alpha_1 p \mathbf{u} \mathrm{d}V \\ = \int_V \left(\dot{W}_M + \dot{W}_T\right) \mathrm{d}V. \end{aligned} \tag{2.2.4b}$$

The system in differential form reads:

$$\partial_t \rho + \nabla \cdot (\rho \mathbf{u}) = 0, \tag{2.2.5a}$$

$$\partial_t (\rho \mathbf{u}) + \nabla \cdot (\rho \mathbf{u} \otimes \mathbf{u}) + \nabla p = \mathbf{0}, \tag{2.2.5b}$$

$$\partial_t (\rho E) + \nabla \cdot (\rho E \mathbf{u}) + \nabla (p\mathbf{u}) = 0, \tag{2.2.5c}$$

$$\partial_t (\alpha_1 \rho_1) + \nabla \cdot (\alpha_1 \rho_1 \mathbf{u}) = 0, \tag{2.2.5d}$$

$$\partial_t (\alpha_1 \rho_1 E_1) + \nabla \cdot (\alpha_1 \rho_1 E_1 \mathbf{u}) + \nabla \cdot (\alpha_1 p \mathbf{u}) = \dot{W}_M + \dot{W}_T. \tag{2.2.5e}$$

Rate-of-work terms

An expression for the so-called rate-of-work terms $\dot{W}_M, \dot{W}_T$ in terms of the existing variables can be derived by making use of primitive equations[4]. We do not show the derivation here, but it can be found in [22]. It yields that the total rate of energy exchange per unit volume between fluid 2 and fluid 1 is

$$\dot{W} = \dot{W}_M + \dot{W}_T, \tag{2.2.6a}$$

$$\dot{W}_M = p\mathbf{u} \cdot \nabla\alpha_1 + (\alpha_1 - \beta_1)\mathbf{u} \cdot \nabla p, \tag{2.2.6b}$$

$$\dot{W}_T = p\alpha_1\alpha_2 \frac{\mathfrak{z}_2 - \mathfrak{z}_1}{\mathfrak{z}} \nabla \cdot \mathbf{u}. \tag{2.2.6c}$$

Here $\beta_1 = \alpha_1\rho_1/\rho$ is the mass fraction of fluid 1.

2.3 Mathematical properties

In this Section we will discuss some properties of the five-equation model [5]. We will only consider the one-dimensional case here.

Structure

The model can be formulated as a set of primitive equations. The derivation is straightforward and we will omit it here. A set of primitive equations reads:

$$\frac{\mathrm{D}\rho}{\mathrm{D}t} + \rho\frac{\partial u}{\partial x} = 0, \tag{2.3.1a}$$

$$\frac{\mathrm{D}u}{\mathrm{D}t} + \frac{1}{\rho}\frac{\partial p}{\partial x} = 0, \tag{2.3.1b}$$

$$\frac{\mathrm{D}p}{\mathrm{D}t} + \rho c^2\frac{\partial u}{\partial x} = 0, \tag{2.3.1c}$$

$$\frac{\mathrm{D}\beta_1}{\mathrm{D}t} = 0, \tag{2.3.1d}$$

$$\frac{\mathrm{D}\alpha_1}{\mathrm{D}t} + \phi\frac{\partial u}{\partial x} = 0, \tag{2.3.1e}$$

where the differential operator

$$\frac{\mathrm{D}}{\mathrm{D}t} := \partial_t + u\partial_x \tag{2.3.2}$$

denotes the *material derivative* operator (also known as *total derivative*) along the characteristic curve $x'(t) = u$. The mixture speed of sound (the speed of sound in the mixture), c, obeys the Wood formula [35]

$$\frac{1}{\rho c^2} = \frac{\alpha_1}{\rho_1 c_1^2} + \frac{\alpha_2}{\rho_2 c_2^2}. \tag{2.3.3}$$

[4] A primitive equation is a differential equation, used in most atmospheric models, of the form $\mathrm{D}a/\mathrm{D}t = \ldots$. where a is a primitive variable (e.g. velocity, density, pressure).

[5] Note that since both five-equation models are only different formulations, all properties of the model hold for both formulations.

The term ρc^2, known as the *acoustic impedance*[6] of the mixture, is the harmonic mean of the *acoustic impedances* of the single fluids. Hence, the speed of sound of the mixture can be less than the speed of sound of the single phases.

The primitive equations (2.3.1) can be cast into the form

$$\partial_t \mathbf{W} + \mathbf{B}(\mathbf{W})\partial_x \mathbf{W} = \mathbf{0}, \tag{2.3.4}$$

with

$$\mathbf{W} = \begin{pmatrix} \rho \\ u \\ p \\ \beta \\ \alpha \end{pmatrix}, \quad \mathbf{B}(\mathbf{W}) = \begin{pmatrix} u & \rho & 0 & 0 & 0 \\ 0 & u & 1/\rho & 0 & 0 \\ 0 & \rho c^2 & u & 0 & 0 \\ 0 & 0 & 0 & u & 0 \\ 0 & \phi & 0 & 0 & u \end{pmatrix}. \tag{2.3.5}$$

The vector $\mathbf{W}$ contains the primitive variables. The wave speeds of the system (2.3.4)-(2.3.5), i.e. the (real) eigenvalues of $\mathbf{B}(\mathbf{W})$, are:

$$\lambda_1 = u - c, \quad \lambda_{2,3,4} = u, \quad \lambda_5 = u + c, \tag{2.3.6}$$

with corresponding right eigenvectors

$$\mathbf{r}_1 = \begin{bmatrix} \rho \\ -c \\ \rho c^2 \\ 0 \\ \phi \end{bmatrix}, \quad \mathbf{r}_2 = \begin{bmatrix} 0 \\ 0 \\ 0 \\ 0 \\ 1 \end{bmatrix}, \quad \mathbf{r}_3 = \begin{bmatrix} 0 \\ 0 \\ 0 \\ 1 \\ 0 \end{bmatrix}, \quad \mathbf{r}_4 = \begin{bmatrix} 1 \\ 0 \\ 0 \\ 0 \\ 0 \end{bmatrix}, \quad \mathbf{r}_5 = \begin{bmatrix} \rho \\ c \\ \rho c^2 \\ 0 \\ \phi \end{bmatrix}. \tag{2.3.7}$$

Hyperbolic system

We now give the definition of a hyperbolic system (i.e. not specific for the five-equation model) which is taken from [32].

Definition 2.3.1. A system

$$\partial_t \mathbf{U} + \mathbf{A}_1 \partial_x \mathbf{U} + \mathbf{A}_2 = \mathbf{0}, \tag{2.3.8}$$

with $\mathbf{U} = \mathbf{U}(x,t) \in \mathbb{R}^m$, $\mathbf{A}_1 = \mathbf{A}_1(\mathbf{U})$ and $\mathbf{A}_2 = \mathbf{A}_2(\mathbf{U})$ is classified as *hyperbolic* at a point (x_0, t_0) if $\mathbf{A}_1$ has m real eigenvalues $\lambda_1, ..., \lambda_m$ and a corresponding set of m linearly independent right eigenvectors $\mathbf{r}_1, ..., \mathbf{r}_m$. System (2.3.8) is classified as *strictly hyperbolic* if the eigenvalues $\lambda_1, ..., \lambda_m$ are all distinct.

As a result, the five-equation model, i.e. system (2.3.4)-(2.3.5), is hyperbolic.

[6] In literature the term ρc is also referred to as *acoustic impedance*.

Characteristic Fields

Consider a system of the form

$$\partial_t \mathbf{U} + \mathbf{A}(\mathbf{U})\partial_x \mathbf{U} = \mathbf{0}, \tag{2.3.9}$$

with eigenvalues λ_i and corresponding right eigenvectors $\mathbf{r}_i$. The wave speed λ_i is said to be a *characteristic field* $\lambda_i = \lambda_i(\mathbf{U})$.

Definition 2.3.2. A field associated with eigenvalue λ (and corresponding eigenvector $\mathbf{r}$) is said to be *linearly degenerate* (LD) if

$$\nabla\lambda\left(\mathbf{U}\right) \cdot \mathbf{r}(\mathbf{U}) = 0, \quad \text{for all} \quad \mathbf{U} \in \mathbb{R}^m, \tag{2.3.10}$$

Definition 2.3.3. A field associated with eigenvalue λ (and corresponding eigenvector $\mathbf{r}$) is said to be *genuinely nonlinear* (GNL) if

$$\nabla\lambda\left(\mathbf{U}\right) \cdot \mathbf{r}(\mathbf{U}) \neq 0, \quad \text{for all} \quad \mathbf{U} \in \mathbb{R}^m. \tag{2.3.11}$$

We now turn back to the five-equation model. Fields associated with $\lambda_{2,3,4}$ (defined in Eq. (2.3.6)) are linearly degenerate and the fields associated with λ_1, λ_5 are genuinely nonlinear. For a proof we refer to [27]. Furthermore, a direct calculation reveals

$$\left(\nabla_{\mathbf{W}}\, u\right) \cdot \mathbf{r}_k\left(\mathbf{W}\right) = 0, \tag{2.3.12a}$$
$$\left(\nabla_{\mathbf{W}}\, p\right) \cdot \mathbf{r}_k\left(\mathbf{W}\right) = 0, \tag{2.3.12b}$$

for $k = 2, 3, 4$, which means that both the velocity as well as the pressure are constant across the *middle wave*, i.e the wave associated with $\lambda_{2,3,4}$. This is an important result which will be used in the approximate Riemann solvers in the Chapter 3,4 and 5.

Riemann Invariants

The five-equation model is a hyperbolic set of PDEs. This means that the PDEs describe quantities which propagate in some direction, while remaining the same strength [21]. These quantities are referred to as *Riemann invariants*. We denote the Riemann invariants with ϕ_k, for $k = 1, ..., 5$. The *characteristic equations* which describe the propagation of the Riemann invariants read:

$$\partial_t \phi_k + \lambda_k \partial_x \phi_k = 0, \tag{2.3.13}$$

for $k = 1, ..., 5$. The wave speed λ_k is also referred to as a *characteristic speed*. The characteristic equations can be written as

$$\frac{\mathrm{D}_k \phi_k}{\mathrm{D}t} = 0, \quad \text{for} \;\; k = 1, ..., 5, \tag{2.3.14}$$

where the differential operator

$$\frac{\mathrm{D}_i}{\mathrm{D}t} := \partial_t + \lambda_i \partial_x \tag{2.3.15}$$

denotes the *material derivative* operator along the characteristic curve $x'(t) = \lambda_i$. In other words, the Riemann invariants are constant along the characteristic curves. This is the reason for using the word 'invariant'. We are interested in obtaining the *Riemann invariants* of the model. The Riemann invariants are used in the Chapters 3 and 4.

We now introduce the Riemann invariants. Our introduction is based on [34]. Let us again consider a system of the form (2.3.9). The matrix $\mathbf{L}(\mathbf{U})$ is a nonsingular matrix with the left eigenvectors of $\mathbf{A}$ as its rows: $\mathbf{L} = [\mathbf{l}_k]$. Premultiplication by $\mathbf{L}$ in Eq. (2.3.9) gives

$$\mathbf{L}\partial_t \mathbf{U} + \mathbf{L}\mathbf{A}\partial_x \mathbf{U} = \mathbf{0}. \tag{2.3.16}$$

This can be written as

$$\mathbf{L}\partial_t \mathbf{U} + \mathbf{\Lambda}\mathbf{L}\partial_x \mathbf{U} = \mathbf{0}, \tag{2.3.17}$$

where $\mathbf{\Lambda} = \text{diag}\,(\lambda_k)$. System (2.3.17) reads componentwise:

$$\sum_k l_{ik}(U_k)\partial_t U_k + \lambda_i(U)\sum_k l_{ik}(U_k)\partial_x U_k = 0, \tag{2.3.18}$$

for $l_{ij} = (\mathbf{L})_{ij}$ and $i = 1, ..., m$.

Definition 2.3.4. If there is an integrating factor μ_i such that

$$\mu_i(\mathbf{U})\sum_k l_{ik}\mathrm{d}U_k = d\phi_i(\mathbf{U}) \tag{2.3.19}$$

then ϕ_i is called a *Riemann Invariant*. The Riemann invariant is constant along the curve $x'(t) = \lambda_i(\mathbf{U})$.

We now turn back to the five-equation model. The left eigenvectors of $\mathbf{B}(\mathbf{W})$ are

$$\begin{aligned} &\mathbf{l}_1 = \left[0, -\rho c, 1, 0, 0\right], \mathbf{l}_2 = \left[-\phi, 0, 0, 0, \rho\right], \mathbf{l}_3 = \left[0, 0, 0, 1, 0\right], \\ &\mathbf{l}_4 = \left[-c^2, 0, 1, 0, 0\right], \mathbf{l}_5 = \left[0, \rho c, 1, 0, 0\right]. \end{aligned} \tag{2.3.20}$$

Next, we define a matrix $\mathbf{L}$ by choosing the left eigenvectors as its rows:

$$\mathbf{L} = \begin{bmatrix} \mathbf{l}_1 \\ \mathbf{l}_2 \\ \mathbf{l}_3 \\ \mathbf{l}_4 \\ \mathbf{l}_5 \end{bmatrix} = \begin{bmatrix} 0 & -\rho c & 1 & 0 & 0 \\ -\phi & 0 & 0 & 0 & \rho \\ 0 & 0 & 0 & 1 & 0 \\ -c^2 & 0 & 1 & 0 & 0 \\ 0 & \rho c & 1 & 0 & 0 \end{bmatrix}. \tag{2.3.21}$$

Using Jordan decomposition, i.e. we write $\mathbf{B} = \mathbf{L}^{-1}\mathbf{\Lambda}\mathbf{L}$ with $\mathbf{\Lambda} = \text{diag}(\lambda_k)$, we obtain:

$$\mathbf{L}\partial_t \mathbf{W} + \mathbf{\Lambda}\mathbf{L}\partial_x \mathbf{W} = \mathbf{0}. \tag{2.3.22}$$

This yields

$$\left(\frac{\partial u}{\partial t} - \frac{1}{\rho c}\frac{\partial p}{\partial t}\right) + (u-c)\left(\frac{\partial u}{\partial x} - \frac{1}{\rho c}\frac{\partial p}{\partial x}\right) = 0, \tag{2.3.23a}$$

$$\left(\rho\frac{\partial \alpha}{\partial t} - \phi\frac{\partial \rho}{\partial t}\right) + u\left(\rho\frac{\partial \alpha}{\partial x} - \phi\frac{\partial \rho}{\partial x}\right) = 0, \tag{2.3.23b}$$

$$\left(\frac{\partial \beta}{\partial t}\right) + u\left(\frac{\partial \beta}{\partial x}\right) = 0, \tag{2.3.23c}$$

$$\left(\frac{\partial p}{\partial t} - c^2\frac{\partial \rho}{\partial t}\right) + u\left(\frac{\partial p}{\partial x} - c^2\frac{\partial \rho}{\partial x}\right) = 0, \tag{2.3.23d}$$

$$\left(\frac{\partial u}{\partial t} + \frac{1}{\rho c}\frac{\partial p}{\partial t}\right) + (u+c)\left(\frac{\partial u}{\partial x} + \frac{1}{\rho c}\frac{\partial p}{\partial x}\right) = 0, \tag{2.3.23e}$$

which can be written as

$$\partial_t \phi_k + \lambda_k \partial_x \phi_k = 0. \tag{2.3.24}$$

for $k = 1, ..., 5$. The Riemann invariants ϕ_k are conserved along the curves and we can write

$$\begin{aligned}
&d\phi_1 = du - \frac{dp}{\rho c} = 0 \qquad \text{along the curve } x'(t) = \lambda_1 = u - c,\\
&d\phi_2 = \rho d\alpha - \phi d\rho = 0 \quad \text{along the curve } x'(t) = \lambda_2 = u,\\
&d\phi_3 = d\beta = 0 \qquad\quad \text{along the curve } x'(t) = \lambda_3 = u,\\
&d\phi_4 = dp - c^2 d\rho = 0 \quad \text{along the curve } x'(t) = \lambda_4 = u,\\
&d\phi_5 = du + \frac{dp}{\rho c} = 0 \qquad \text{along the curve } x'(t) = \lambda_5 = u - c.
\end{aligned} \tag{2.3.25}$$

This result is also obtained in [21].

Alternatively, to obtain the Riemann invariants one can also proceed as follows. The *Generalized Riemann invariants* (GRIs) applied to the i-th characteristic field are written as[7]

$$\frac{dw(1)}{r_i(1)} = \frac{dw(2)}{r_i(2)} = ... = \frac{dw(n)}{r_i(n)}, \tag{2.3.26}$$

where $r_i(k)$ is the k-th component of $\mathbf{r}_i$ and $w(k)$ is the k-th component of $\mathbf{W}$. The GRIs should be interpreted as a set of ordinary differential equations. The GRIs relate the changes of the primitive variables $dw(g)$ to the corresponding right eigenvector $r_i(g)$. By taking a pair of these ODEs, we obtain a Riemann invariant:

$$\begin{aligned}
&\frac{dw(k)}{r_i(k)} = \frac{dw(l)}{r_i(l)}, \quad 1 \le k, l \le n,\\
&r_i(l)dw(k) - r_i(k)dw(l) = 0,
\end{aligned} \tag{2.3.27}$$

[7]Let us remark that this is only a formal matter of notation. For a detailed, more precise discussion we refer to the book of Jeffery [**?**].

which is constant inside the wave

$$\int r_i(l)dw(k) - \int r_i(k)dw(l) = \text{constant}. \tag{2.3.28}$$

We now apply the GRIs to the different characteristic fields of the five-equation model, i.e. we have $n = 5$. First, for the linearly degenerate fields we write:

$$\lambda_2 : \ \frac{d\rho}{0} = \frac{du}{0} = \frac{dp}{0} = \frac{d\beta}{0} = \frac{d\alpha}{1}, \tag{2.3.29a}$$

$$\lambda_3 : \ \frac{d\rho}{0} = \frac{du}{0} = \frac{dp}{0} = \frac{d\beta}{1} = \frac{d\alpha}{0}, \tag{2.3.29b}$$

$$\lambda_4 : \ \frac{d\rho}{1} = \frac{du}{0} = \frac{dp}{0} = \frac{d\beta}{0} = \frac{d\alpha}{0}. \tag{2.3.29c}$$

This means that across $\lambda_{2,3,4}$ all variables but α, ρ, β respectively, i.e. p, u, are constant. Next, for the linearly degenerate field $\lambda_1(\mathbf{W}) = u - c$ we obtain

$$\frac{d\rho}{\rho} = \frac{du}{-c} = \frac{dp}{\rho c^2} = \frac{d\beta}{0} = \frac{d\alpha}{\phi}, \tag{2.3.30}$$

with corresponding Riemann invariants

$$d\phi_2 = \rho d\alpha - \phi d\rho, \quad d\phi_3 = d\beta, \quad d\phi_4 = dp - c^2 d\rho, \quad d\phi_5 = du + \frac{dp}{\rho c}. \tag{2.3.31}$$

Similarly, for $\lambda_5(\mathbf{W}) = u + c$ we obtain the Riemann invariants

$$d\phi_1 = du - \frac{dp}{\rho c}, \quad d\phi_2 = \rho d\alpha - \phi d\rho, \quad d\phi_3 = d\beta, \quad d\phi_4 = dp - c^2 d\rho. \tag{2.3.32}$$

And again we have obtained all Riemann invariants.

2.4 Riemann problem

In this thesis we deal with computing solutions containing discontinuities, such as shock waves. In particular, we deal with Riemann problems. In these problems, the PDE is combined with initial conditions consisting of a single discontinuity at position $x = x_0$:

$$\mathbf{W}(x,0) = \begin{cases} \mathbf{W}_L & x < x_0, \\ \mathbf{W}_R & x \geq x_0. \end{cases} \tag{2.4.1}$$

We give a short introduction to Riemann Problems for (i) the linear advection equation and (ii) a general non-linear hyperbolic system. For both parts we follow [32].

2.4.1 The linear advection equation

The one-dimensional linear advection equation can be written as

$$\partial_t u + a\partial_x u = 0, \tag{2.4.2}$$

with $u = u(x,t)$ the unknown quantity and a the given constant advection speed. For the initial condition we take

$$u(x,0) = u_0(x) = \begin{cases} u_L & x < 0, \\ u_R & x \geq 0, \end{cases} \tag{2.4.3}$$

where u_l, u_R are constant values, see Figure 2.1.

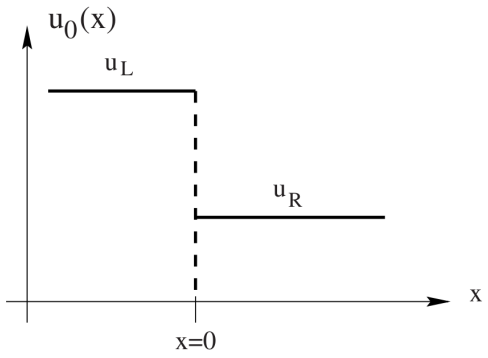

Figure 2.1: Initial condition Riemann Problem consisting of two constant states (taken from [32]).

The PDE (2.4.2) combined with the initial condition (2.4.3) is called a *Riemann Problem*. The wave solution is given by

$$u(x,t) = u_0(x - at). \tag{2.4.4}$$

The initial profile will simply be translated with velocity a by the PDE. The shape remains unchanged. So the solution can be written as

$$u(x,t) = u_0(x - at) = \begin{cases} u_L & x/t < a, \\ u_R & x/t \geq a. \end{cases} \tag{2.4.5}$$

We can represent the solution of the Riemann Problem in the $x - t$-plane, see Figure 2.2.

2.4.2 A general non-linear hyperbolic system

Consider the Riemann problem for a general $m \times m$ non-linear hyperbolic system

$$\begin{aligned} &\partial_t \mathbf{U} + \partial_x \mathcal{G}(\mathbf{U}) = 0, \\ &\mathbf{U}(x,0) = \begin{cases} \mathbf{U}_L & x < 0, \\ \mathbf{U}_R & x \geq 0. \end{cases} \end{aligned} \tag{2.4.6}$$

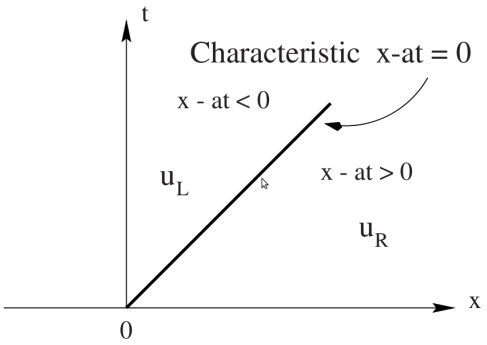

Figure 2.2: The solution of the Riemann Problem in the $x-t$-plane (taken from [32]).

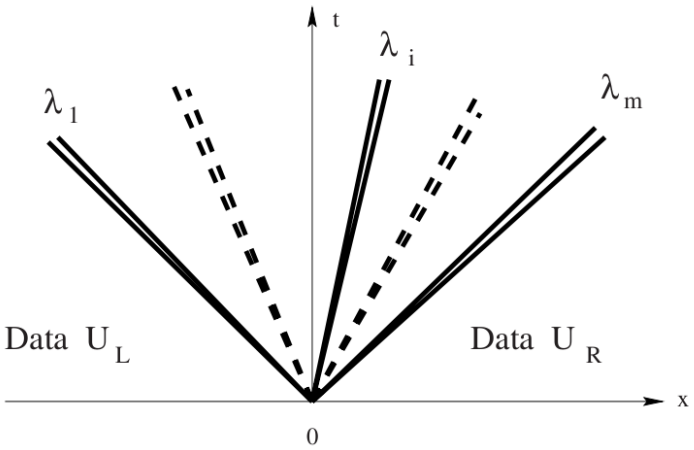

Figure 2.3: Structure of the solution of the Riemann problem (taken from [32]).

The solution consists of $m+1$ states which are separated by m waves, see Figure 2.3. There is a wave family for each eigenvalue λ_k.
The waves of the Riemann problem can be classified as

- *contact discontinuity*,
- *rarefaction wave* (also called *expansion wave* or *wave fan*),
- *shock wave*.

The characteristics of the problem (i) run into each other at a shock wave (ii) are parallel at a contact discontinuity and (iii) diverge from the discontinuity at a rarefaction wave, see Figure 2.4. The speed of the shock wave and the contact discontinuity is denoted with S_i. For a shock wave the *entropy condition* applies

$$\lambda_k(\mathbf{U}_L) > S_i > \lambda_k(\mathbf{U}_R). \tag{2.4.7}$$

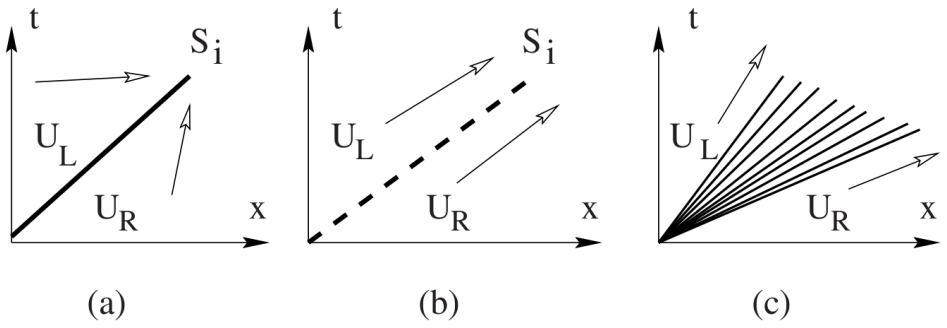

Figure 2.4: The possible wave solutions of the Riemann problem: (i) shock wave, (ii) contact discontinuity and (iii) rarefaction wave (taken from [32]).

This means that the speed at the left side of the shock is higher than at the right side. For a contact wave speeds are equal:

$$\lambda_k(\mathbf{U}_L) = S_i = \lambda_k(\mathbf{U}_R). \tag{2.4.8}$$

And finally, for a rarefaction wave the characteristics diverge

$$\lambda_k(\mathbf{U}_L) < \lambda_k(\mathbf{U}_R). \tag{2.4.9}$$

The characteristic field associated with a contact discontinuity is linearly degenerate, the characteristic fields associated with a shock wave or a rarefaction wave are genuinely nonlinear. Many more details can be found in [32].
We turn back to the five-equation model. The wave associated with the $\lambda_{2,3,4}(\mathbf{W})$ characteristic field is the so-called *contact discontinuity* (since the associated field is classified as LD) and those associated with $\lambda_1(\mathbf{W}), \lambda_5(\mathbf{W})$ are either an *expansion wave* or a *shock wave* (since the associated fields are classified as GNL).

2.5 Finite volume approximation

Let us first consider a conservative PDE, i.e.

$$\partial_t \mathbf{Q}(x,t) + \partial_x \mathcal{F}(\mathbf{Q}) = 0. \tag{2.5.1}$$

While dealing with Riemann Problems the choice of the formulation of the model is important. Using other than conservative variables will cause problems at the discontinuities, see e.g. [32]. Therefore, conservative methods have to be used. The Finite volume (FV) method is the conservative method which we will use in this thesis. In the FV method we cover the domain with finite cells (also called finite volumes or control volumes). The discrete values of the domain are given by the averages over the cells. The fluxes are located at the edges of the finite volumes, see Figure 2.5. More precisely, we define cell i as

$$\Omega_i = \left(x_{i-1/2}, x_{i+1/2}\right), \tag{2.5.2}$$

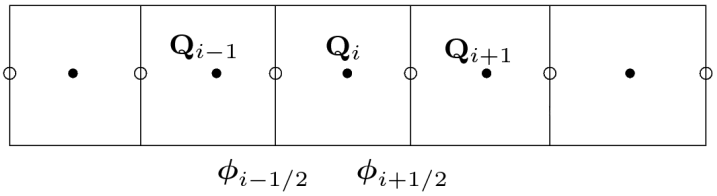

Figure 2.5: The finite volume mesh consisting of the control volumes. We show the cells as boxes here (like it is two-dimensional).

and approximate the conservative variables at this cell at time n by

$$\mathbf{Q}_i^n \doteq \frac{1}{\Delta x_i}\int_{\Omega_i} \mathbf{Q}(x,t_n)\mathrm{d}x, \tag{2.5.3}$$

with $\Delta x_i = |\Omega_i|$. The conservation law (2.5.1) can be written in integral form as

$$\frac{\mathrm{d}}{\mathrm{d}t}\int_{x_1}^{x_2} \mathbf{Q}(x,t)\mathrm{d}x = \mathcal{F}_1(t) - \mathcal{F}_2(t), \tag{2.5.4}$$

where $\mathcal{F}_1(t) = \mathcal{F}(x_1,t)$ and $-\mathcal{F}_2(t) = -\mathcal{F}(x_2,t)$ represent fluxes into the section. Integration gives

$$\begin{aligned}\frac{1}{\Delta x_i}\int_{\Omega_i} \mathbf{Q}\left(x,t_{n+1}\right)\mathrm{d}x = \quad & \frac{1}{\Delta x_i}\int_{\Omega_i} \mathbf{Q}\left(x,t_n\right)\mathrm{d}x \\ & -\frac{1}{\Delta x_i}\left[\int_{t_n}^{t_{n+1}} \mathcal{F}\left(x_{i+1/2},t\right)\mathrm{d}t - \int_{t_n}^{t_{n+1}} \mathcal{F}\left(x_{i-1/2},t\right)\mathrm{d}t\right].\end{aligned} \tag{2.5.5}$$

By approximating the first two integrals as in (2.5.3) the form of the numerical method is obtained

$$\mathbf{Q}_i^{n+1} = \mathbf{Q}_i^n - \frac{\Delta t}{\Delta x_i}\left(\boldsymbol{\phi}_{i+1/2}^n - \boldsymbol{\phi}_{i-1/2}^n\right), \tag{2.5.6}$$

with $\Delta t = t_{n+1} - t_n$ and $\boldsymbol{\phi}_{i+1/2}^n$ an approximation of the average flux at the cell face $i+1/2$. We choose to use explicit time integration to take into account the propagation of pressure waves (shock or rarefaction waves). Furthermore, explicit time integration is the easiest and it is used for the solvers: HLLC-type solver [11] and the Osher-type solver [22]. Since higher order time integration methods may lead to oscillations, a first order time integration method is used (see also Chapter 6).

The five-equation model is not a conservative model, it is of the form

$$\partial_t \mathbf{Q} + \partial_x \mathcal{F}(\mathbf{Q}) + \mathcal{R}(\mathbf{Q}, \partial_x \mathbf{Q}) = \mathbf{0}, \tag{2.5.7}$$

where $\mathcal{R}$ denote the non-conservative terms. We take a non-moving equidistant grid: $\Delta x = \Delta x_i$ for all i. The numerical approximation [8] reads

$$\mathbf{Q}_i^{n+1} = \mathbf{Q}_i^n - \frac{\Delta t}{\Delta x}\left(\boldsymbol{\phi}_{i+1/2}^n - \boldsymbol{\phi}_{i-1/2}^n\right) - \frac{\Delta t}{\Delta x}\mathcal{R}_i^n, \tag{2.5.8}$$

where $\mathcal{R}_i^n$ is an approximation of the non-conservative terms at $x = x_i, t = n$.

[8] This approximation is used in the numerical methods presented in Chapter 3 and 4. The approximation in Chapter 5 is different, since in this Chapter the model is split into submodels covering the different physical phenomena.

2.5.1 Spatial accuracy

The spatial accuracy of the numerical method is determined by the spatial reconstruction of the variables at the cell boundaries. The simplest way for this reconstruction, leading to first order spatial accuracy, is to take

$$\begin{aligned} \mathbf{W}_{i-1/2} &= \mathbf{W}_i, \\ \mathbf{W}_{i+1/2} &= \mathbf{W}_{i+1}. \end{aligned} \tag{2.5.9}$$

Positive, higher order accuracy can be obtained by using the concept of flux limiters. The idea is to limit the spatial derivatives to physically realizable values. The flux limiters only operate when dealing with sharp wave fronts. For each boundary cell we introduce a left and a right state, see Figure 2.6.

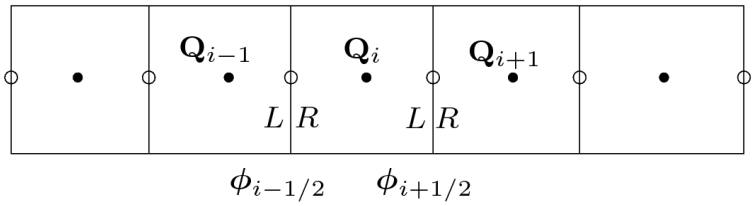

Figure 2.6: The left and right states on a finite volume mesh consisting of the control volumes.

The spatial reconstruction when using flux limiters is given by:

$$\begin{aligned} w^R_{i-1/2} &= w_i + \frac{1}{2}\varphi\left(r^R_i\right)(w_i - w_{i+1}), \quad r^R_i = \frac{w_i - w_{i-1}}{w_{i+1} - w_i}, \\ w^L_{i+1/2} &= w_i + \frac{1}{2}\varphi\left(r^L_i\right)(w_i - w_{i-1}), \quad r^L_i = \frac{w_{i+1} - w_i}{w_i - w_{i-1}}, \end{aligned} \tag{2.5.10}$$

for all components w of the primitive variables $\mathbf{W}$. The value r_i is an approximation for the slope; it is the ratio of successive gradients on the solution mesh. In this thesis we use the flux limiter of Koren [20]:

$$\varphi(r) = \max\left(0, \min\left(2r, \frac{1}{3} + \frac{2}{3}r, 2\right)\right). \tag{2.5.11}$$

This limiter is not differentiable. When $\varphi(r) = 1/3 + 2r/3$ it provides third order accuracy [20].

2.5.2 Stability

When using explicit schemes, one has to consider the numerical stability of the scheme. A numerical method is said to be stable if the total variation of the numerical solution at a fixed time remains bounded as the time step size goes towards zero. Here, the numerical stability is determined by the Courant-Friedrichs-Lewy (CFL) number. The CFL number is defined as

$$\mathcal{C} = \frac{\Delta t}{\Delta x}\max\left(|u| + c\right). \tag{2.5.12}$$

The CFL number describes the ratio of the distance covered in time step Δt and the grid size. Without limiter the stability condition reads

$$\mathcal{C} < 1, \tag{2.5.13}$$

i.e. a grid cell can not be skipped. When dealing with two successive Riemann problems at the same cell, the stricter CFL restriction holds [9]:

$$\mathcal{C} < 1/2, \tag{2.5.14}$$

see Chapter 5. In the problems we have encountered, we use the limit (2.5.13). When using a flux limiter in the spatial reconstruction, the requirement on the time step is stricter; the positivity requirement for forward Euler is (2.5.14).

2.5.3 Boundary conditions

All the test cases that are considered are so-called *shock tube problems*. See Chapter 6 for more details on shock tube problems. In the simulations we consider a finite length shock tube and take at the boundaries the values of the neighbouring cells. However, this is not important since the test cases are selected such that the waves do not reach the boundary of the computational domain during the computation. Therefore, at the boundaries nothing should happen during the calculations.

3

An Osher-type solver for the five-equation model

In this Chapter we present an Osher-type solver for Kapila's model. This Osher-type solver is very similar to the one of Kreeft and Koren [22]. However, applying this approach to the model of Kapila et al. [18] is new. This is the first new work of this Thesis. For the treatment of the non-conservative terms we also use the approach presented in [22]. The motivation for this Chapter is as follows: As Kapila's model only contains a single non-conservative product, the integration of the non-conservative part is less involved than for the model of Kreeft and Koren.
This Chapter is organised as follows. First, we derive the Riemann Solver of Osher in Section 3.1. Next, we present the results of applying this solver to the conservative part of Kapila's model in Section 3.2. Finally, the integration of the non-conservative term is presented in Section 3.3.

3.1 Derivation Riemann solver of Osher

In this Section we present the main ideas and derivation of the approximate Riemann solver of Osher [28]. This derivation is partly based on the book of Toro [32].
Let us consider the system of m conservation laws:

$$\partial_t \mathbf{Q} + \partial_x \mathcal{F}(\mathbf{Q}) = 0 \tag{3.1.1}$$

with conservative scheme (see also the previous Chapter)

$$\mathbf{Q}_i^{n+1} = \mathbf{Q}_i^n - \frac{\Delta t}{\Delta x}\left[\boldsymbol{\phi}_{i+1/2}^n - \boldsymbol{\phi}_{i-1/2}^n\right]. \tag{3.1.2}$$

The objective is to determine an expression for the numerical flux vector $\boldsymbol{\phi}_{i+1/2}^n$. The system of conservation laws (3.1.1) is assumed to be strictly hyperbolic with eigenvalues

$$\lambda_1(\mathbf{Q}) < \lambda_2(\mathbf{Q}) < \cdots < \lambda_m(\mathbf{Q}), \tag{3.1.3}$$

and corresponding eigenvectors

$$\mathbf{r}_1(\mathbf{Q}), \ldots, \mathbf{r}_m(\mathbf{Q}). \tag{3.1.4}$$

The Jacobian matrix

$$\mathbf{A}(\mathbf{Q}) = \partial\mathcal{F}/\partial\mathbf{Q}, \tag{3.1.5}$$

can be diagonalized as

$$\mathbf{A}(\mathbf{Q}) = \mathbf{R}(\mathbf{Q})\mathbf{\Lambda}(\mathbf{Q})\mathbf{R}^{-1}(\mathbf{Q}), \tag{3.1.6}$$

where the matrix $\mathbf{R}(\mathbf{Q})$ is a non-singular matrix with the right eigenvectors as its columns

$$\mathbf{R}(\mathbf{Q}) = [\mathbf{r}_1(\mathbf{Q}), \ldots \mathbf{r}_m(\mathbf{Q})] \tag{3.1.7}$$

and $\mathbf{\Lambda}(\mathbf{Q}) = \mathrm{diag}(\lambda_1(\mathbf{Q}), \ldots, \lambda_m(\mathbf{Q}))$.

Splitting of the flux

The idea of Osher is to split the flux into two parts: (i) A part corresponding to the positive eigenvalues and (ii) a part corresponding to the negative eigenvalues. This is done as follows. Introduce the notation for the positive and negative part of the eigenvalues:

$$\lambda_i^+(\mathbf{Q}) = \max(\lambda_i(\mathbf{Q}), 0), \quad \lambda_i^-(\mathbf{Q}) = \min(\lambda_i(\mathbf{Q}), 0), \tag{3.1.8}$$

with corresponding diagonal matrices $\mathbf{\Lambda}^+(\mathbf{Q})$ and $\mathbf{\Lambda}^-(\mathbf{Q})$:

$$\mathbf{\Lambda}(\mathbf{Q}) = \mathbf{\Lambda}^+(\mathbf{Q}) + \mathbf{\Lambda}^-(\mathbf{Q}). \tag{3.1.9}$$

Using the notation

$$\mathbf{A}^+(\mathbf{Q}) = \mathbf{R}(\mathbf{Q})\mathbf{\Lambda}^+(\mathbf{Q})\mathbf{R}^{-1}(\mathbf{Q}), \tag{3.1.10a}$$
$$\mathbf{A}^-(\mathbf{Q}) = \mathbf{R}(\mathbf{Q})\mathbf{\Lambda}^-(\mathbf{Q})\mathbf{R}^{-1}(\mathbf{Q}). \tag{3.1.10b}$$

the Jacobian matrix can be split as:

$$\mathbf{A}(\mathbf{Q}) = \mathbf{A}^+(\mathbf{Q}) + \mathbf{A}^-(\mathbf{Q}), \tag{3.1.11}$$

where $\mathbf{A}^+(\mathbf{Q})$ has nonnegative eigenvalues and $\mathbf{A}^-(\mathbf{Q})$ has nonpositive eigenvalues. Osher now assumes that the matrices $\mathbf{A}^+$ and $\mathbf{A}^-$ are also Jacobian matrices, i.e. there exist flux vectors $\mathcal{F}^+$ and $\mathcal{F}^-$ such that

$$\mathcal{F}(\mathbf{Q}) = \mathcal{F}^+(\mathbf{Q}) + \mathcal{F}^-(\mathbf{Q}), \tag{3.1.12a}$$
$$\mathbf{A}^+(\mathbf{Q}) = \partial\mathcal{F}^+/\partial\mathbf{Q}, \tag{3.1.12b}$$
$$\mathbf{A}^-(\mathbf{Q}) = \partial\mathcal{F}^-/\partial\mathbf{Q}. \tag{3.1.12c}$$

Osher's numerical flux

Using the initial data of the Riemann problem for the conservation laws (3.1.1) denoted by

$$\mathbf{Q}_0 \equiv \mathbf{Q}_L = \mathbf{Q}_i^n, \tag{3.1.13a}$$
$$\mathbf{Q}_1 \equiv \mathbf{Q}_R = \mathbf{Q}_{i+1}^n, \tag{3.1.13b}$$

and a single wave (see Chapter 2), the numerical flux can be written as

$$\boldsymbol{\phi}_{i+1/2} = \mathcal{F}^+(\mathbf{Q}_0) + \mathcal{F}^-(\mathbf{Q}_1). \tag{3.1.14}$$

For a derivation of (3.1.14) we refer to [33, 28]. By using (3.1.10)-(3.1.14) the numerical flux can be cast into three different forms

$$\boldsymbol{\phi}_{i+1/2} = \mathcal{F}(\mathbf{Q}_0) + \int_{\mathbf{Q}_0}^{\mathbf{Q}_1} \mathbf{A}^-(\mathbf{Q})\mathrm{d}(\mathbf{Q}), \tag{3.1.15a}$$
$$\boldsymbol{\phi}_{i+1/2} = \mathcal{F}(\mathbf{Q}_1) - \int_{\mathbf{Q}_0}^{\mathbf{Q}_1} \mathbf{A}^+(\mathbf{Q})\mathrm{d}(\mathbf{Q}), \tag{3.1.15b}$$
$$\boldsymbol{\phi}_{i+1/2} = \frac{1}{2}\left(\mathcal{F}(\mathbf{Q}_0) + \mathcal{F}(\mathbf{Q}_1)\right) - \frac{1}{2}\int_{\mathbf{Q}_0}^{\mathbf{Q}_1} |\mathbf{A}(\mathbf{Q})|\mathrm{d}(\mathbf{Q}). \tag{3.1.15c}$$

These fluxes are very similar to the Godunov flux for linear systems and the Roe fluxes [32]. In Godunov's method for linear systems the Godunov flux reads

$$\boldsymbol{\phi}_{i+1/2}^{\text{Godu}} = \frac{1}{2}\left(\mathcal{F}(\mathbf{Q}_0) + \mathcal{F}(\mathbf{Q}_1)\right) - \frac{1}{2}|\mathbf{A}|\left(\mathbf{Q}_1 - \mathbf{Q}_0\right), \tag{3.1.16}$$

where $\mathcal{F}(\mathbf{Q}) = \mathbf{A}\mathbf{Q}$. In Roe's approach the Jacobian matrix is replaced by a constant Jacobian matrix depending on $\mathbf{Q}_L, \mathbf{Q}_R$:

$$\tilde{\mathbf{A}} = \tilde{\mathbf{A}}\left(\mathbf{Q}_L, \mathbf{Q}_R\right). \tag{3.1.17}$$

Also the Roe's numerical flux can be expressed into three different forms:

$$\tilde{\boldsymbol{\phi}}_{i+1/2} = \mathcal{F}(\mathbf{Q}_0) + \sum_{\tilde{\lambda}_i \geq 0} \tilde{\alpha}_i \tilde{\lambda}_i \tilde{\mathbf{r}}_i, \tag{3.1.18a}$$
$$\tilde{\boldsymbol{\phi}}_{i+1/2} = \mathcal{F}(\mathbf{Q}_1) - \sum_{\tilde{\lambda}_i \leq 0} \tilde{\alpha}_i \tilde{\lambda}_i \tilde{\mathbf{r}}_i, \tag{3.1.18b}$$
$$\tilde{\boldsymbol{\phi}}_{i+1/2} = \frac{1}{2}\left(\mathcal{F}(\mathbf{Q}_0) + \mathcal{F}(\mathbf{Q}_1)\right) - \frac{1}{2}\sum_{i=1}^{m} \tilde{\alpha}_i |\tilde{\lambda}_i| \tilde{\mathbf{r}}_i, \tag{3.1.18c}$$

where the same notation as above with a $\sim$ is used to distinguish between Osher and Roe. Furthermore the variables $\tilde{\alpha}_i = \tilde{\alpha}_i\left(\mathbf{Q}_L, \mathbf{Q}_R\right)$ are called the wave strengths, which we do not specify here.

In general, the evaluation of the integrals in (3.1.15) depends on the integration path chosen. Osher's approach is to select integration paths which make the integration tractable.

Suppose the states $\mathbf{Q}_L$ and $\mathbf{Q}_R$ are connected by m waves, see Chapter 2. We choose a set of partial integration paths $\{\mathbf{I}_k(\mathbf{Q})\}, k = 1, \dots m$ such that $\mathbf{I}_k$ is tangential to $\mathbf{r}_k(\mathbf{Q})$ and each two successive paths $\mathbf{I}_k$ and $\mathbf{I}_{k+1}$ intersect at a single point

$$\mathbf{Q}_{k/m} = \mathbf{I}_k \cap \mathbf{I}_{k+1}. \tag{3.1.19}$$

The initial data of the Riemann problem can be interpreted as

$$\mathbf{Q}_0 \equiv \mathbf{Q}_{(k-1)/m}, \quad \mathbf{Q}_1 \equiv \mathbf{Q}_{k/m}. \tag{3.1.20}$$

The total integration path is found by taking the union of all partial integration paths, i.e.

$$\mathbf{I}(\mathbf{Q}) = \bigcup_{k=1}^{m} \mathbf{I}_k. \tag{3.1.21}$$

Suppose the partial integration paths are parameterized by $\mathbf{Q}(\xi)$, then we have

$$\frac{\mathrm{d}\mathbf{Q}(\xi)}{\mathrm{d}\xi} = \mathbf{r}_k(\mathbf{Q}(\xi)) \quad \text{for} \quad \xi_k \leq \xi \leq \xi_{k+1}. \tag{3.1.22}$$

To order the integration paths, two different possibilities have been proposed. These are (i) the *original* Osher ordering, in short *O-ordering* and (ii) the *physical* ordering, or in short *P-ordering*. The first one was originally introduced by Osher [28], while the second one was proposed by Hemker and Spekreijse [14]. In the P-ordering the ordering of the integration paths is according to increasing eigenvalues, while the O-ordering is inverted.

We choose to evaluate the first integral (3.1.15a). By performing a change of variables, we have

$$\begin{aligned} \int_{\mathbf{I}_k} \mathbf{A}^-(\mathbf{Q})\mathrm{d}(\mathbf{Q}) &= \int_{\xi_k}^{\xi_{k+1}} \mathbf{A}^-(\mathbf{Q}(\xi)) \frac{\mathrm{d}\mathbf{Q}(\xi)}{\mathrm{d}\xi}\mathrm{d}\xi \\ &= \int_{\xi_k}^{\xi_{k+1}} \mathbf{A}^-(\mathbf{Q}(\xi))\, \mathbf{r}_k(\mathbf{Q}(\xi))\, \mathrm{d}\xi \\ &= \int_{\xi_k}^{\xi_{k+1}} \lambda_k^- \mathbf{r}_k(\mathbf{Q}(\xi))\, \mathrm{d}\xi. \end{aligned} \tag{3.1.23}$$

Note that for positive eigenvalues the integral in (3.1.23) vanishes. Therefore, we now distinguish several cases regarding the eigenvalues. Suppose that the eigenvalues are either linearly degenerate or genuinely nonlinear, for the definitions see Chapter 2. Let us first consider the linearly degenerate case. A rewriting as

$$\frac{\mathrm{d}\lambda_k}{\mathrm{d}\xi}(\mathbf{Q}(\xi)) = \nabla\lambda_k(\mathbf{Q}) \cdot \frac{\mathrm{d}\mathbf{Q}(\xi)}{\mathrm{d}\xi} = \nabla\lambda_k(\mathbf{Q}) \cdot \mathbf{r}_k(\mathbf{Q}) = \mathbf{0}, \tag{3.1.24}$$

reveals that λ_k is constant along I_k for the linearly degenerate case. As for positive λ_k the integral in (3.1.23) vanishes, consider now $\lambda_k < 0$. This means that

$$\int_{\mathbf{I}_k} \mathbf{A}^-(\mathbf{Q})\mathrm{d}(\mathbf{Q}) = \int_{\xi_k}^{\xi_{k+1}} \frac{\mathrm{d}\mathcal{F}}{\mathrm{d}\mathbf{Q}} \frac{\mathrm{d}\mathbf{Q}}{\mathrm{d}\xi}\mathrm{d}\xi = \mathcal{F}(\mathbf{Q}(\xi_{k+1})) - \mathcal{F}(\mathbf{Q}(\xi_k)). \tag{3.1.25}$$

The numerical flux of path I_k can now be written as, by substituting the integral into (3.1.15a)):

$$(\boldsymbol{\phi}_{i+1/2})_{I_k} = \begin{cases} \mathcal{F}(\mathbf{Q}_k) & \text{if} \quad \lambda_k \geq 0, \\ \mathcal{F}(\mathbf{Q}_{k+1}) & \text{if} \quad \lambda_k < 0. \end{cases} \tag{3.1.26}$$

where $\mathbf{Q}_k = \mathbf{Q}(\xi_k)$. When λ_k is genuinely nonlinear (3.1.24) reveals that λ_k is strictly monotonic along I_k, i.e. it changes sign at most once. If λ_k appears not to change sign, we are back in the linearly degenerate case. Suppose λ_k changes sign at $\xi = \xi_s$. We can now consider two different cases, either λ_k turns from positive to negative at $\xi = \xi_s$ or vice versa. In both cases in the evaluation of the integral the integration path should be split. A computation of the integrals and collecting all the results leads to the Osher's Numerical flux:

$$(\boldsymbol{\phi}_{i+1/2})_{I_k} = \begin{cases} \mathcal{F}(\mathbf{Q}_k) & \text{if} \quad \lambda_k \geq 0, \\ \mathcal{F}(\mathbf{Q}_{k+1}) & \text{if} \quad \lambda_k \leq 0, \\ \mathcal{F}(\mathbf{Q}_k) + \mathcal{F}(\mathbf{Q}_{k+1}) - \mathcal{F}(\mathbf{Q}_s) & \text{if} \quad \lambda_k(\mathbf{Q}_k) \geq 0, \lambda_k(\mathbf{Q}_s) = 0, \\ & \qquad \lambda_k(\mathbf{Q}_{k+1}) \leq 0, \\ \mathcal{F}(\mathbf{Q}_s) & \text{if} \quad \lambda_k(\mathbf{Q}_k) \leq 0, \lambda_k(\mathbf{Q}_s) = 0, \\ & \qquad \lambda_k(\mathbf{Q}_{k+1}) \geq 0, \end{cases} \tag{3.1.27}$$

where $\mathbf{Q}_s = \mathbf{Q}(\xi_s)$ is called a *sonic point*.

3.2 Osher's fluxes for the five-equation two-phase flow model

Here we discuss the Osher's fluxes for the five-equation model. This has already been done for Kreeft and Koren's model but is new for Kapila's model. The actual flux for the two different five equation models differs in the last component, since the first four equations are the same. However, the approach of determining Osher's numerical flux is for both five-equation models the same.
For the fifth equation of Kapila's model, we take formulation

$$\partial_t \alpha_1 + \partial_x(\alpha_1 u) = (\alpha_1 - \phi)\partial_x u, \tag{3.2.1}$$

with the non-conservative term $(\alpha_1 - \phi)\partial_x u$. The integration path for the five-equation model consists of three subpaths corresponding to the wave speeds $\lambda_1, \lambda_{2,3,4}$ and λ_5. The wave speed $\lambda_1 = \lambda_1(\xi)$ changes sign at $\lambda_1((\xi_s)_L) = 0$ and $\lambda_5 = \lambda_5(\xi)$ at $\lambda_5((\xi_s)_R) = 0$. The corresponding two sonic points are denoted as $(\mathbf{Q}_s)_L$ and $(\mathbf{Q}_s)_R$ respectively. Furthermore, we denote $\mathcal{F}_k = \mathcal{F}(\mathbf{Q}_k)$ with $k = 1, ..., 5$ and $\mathcal{F}_{Q_K} = \mathcal{F}((\mathbf{Q}_s)_K)$ with $K = L, R$. We show the integration path for the five-equation model in Figure 3.1.
To obtain the numerical flux of Osher one has to examine the sign of the wave speeds at the different subpaths. The wave speeds at the different points are $u_1 - c, u_2 - c, u_{2,3,4}, u_4 + c, u_5 + c$, where the subscript refers to the number of the point. This leads to $2^5 = 32$ different cases. A closer examination reveals that fortunately only 16 cases are actually possible. For instance, the case in which $u_{2,3,4} \leq 0$ and $u_2 - c \geq 0$ is a contradictory case. The realisable cases are shown in Table 3.1. Here we introduce the notation $\mu_1 = u_1 - c, \mu_5 = u_5 - c$ to reduce the size of the Table. The question now remains how to determine the intersection and sonic points (at which the sign of the eigenvalue changes). To do so, Generalized Riemann Invariants are used. Since this is the same as for the new formulation of the five-equation model, we refer to [21] for details.

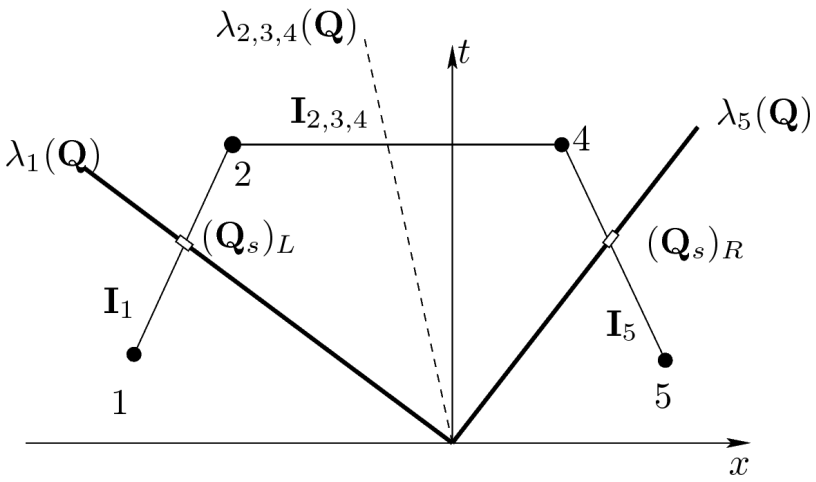

Figure 3.1: Integration path

	$\mu_1 \geq 0, \mu_5 \geq 0$	$\mu_1 \geq 0, \mu_5 \leq 0$	$\mu_1 \leq 0, \mu_5 \geq 0$	$\mu_1 \leq 0, \mu_5 \leq 0$
$u_{2,3,4} \geq 0, u_2 - c \geq 0$	$\mathcal{F}_1$	$\mathcal{F}_1 - \mathcal{F}_{Q_R} + \mathcal{F}_5$	$\mathcal{F}_{Q_L}$	$\mathcal{F}_{Q_L} - \mathcal{F}_{Q_R} + \mathcal{F}_5$
$u_{2,3,4} \geq 0, u_2 - c \leq 0$	$\mathcal{F}_1 - \mathcal{F}_{Q_L} + \mathcal{F}_2$	$\mathcal{F}_1 + \mathcal{F}_{Q_L} + \mathcal{F}_2 - \mathcal{F}_{Q_R} + \mathcal{F}_5$	$\mathcal{F}_2$	$\mathcal{F}_2 - \mathcal{F}_{Q_R} + \mathcal{F}_5$
$u_{2,3,4} \leq 0, u_4 + c \geq 0$	$\mathcal{F}_1 - \mathcal{F}_{Q_L} + \mathcal{F}_4$	$\mathcal{F}_1 - \mathcal{F}_{Q_L} + \mathcal{F}_4 - \mathcal{F}_{Q_R} + \mathcal{F}_5$	$\mathcal{F}_5$	$\mathcal{F}_4 - \mathcal{F}_{Q_R} + \mathcal{F}_5$
$u_{2,3,4} \leq 0, u_4 + c \leq 0$	$\mathcal{F}_1 - \mathcal{F}_{Q_L} + \mathcal{F}_R$	$\mathcal{F}_1 - \mathcal{F}_{Q_L} + \mathcal{F}_5$	$\mathcal{F}_{Q_R}$	$\mathcal{F}_5$

Table 3.1: Numerical flux Osher table.

3.3 Integration of the non-conservative term Kapila's of model

In this Section we discuss the treatment of the non-conservative part

$$\int_\Omega (\alpha_1 - \phi)\partial_x u \mathrm{d}x \tag{3.3.1}$$

of the equation, which is new for Kapila's model. We choose to apply the approach of Kreeft and Koren to our non-conservative term. We will only present the key ideas and main results, for more details on this approach we refer to the paper of Kreeft and Koren.

The integration of non-conservative part (3.3.1) over a finite volume consists of two parts: (i) a part linked to continuous solution in the cell interior and (ii) a part linked to the discontinuous solution over the cell faces. This is illustrated in Figure 3.2. We split the integration at the cell faces from the integration in the cell interior. Since the non-conservative term is not Riemann integrable at the cell faces, this integration is done in the solution space. The partitioning of (3.3.1) results in

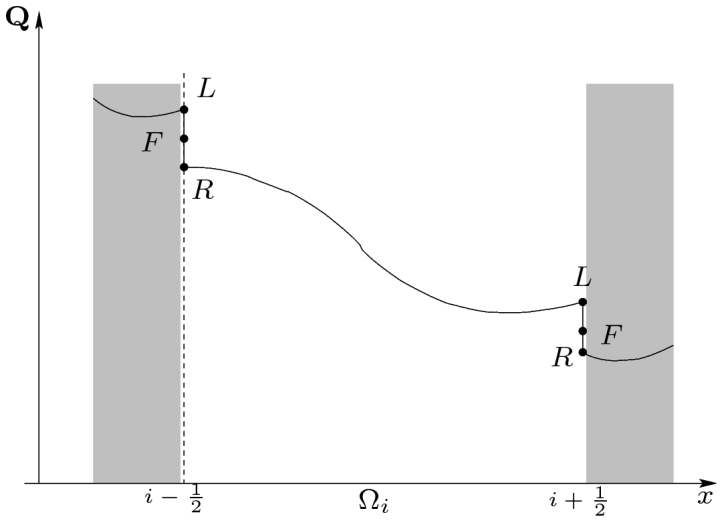

Figure 3.2: Distribution of a solution in and around finite volume Ω_i.

(with an abuse of notation for the first and third integral following Kreeft and Koren [22]):

$$\int_{\Omega_i}(\alpha_1-\phi)\partial_x u\mathrm{d}x=\int_{\mathbf{Q}^F_{i-1/2}}^{\mathbf{Q}^R_{i-1/2}}(\alpha_1-\phi)\mathrm{d}\mathbf{Q}+\int_{x_{i-1/2}}^{x_{i+1/2}}(\alpha_1-\phi)\partial_x u\mathrm{d}x+\int_{\mathbf{Q}^L_{i+1/2}}^{\mathbf{Q}^F_{i+1/2}}(\alpha_1-\phi)\mathrm{d}\mathbf{Q}. \tag{3.3.2}$$

Integration in cell interior

To evaluate the second integral in (3.3.2) a finite volume approximation has to be used. When using a first order approximation the integral would vanish. We choose to use a second order approximation in which the functions are assumed to be piecewise linear, as is visualized in Figure 3.3.
This means that the functions u,α,ϕ are of the form (for the right side of the cell, the left side is similar):

$$f(x)=f(x_i)+(f(x_{i+1/2})-f(x_i))\frac{x-x_i}{x_{i+1/2}-x}. \tag{3.3.3}$$

The integration results in

$$\begin{aligned}\int_{x_{i-1/2}}^{x_{i+1/2}}(\alpha_1-\phi)\partial_x u\mathrm{d}x=&\int_{x_{i-1/2}}^{x_i}(\alpha_1-\phi)\partial_x u\mathrm{d}x+\int_{x_i}^{x_{i+1/2}}(\alpha_1-\phi)\partial_x u\mathrm{d}x\\ \doteq&\ \tfrac{1}{2}\left[(\alpha_1)_{i-1/2}-\phi_{i-1/2}+(\alpha_1)_i-\phi_i\right](u_i-u_{i-1/2})\\ &+\tfrac{1}{2}\left[(\alpha_1)_i-\phi_i+(\alpha_1)_{i+1/2}-\phi_{i+1/2}\right](u_{i+1/2}-u_i).\end{aligned} \tag{3.3.4}$$

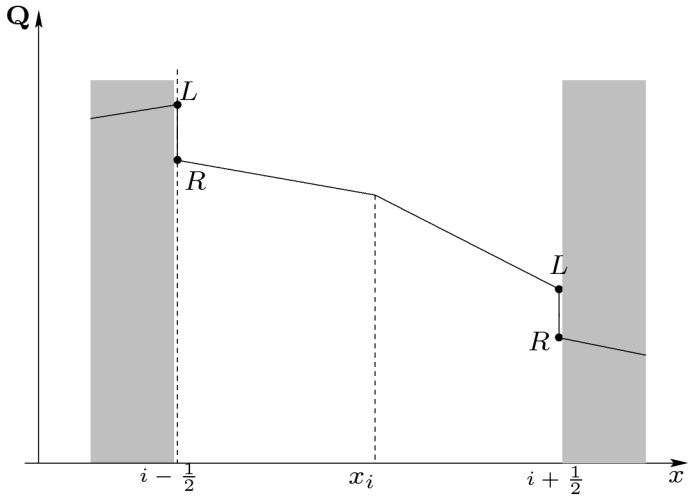

Figure 3.3: Piecewise linear solution in cell interior.

Integration at cell faces

In correspondence to the Osher solver for the conservative part, we use a P-variant ordering of the wave paths. The wave paths are the same as in [22], see Figure 3.4, however one has to keep in mind that the solution space $\mathbf{Q}$ is different from the solution space in [22]. The intermediate states at the intersection points of the wave paths are denoted by Q^{LM}, Q^{RM}, see Figure 3.4.

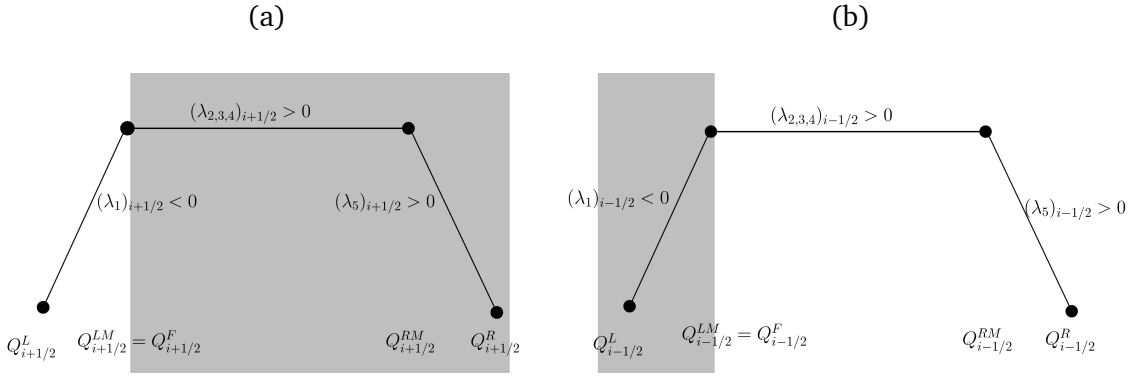

Figure 3.4: Cell faces (a) $i-1/2$ and (b) $i+1/2$

For the integration parameter we choose to take the velocity u. For this choice we have the following reasons:

1. It is in correspondence with Kreeft & Koren [22].
2. The integrand simplifies.
3. No Riemann Invariants have to be used in the integrand. This is in contrast to the model of Kreeft & Koren.

The first and third integral in (3.3.2) can be written as

$$\int_{u_{i-1/2}^F}^{u_{i-1/2}^R}(\alpha_1-\phi)\mathrm{d}u, \tag{3.3.5a}$$

$$\int_{u_{i+1/2}^L}^{u_{i+1/2}^F}(\alpha_1-\phi)\mathrm{d}u, \tag{3.3.5b}$$

respectively. Next, we split the first integral again, according to the wave configuration, into

$$\int_{u_{i-1/2}^F}^{u_{i-1/2}^R}(\alpha_1-\phi)\mathrm{d}u=\int_{u_{i-1/2}^F}^{u_{i-1/2}^{RM}}(\alpha_1-\phi)\mathrm{d}u+\int_{u_{i-1/2}^{RM}}^{u_{i-1/2}^R}(\alpha_1-\phi)\mathrm{d}u. \tag{3.3.6}$$

Note that the first integral in (3.3.6) vanishes since the velocity is constant across the middle subpath. The corresponding integral in the model of Kreeft and Koren does not entirely vanish. This is due to the fact that the term $\mathrm{d}\alpha_1/\mathrm{d}u$ appears in that integral and the volume fraction is not constant across the middle wave. We are left with the integrals

$$\int_{u_{i-1/2}^{RM}}^{u_{i-1/2}^R}(\alpha_1-\phi)\mathrm{d}u, \tag{3.3.7a}$$

$$\int_{u_{i+1/2}^L}^{u_{i+1/2}^F}(\alpha_1-\phi)\mathrm{d}u, \tag{3.3.7b}$$

for which Simpson's 3/8 rule is used in the calculation.

4

An HLLC-type solver for the five-equation model

In this Chapter we present an HLLC-type solver for the two-phase flow model. The original HLLC scheme, developed by E. F. Toro et al. [33], is an extension of the HLL (referring to the developers) scheme proposed by Harten, Lax and van Leer [13]. In both schemes an approximation for the intercell numerical flux is obtained directly. This leads to relatively simple and fast approximate Riemann solvers. The main idea of the schemes is to assume a wave configuration of the solution and to use integral relations of the Riemann Problem.
An HLLC-type solver for the conservative terms of the models is derived. It is important to note that the HLLC-type scheme for Kapila's model is not new; it has been developed by F. Daude et al. in [11]. However, as the derivation of the scheme for the model of Kreeft and Koren, which is new, uses the HLLC-type scheme for Kapila's model, we have chosen to present both here. The non-conservative part is treated differently for the two models. On the one hand we use an HLLC-type approach in Kapila's model, while on the other hand we use an Osher-type approach for the Kreeft and Koren model.
This Chapter is organized as follows. First, in Section 4.1 we present the derivation of the HLLC scheme, based on [33]. Next, in Section 4.2 we apply the HLLC-scheme to both five-equation models. Finally, in Section 4.3 we present the treatment of the non-conservative terms. We postpone the numerical simulations to Chapter 6.

4.1 Derivation HLLC approximate Riemann Solver

In this Section we briefly present the derivation of the HLLC-type scheme[1]. The HLLC scheme proposed by Toro as an extension of the HLL scheme is a method to compute an approximation to the flux *directly*. In the HLLC scheme the missing contact wave is restored. The 'C' of HLLC stands for Contact, referring to the extra contact wave. Therefore, in contrast to the approximate Riemann solver of Osher, no Riemann Invariants have to be used. In the HLLC approximate Riemann

[1]This derivation assumes that the considered model consists of three different waves, which holds for both the Euler equations of gas dynamics and the five-equation model. This approach can easily be generalized for models consisting of more waves, for e.g. the seven equation model.

solver we assume that the solution consists of different states separated according to the wave configuration of the equations. The states are separated by the signal waves $\mathcal{S}$. The slowest and fastest signal waves, present in both the HLL scheme as well as in the HLLC scheme, are denoted with $\mathcal{S}_L$ and $\mathcal{S}_R$ respectively. The additional middle wave of the HLLC scheme is denoted by $\mathcal{S}_M$. We specify the choice of these signal waves later. The three waves separate the solution into four states. More precisely, the HLLC approximate Riemann Solver proposed by Toro [33] is given by [2]

$$\tilde{\mathbf{Q}}(x,t) = \begin{cases} \mathbf{Q}_L & \text{if} \quad x/t \leq \mathcal{S}_L, \\ \mathbf{Q}_L^* & \text{if} \quad \mathcal{S}_L \leq x/t < \mathcal{S}_M, \\ \mathbf{Q}_R^* & \text{if} \quad \mathcal{S}_M \leq x/t < \mathcal{S}_R, \\ \mathbf{Q}_R & \text{if} \quad \mathcal{S}_R \leq x/t, \end{cases} \tag{4.1.1}$$

see Figure 4.1. The middle two states are referred to as the *star region*.

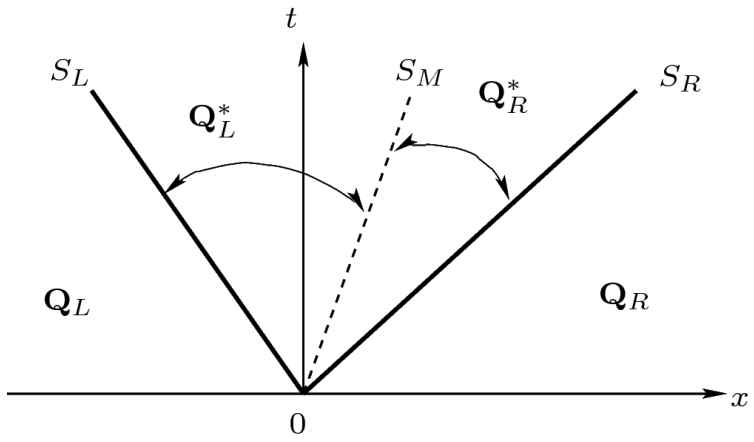

Figure 4.1: HLLC Riemann Solver

Let us consider a control volume $[x_L, x_R] \times [0, T]$ as in Figure 4.2 in which the entire wave structure of the Riemann problem is shown. Here, $T > 0$ is a fixed time. The integral form of the conservation law (2.5.1) in the control volume reads

$$\int_{x_L}^{x_R} \mathbf{Q}(x,T)\mathrm{d}x = \int_{x_L}^{x_R} \mathbf{Q}(x,0)\mathrm{d}x + \int_0^T \mathcal{F}(\mathbf{Q}(x_L,t))\mathrm{d}t - \int_0^T \mathcal{F}(\mathbf{Q}(x_R,t))\mathrm{d}t, \tag{4.1.2}$$

which is evaluated as

$$\int_{x_L}^{x_R} \mathbf{Q}(x,T)\mathrm{d}x \doteq x_R\mathbf{Q}_R - x_L\mathbf{Q}_L + T(\mathcal{F}_L - \mathcal{F}_R), \tag{4.1.3}$$

[2] In the original HLL scheme the middle wave $\mathcal{S}_M$ is not present. In the star region the approximate HLL Riemann solver is given by $\mathbf{Q}^{HLL}$.

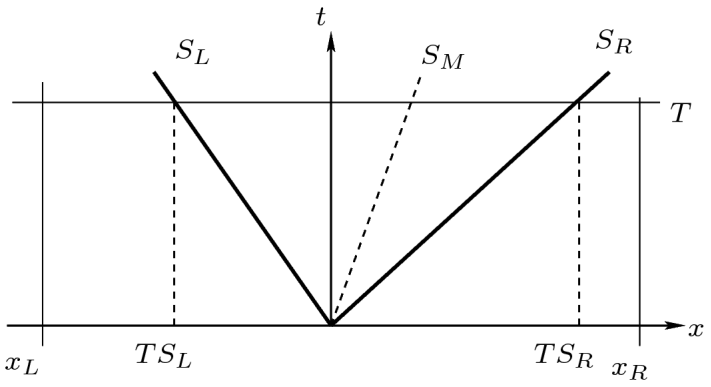

Figure 4.2: Control volume

with $\mathcal{F}_K = \mathcal{F}(\mathbf{Q}_K), K = L, R$. On the other hand, splitting of the integration domain (into $[x_L, T\mathcal{S}_L], [T\mathcal{S}_L, T\mathcal{S}_R]$ and $[T\mathcal{S}_R, x_R]$) leads to

$$\int_{x_L}^{x_R} \mathbf{Q}(x,T)\mathrm{d}x = (T\mathcal{S}_L - x_L)\mathbf{Q}_L + \int_{T\mathcal{S}_L}^{T\mathcal{S}_R} \mathbf{Q}(x,T)\mathrm{d}x + (x_R - T\mathcal{S}_R)\mathbf{Q}_R. \tag{4.1.4}$$

Combining of (4.1.3) and (4.1.4) we obtain the expression

$$\frac{1}{T(\mathcal{S}_R - \mathcal{S}_L)} \int_{T\mathcal{S}_L}^{T\mathcal{S}_R} \mathbf{Q}(x,T)\mathrm{d}x = \frac{\mathcal{S}_R\mathbf{Q}_R - \mathcal{S}_L\mathbf{Q}_L + \mathcal{F}_L - \mathcal{F}_R}{\mathcal{S}_R - \mathcal{S}_L} \equiv \mathbf{Q}^{HLL}. \tag{4.1.5}$$

Splitting the integration in the integral in Eq. (4.1.5) gives

$$\frac{\mathcal{S}_M - \mathcal{S}_L}{\mathcal{S}_R - \mathcal{S}_L}\mathbf{Q}_{*,L} + \frac{\mathcal{S}_R - \mathcal{S}_M}{\mathcal{S}_R - \mathcal{S}_L}\mathbf{Q}_{*,R} = \mathbf{Q}^{HLL}, \tag{4.1.6}$$

with

$$\mathbf{Q}_{*,L} = \frac{1}{T(\mathcal{S}_M - \mathcal{S}_L)} \int_{T\mathcal{S}_L}^{T\mathcal{S}_M} \mathbf{Q}(x,T)\mathrm{d}x, \tag{4.1.7a}$$

$$\mathbf{Q}_{*,R} = \frac{1}{T(\mathcal{S}_R - \mathcal{S}_M)} \int_{T\mathcal{S}_M}^{T\mathcal{S}_R} \mathbf{Q}(x,T)\mathrm{d}x \tag{4.1.7b}$$

which is referred to as the *Consistency condition*. To determine the HLLC numerical flux vector, we consider the same four states as in the HLLC approximate Riemann solver (4.1.1), i.e. the flux reads:

$$\phi^{\text{HLLC}} = \begin{cases} \mathcal{F}_L & \text{if} \quad 0 \leq \mathcal{S}_L, \\ \mathcal{F}_L^* & \text{if} \quad \mathcal{S}_L \leq 0 < \mathcal{S}_M, \\ \mathcal{F}_R^* & \text{if} \quad \mathcal{S}_M \leq 0 < \mathcal{S}_R, \\ \mathcal{F}_R & \text{if} \quad \mathcal{S}_R \leq 0. \end{cases} \tag{4.1.8}$$

In contrast to the left and right state ($\mathcal{F}_K = \mathcal{F}(\mathbf{Q}_K), K = L, R$), we do not take for $\mathcal{F}_K^*$ the flux at $\mathbf{Q}_K^*$. The fluxes in the star region are obtained in a similar way as in the derivation of the Consistency condition. By integrating over the control volumes $\mathcal{C}_1, C_2, C_3$ respectively, we obtain, after some rewriting, the relations [3]

$$\mathcal{F}_L^* = \mathcal{F}_L + \mathcal{S}_L \left(\boldsymbol{Q}_L^* - \boldsymbol{Q}_L \right), \qquad \mathcal{C}_1 = [x_L, T\mathcal{S}_M] \times [0, T], \tag{4.1.10a}$$

$$\mathcal{F}_R^* = \mathcal{F}_L^* + \mathcal{S}_M \left(\boldsymbol{Q}_R^* - \boldsymbol{Q}_L^* \right), \qquad \mathcal{C}_2 = [T\mathcal{S}_L, T\mathcal{S}_R] \times [0, T], \tag{4.1.10b}$$

$$\mathcal{F}_R^* = \mathcal{F}_R + \mathcal{S}_R \left(\boldsymbol{Q}_R^* - \boldsymbol{Q}_R \right), \qquad \mathcal{C}_3 = [T\mathcal{S}_M, x_R] \times [0, T]. \tag{4.1.10c}$$

Together with estimates $\mathcal{S}_L, \mathcal{S}_R, \mathcal{S}_M$ for the wave speeds, this concludes the derivation of the HLLC scheme.

4.2 Application to the five-equation model

In this Section we apply the HLLC scheme to the five-equation model (both formulations). We consider only the conservative part of the model, the non-conservative part of the model is treated in the next Section.
As mentioned in the previous Section, the HLLC scheme is directly applicable to the five-equation model since the model consists of three different waves ($\lambda_1 = u - c, \lambda_{2,3,4} = u, \lambda_1 = u + c$), see Chapter 2. The star states are now given by $\boldsymbol{Q}_K^* = (\rho_K^*, (\rho u)_K^*, (\rho E)_K^*, (\alpha_1 \rho_1)_K^*, (Q_5)_K^*)$, with $Q_5 = \alpha_1$, for Kapila's model and $Q_5 = \alpha_1 \rho_1 E_1$ for the model of Kreeft and Koren. The velocity and pressure are both constant along the middle wave, see Chapter 2. Therefore, we impose the conditions

$$u_L^* = u_R^* \equiv u^* \tag{4.2.1a}$$

$$p_L^* = p_R^* \equiv p^*. \tag{4.2.1b}$$

As the middle wave speed $\mathcal{S}_M$ is associated with the eigenvalue $\lambda_{2,3,4}$ we take, in correspondence with Toro [32], $\mathcal{S}_M = u^*$. The speeds $\mathcal{S}_L$ and $\mathcal{S}_R$ corresponding to the fastest waves at each side of the interface can be estimated in several ways. We choose (see next page for explanation) to take the one proposed by Batten et al. [5]:

$$\begin{aligned} \mathcal{S}_L &= \min \left(u_L - c_L, u - c^{Roe} \right), \\ \mathcal{S}_R &= \max \left(u_R + c_R, u + c^{Roe} \right), \end{aligned} \tag{4.2.2}$$

where the Roe average of a quantity $\mathbf{g}$ is given by

$$\mathbf{g}^{Roe} := \frac{\sqrt{\rho_L}\mathbf{g}_L + \sqrt{\rho_R}\mathbf{g}_R}{\sqrt{\rho_L} + \sqrt{\rho_R}}. \tag{4.2.3}$$

[3] In the original HLL scheme these relations are replaced by

$$\mathcal{F}^{HLL} = \mathcal{F}_L + \mathcal{S}_L \left(\boldsymbol{Q}^{HLL} - \boldsymbol{Q}_L \right),$$
$$\mathcal{F}^{HLL} = \mathcal{F}_R + \mathcal{S}_R \left(\boldsymbol{Q}^{HLL} - \boldsymbol{Q}_R \right),$$

and are obtained after integrating over $[x_L, 0] \times [0, T]$ and $[0, x_R] \times [0, T]$ respectively. Alternatively, the relations are obtained by applying the so-called Rankine-Hugoniot condition across each of the waves.

The reason for this choice is the following. In the case of the Euler equations of gas dynamics, the wave speed of a shock wave is given by either $u - \hat{c}$ (left running) or $u + c^{Roe}$ (right running). On the other hand, for an expansion fan the slowest wave speed is $u_L - c_L$ (left running) and the fastest wave speed is $u_R + c_R$ (right running). The estimate of Batten et al. takes both effects into account. We now determine the components of $\mathbf{Q}_K^*$ by using (4.2.1) in the relations (4.1.10). For the bulk mass component of Eq. (4.1.10), this leads to

$$\rho_K^* = \rho_K \frac{\mathcal{S}_K - u_K}{\mathcal{S}_K - \mathcal{S}_M}, \tag{4.2.4}$$

with again $K = L, R$. Next, we find an expression for the pressure values p_K^* by using the momentum component of Eq. (4.1.10) and subsequently a substitution of (4.2.4). This gives

$$p_K^* = p_K + \rho_K(\mathcal{S}_K - u_K)(\mathcal{S}_M - u_K). \tag{4.2.5}$$

After using the condition $p_L^* = p_R^*$, the middle wave speeds $\mathcal{S}_M$ is found to be

$$\mathcal{S}_M = \frac{p_L - p_R + \rho_R u_R\left(\mathcal{S}_R - u_R\right) - \rho_L u_L\left(\mathcal{S}_L - u_L\right)}{\rho_R\left(\mathcal{S}_R - u_R\right) - \rho_L\left(\mathcal{S}_L - u_L\right)}. \tag{4.2.6}$$

For the bulk energy component of Eq. (4.1.10) we obtain, after substitution of (4.2.5),

$$\rho_K^* E_K^* = \rho_K \frac{\mathcal{S}_K - u_K}{\mathcal{S}_K - \mathcal{S}_M}\left[E_K + (\mathcal{S}_M - u_K)\left(\mathcal{S}_M + \frac{p_K}{\rho_K\left(\mathcal{S}_K - u_K\right)}\right)\right]. \tag{4.2.7}$$

These results have already been found by Toro [33]. In a similar fashion, we obtain the remaining fluxes of the single fluid. We get from Eq. (4.1.10) for component of the mass of phase 1:

$$(\alpha_1^*\rho_1^*)_K = (\alpha_1\rho_1)_K \frac{\mathcal{S}_K - u_K}{\mathcal{S}_K - \mathcal{S}_M}. \tag{4.2.8}$$

What remains is to determine the fluxes for the fifth equation of the model. For Kapila's model we follow the approach of Daude et al. [11]. Write the equation for volume fraction α_1 in the form

$$\partial_t \alpha_1 + \partial_x(\alpha_1 u) = (\alpha_1 - \phi)\partial_x u, \tag{4.2.9}$$

where the second term on the left-hand side is a conservative flux. As we treat the non-conservative part of the model differently, we do not take it into account here. Applying the form (4.1.10) to (4.2.9), we obtain:

$$(\alpha_1^*)_K = (\alpha_1)_K \frac{\mathcal{S}_K - u_K}{\mathcal{S}_K - \mathcal{S}_M}. \tag{4.2.10}$$

Next, we consider the fifth equation of the model of Kreeft and Koren. Applying Eq. (4.1.10) gives the new equation

$$\begin{aligned}(\alpha_1\rho_1 E_1 u)_K^* + (\alpha_1 p u)_K^* = \;& (\alpha_1\rho_1 E_1)_K u_K + (\alpha_1 p u)_K \\ & + S_K\left((\alpha_1\rho_1 E_1)_K^* - (\alpha_1\rho_1 E_1)_K\right).\end{aligned} \tag{4.2.11}$$

Substituting the estimate (4.2.10) into (4.2.11) and a lot a rewriting eventually gives

$$\begin{aligned}(\alpha_1\rho_1E_1)_K^* = \quad & (\alpha_1)_K\rho_K S_M\left[\frac{\mathcal{S}_K-u_K}{\mathcal{S}_K-\mathcal{S}_M}\right]^2(\mathcal{S}_M-u_K)\\ & +(\alpha_1\rho_1E_1)_K\frac{\mathcal{S}_K-u_K}{\mathcal{S}_K-\mathcal{S}_M}\\ & +(\alpha_1)_Kp_KS_K\frac{\mathcal{S}_M-u_K}{(\mathcal{S}_K-\mathcal{S}_M)^2}.\end{aligned} \tag{4.2.12}$$

By collecting all the results the solution vectors can be formed:

$$(\mathbf{Q}_K^*)^{\mathrm{M}} = \frac{1}{\mathcal{S}_K-\mathcal{S}_M}\begin{bmatrix}\rho_K\left(\mathcal{S}_K-u_K\right)\\ \rho_K\mathcal{S}_M\left(\mathcal{S}_K-u_K\right)\\ \rho_K\left(\mathcal{S}_K-u_K\right)\left[E_K+\left(\mathcal{S}_M-u_K\right)\left(\mathcal{S}_M+\frac{p_K}{\rho_K(\mathcal{S}_K-u_K)}\right)\right]\\ (\alpha_1\rho_1)_K\left(\mathcal{S}_K-u_K\right)\\ (\mathbf{Q}_K^*)_5^{\mathrm{M}}\end{bmatrix} \tag{4.2.13}$$

for $K=L,R$ and M=KP for Kapila's model and M=KK for the model of Kreeft and Koren. The fifth term is given by:

$$(\mathbf{Q}_K^*)_5^{\mathrm{KP}} = (\alpha_1)_K\left(\mathcal{S}_K-u_K\right), \tag{4.2.14a}$$

$$\begin{aligned}(\mathbf{Q}_K^*)_5^{\mathrm{KK}} =& (\alpha_1)_K\rho_K\mathcal{S}_M(\mathcal{S}_K-u_K)\frac{\mathcal{S}_K-u_K}{\mathcal{S}_K-\mathcal{S}_M}(\mathcal{S}_M-u_K)+(\alpha_1\rho_1E_1)_K(\mathcal{S}_K-u_K)\\ & +(\alpha_1)_Kp_K\mathcal{S}_K\frac{\mathcal{S}_M-u_K}{\mathcal{S}_K-\mathcal{S}_M}.\end{aligned} \tag{4.2.14b}$$

Substitution of the solution vectors into relation (4.1.10) gives the fluxes:

$$(\mathcal{F}_K^*)^{\mathrm{M}} = \frac{1}{\mathcal{S}_K-\mathcal{S}_M}\begin{bmatrix}\rho_K\left(\mathcal{S}_K-u_K\right)\mathcal{S}_M\\ \rho_Ku_K\left(\mathcal{S}_K-u_K\right)\mathcal{S}_M+p_M\mathcal{S}_K-p_K\mathcal{S}_M\\ \rho_KE_K\left(\mathcal{S}_K-u_K\right)\mathcal{S}_M+p_M\mathcal{S}_K\mathcal{S}_M-p_K\mathcal{S}_Mu_K\\ (\alpha_1\rho_1)_K\left(\mathcal{S}_K-u_K\right)\mathcal{S}_M\\ (\mathcal{F}_K^*)_5^{\mathrm{M}}\end{bmatrix}. \tag{4.2.15}$$

with

$$(\mathcal{F}_K^*)_5^{\mathrm{KP}} = (\alpha_1)_K\left(\mathcal{S}_K-u_K\right)\mathcal{S}_M, \tag{4.2.16a}$$

$$\begin{aligned}(\mathcal{F}_K^*)_5^{\mathrm{KK}} =& \mathcal{S}_K(\alpha_1)_K\rho_K\mathcal{S}_M(\mathcal{S}_K-u_K)\frac{\mathcal{S}_K-u_K}{\mathcal{S}_K-\mathcal{S}_M}(\mathcal{S}_M-u_K)\\ & +(\alpha_1\rho_1E_1)_K\mathcal{S}_M(\mathcal{S}_K-u_K)\\ & +\mathcal{S}_K(\alpha_1)_Kp_K\mathcal{S}_K\frac{\mathcal{S}_M-u_K}{\mathcal{S}_K-\mathcal{S}_M}.\end{aligned} \tag{4.2.16b}$$

4.3 Estimating the non-conservative terms

The non-conservative terms require a different treatment than the conservative ones. In the following we discuss the treatment of the non-conservative term(s) of the two five-equation models.

4.3.1 Kapila's model

To estimate the non-conservative product in Kapila's model, we follow Daude et al. [11], and therefore use results of the conservative terms (previous Subsection). The non-conservative term reads

$$\mathcal{R}(\mathbf{Q}, \partial_x \mathbf{Q}) = \mathcal{B}(\mathbf{Q})\, \partial_x u, \tag{4.3.1}$$

with $\mathcal{B}(\mathbf{Q}) = (0, 0, 0, 0, \alpha_1 - \phi)^T$. In the Finite volume approximation, we approximate the term $\mathcal{B}$ at first order, similar to [11], which leads to

$$\int_{C_i} \mathcal{B}(\mathbf{Q}_i)\, \partial_x u \, \mathrm{d}C_i \doteq \mathcal{B}(\mathbf{Q}_i) \int_{C_i} \partial_x u \, \mathrm{d}C_i, \tag{4.3.2}$$

where C_i denotes cell i. In the (volume) integral we use Gauss' integral theorem resulting in

$$\int_{C_i} \partial_x u \mathrm{d}C_i \doteq u_{i+1/2}(\mathbf{Q}_L, \mathbf{Q}_R) - u_{i-1/2}(\mathbf{Q}_L, \mathbf{Q}_R). \tag{4.3.3}$$

In an HLLC-type way the velocity 'jumps' from one state to another. To take this into account, we use the HLLC-type estimate proposed in [17]:

$$u_l(\mathbf{Q}_L, \mathbf{Q}_R) = \begin{cases} u_L & \text{if} \quad 0 \leq \mathcal{S}_L, \\ (u_E)_L & \text{if} \quad \mathcal{S}_L \leq 0 < \mathcal{S}_M, \\ (u_E)_R & \text{if} \quad \mathcal{S}_M \leq 0 < \mathcal{S}_R, \\ u_R & \text{if} \quad \mathcal{S}_R \leq 0, \end{cases} \tag{4.3.4}$$

where $l = i + 1/2, i - 1/2$. For the velocity in the star region we take

$$(u_E)_K = \mathcal{S}_M \frac{\mathcal{S}_K - u_K}{\mathcal{S}_K - \mathcal{S}_M}. \tag{4.3.5}$$

This estimate is linked to the conservative form of the advection equation as follows. Write the advection equation ($\mathrm{D}q/\mathrm{D}t = 0$) of a quantity q in the following conservative form (i.e. make use of the conservation of bulk mass)

$$\partial_t(\rho q) + \nabla \cdot (\rho q \mathbf{u}) = 0. \tag{4.3.6}$$

The estimate $(u_E)_K$, used in the star region, appears in the advective part of Eq. (4.3.6) as follows

$$\rho_K^* q_K^* \mathcal{S}_M = \rho_K \mathcal{S}_M \frac{\mathcal{S}_K - u_K}{\mathcal{S}_K - \mathcal{S}_M} q_K = \rho_K (u_E)_K q_K. \tag{4.3.7}$$

Alternatively, this estimate is is linked to the advective part of the flux. Let us split the flux into two parts: (i) One advection part, denoted with a, and (ii) one part consisting of pressure terms, denoted with p, i.e.:

$$\mathcal{F}_K^* = (\mathcal{F}_a^*)_K + \left(\mathcal{F}_p^*\right)_K, \tag{4.3.8}$$

where

$$(\mathcal{F}_a^*)_K^{\mathrm{M}} = \begin{pmatrix} \rho u \\ \rho u^2 \\ \rho E u \\ \alpha_1\rho_1 u \\ \mathcal{F}_{5,a}^{\mathrm{M}} \end{pmatrix}_K^*, \quad \left(\mathcal{F}_p^*\right)_K^{\mathrm{M}} = \begin{pmatrix} 0 \\ p \\ pu \\ 0 \\ \mathcal{F}_{5,p}^{\mathrm{M}} \end{pmatrix}_K^*, \tag{4.3.9}$$

with

$$\mathcal{F}_{5,a}^{\mathrm{KP}} = \alpha_1 u, \tag{4.3.10a}$$
$$\mathcal{F}_{5,p}^{\mathrm{KP}} = 0, \tag{4.3.10b}$$
$$\mathcal{F}_{5,a}^{\mathrm{KK}} = \alpha_1\rho_1 u E_1, \tag{4.3.10c}$$
$$\mathcal{F}_{5,p}^{\mathrm{KK}} = \alpha_1 p u, \tag{4.3.10d}$$

and M=KP, KK the fluxes for Kapila's model and the model of Kreeft and Koren, respectively. The superscript $*$ and the subscript K should be taken componentwise. Using the expressions of the previous Section, we find

$$(\mathcal{F}_a^*)_K^{\mathrm{M}} = \mathcal{S}_M \frac{\mathcal{S}_K - u_K}{\mathcal{S}_K - \mathcal{S}_M}\mathbf{Q}_K = (u_E)_K\mathbf{Q}_K, \tag{4.3.11a}$$

$$\left(\mathcal{F}_p^*\right)_K^{\mathrm{M}} = \frac{1}{\mathcal{S}_K - \mathcal{S}_M}\begin{pmatrix} 0 \\ p^*\mathcal{S}_K - p_K\mathcal{S}_M \\ \mathcal{S}_M\left(p^*\mathcal{S}_K - p_K u_K\right) \\ 0 \\ \left(\mathcal{F}_p^*\right)_{K,5}^{\mathrm{M}} \end{pmatrix}. \tag{4.3.11b}$$

with

$$\left(\mathcal{F}_p^*\right)_{K,5}^{\mathrm{KP}} = 0, \tag{4.3.12a}$$
$$\begin{aligned}\left(\mathcal{F}_p^*\right)_{K,5}^{\mathrm{KK}} =& \mathcal{S}_K(\alpha_1)_K p_K \mathcal{S}_K \frac{\mathcal{S}_M - u_K}{\mathcal{S}_K - \mathcal{S}_M} \\ &+ \mathcal{S}_K(\alpha_1)_K\rho_K\mathcal{S}_M(\mathcal{S}_K - u_K)\frac{\mathcal{S}_K - u_K}{\mathcal{S}_K - \mathcal{S}_M}(\mathcal{S}_M - u_K).\end{aligned} \tag{4.3.12b}$$

The splitting of the flux reveals that the velocity estimate (4.3.5) is linked to the advective part of the flux (4.3.11a).

4.3.2 Kreeft and Koren's model

For the model of Kreeft and Koren we use the Osher-type treatment for the non-conservative terms [4],[5]. This has been discussed in Section 3.3.

[4] One might argue as follows. Why not use an HLLC-type approach for the treatment of the non-conservative terms, as in Section 4.3.1? The term $p\phi\partial_x u$ can indeed be treated in an HLLC-type way. For the other terms this is not trivial. Several estimates (based on a splitting of the flux) have been tested with, unfortunately, bad results.

[5] Note that for this model the Riemann Invariants are used here.

5

An all-regime Lagrange-Projection like scheme for Kapila's model

In this Chapter we propose a new all regime Lagrange-Projection like numerical scheme for the five-equation two-phase flow model. In the five equation model we encounter fast acoustic waves as well as slow material waves. The key idea is to decouple these two different physical phenomenon. This is proposed by Chalons et al. [9] for the Euler equations of gas dynamics. In this Chapter we extend a kind of this approach to the five-equation model.
For the acoustic part of the model we use a relaxation approach to deal with a larger but simpler system. We propose to use an HLLC-type solver for the conservative part of the relaxed system. The non-conservative term, which is included in the acoustic system, is approximated with a finite difference-type approach. For the transport part a classical upwind scheme is used. As the acoustic part of the scheme does not behave well in the low Mach regime, the correction of Chalons et al. is used to solve this.
This Chapter is organised as follows. First, in Section 5.1 we discuss the splitting of the five-equation two-phase flow model into an acoustic and a transport part. We start with considering the acoustic system. In Section 5.2 we present an approximate HLLC-type scheme of a relaxed system. Next, in Section 5.3 we give the upwind scheme for the transport system. The behaviour of the scheme (both the acoustic as well as the transport part) with respect to the low Mach regime is given in Section 5.4. The modified acoustic scheme with a correction for the low Mach regime is presented in Section 5.5. We conclude this Chapter with a short note on the modified scheme. The numerical simulations are postponed to Chapter 6.

5.1 Splitting of the different physical phenomena

In this Section we discuss the strategy of splitting the two different physical phenomena. In the model we have the two physical phenomena: An acoustic part describing the pressure wave propagation and a transport part describing the movement of the waves according to the material velocity. The corresponding typical velocities are the material velocity and the speed of sound, respectively,

see Section 2.3. The proposed splitting decouples the two physical phenomena.

Let us repeat the five-equation two-phase flow model of Kapila et al. for convenience, see Chapter 2:

$$\begin{aligned}
&\partial_t \rho && +\nabla\cdot(\rho\mathbf{u}) && && = 0, && \text{(5.1.1a)}\\
&\partial_t(\rho\mathbf{u}) && +\nabla\cdot(\rho\mathbf{u}\otimes\mathbf{u}) && +\nabla p && = \mathbf{0}, && \text{(5.1.1b)}\\
&\partial_t(\rho E) && +\nabla\cdot(\rho E\mathbf{u}) && +\nabla\cdot(p\mathbf{u}) && = 0, && \text{(5.1.1c)}\\
&\partial_t(\alpha_1\rho_1) && +\nabla\cdot(\alpha_1\rho_1\mathbf{u}) && && = 0, && \text{(5.1.1d)}\\
&\partial_t\alpha_1 && +(\mathbf{u}\cdot\nabla)\alpha_1 && +\phi\nabla\cdot\mathbf{u} && = 0. && \text{(5.1.1e)}
\end{aligned}$$

By using chain rule arguments the five-equation model can be written as

$$\begin{aligned}
&\partial_t \rho && +\rho\nabla\cdot\mathbf{u} && && +(\mathbf{u}\cdot\nabla)\,\rho && = 0, && \text{(5.1.2a)}\\
&\partial_t(\rho\mathbf{u}) && +\rho\mathbf{u}\nabla\cdot\mathbf{u} && +\nabla p && +(\mathbf{u}\cdot\nabla)\,(\rho\mathbf{u}) && = \mathbf{0}, && \text{(5.1.2b)}\\
&\partial_t(\rho E) && +\rho E\nabla\cdot\mathbf{u} && +\nabla\cdot(p\mathbf{u}) && +(\mathbf{u}\cdot\nabla)\,(\rho E) && = 0, && \text{(5.1.2c)}\\
&\partial_t(\alpha_1\rho_1) && +\alpha_1\rho_1\nabla\cdot\mathbf{u} && && +(\mathbf{u}\cdot\nabla)\,(\alpha_1\rho_1) && = 0, && \text{(5.1.2d)}\\
&\partial_t\alpha_1 && +\phi\nabla\cdot\mathbf{u} && && +(\mathbf{u}\cdot\nabla)\,\alpha_1 && = 0. && \text{(5.1.2e)}
\end{aligned}$$

In the splitting the transport terms are separated from the other terms. The two submodels are (i) the acoustic system:

$$\begin{aligned}
&\partial_t \rho && +\rho\nabla\cdot\mathbf{u} && && = 0, && \text{(5.1.3a)}\\
&\partial_t(\rho\mathbf{u}) && +\rho\mathbf{u}\nabla\cdot\mathbf{u} && +\nabla p && = \mathbf{0}, && \text{(5.1.3b)}\\
&\partial_t(\rho E) && +\rho E\nabla\cdot\mathbf{u} && +\nabla\cdot(p\mathbf{u}) && = 0, && \text{(5.1.3c)}\\
&\partial_t(\alpha_1\rho_1) && +\alpha_1\rho_1\nabla\cdot\mathbf{u} && && = 0, && \text{(5.1.3d)}\\
&\partial_t\alpha_1 && +\phi\nabla\cdot\mathbf{u} && && = 0, && \text{(5.1.3e)}
\end{aligned}$$

and (ii) the transport system, which reads as:

$$\begin{aligned}
&\partial_t \rho && +(\mathbf{u}\cdot\nabla)\,\rho && = 0, && \text{(5.1.4a)}\\
&\partial_t(\rho\mathbf{u}) && +(\mathbf{u}\cdot\nabla)\,(\rho\mathbf{u}) && = \mathbf{0}, && \text{(5.1.4b)}\\
&\partial_t(\rho E) && +(\mathbf{u}\cdot\nabla)\,(\rho E) && = 0, && \text{(5.1.4c)}\\
&\partial_t(\alpha_1\rho_1) && +(\mathbf{u}\cdot\nabla)\,(\alpha_1\rho_1) && = 0, && \text{(5.1.4d)}\\
&\partial_t\alpha_1 && +(\mathbf{u}\cdot\nabla)\,\alpha_1 && = 0. && \text{(5.1.4e)}
\end{aligned}$$

We discretize (5.1.1) by successively approximating the solution of the acoustic system and the transport system. This splitting approach is first order accurate in time. Note that the acoustic system contains all the pressure terms. Furthermore, we have chosen to include the non-conservative term of the model in the acoustic system since it is a fast phenomenon (it includes the speed of sound). As we will only consider one-dimensional problems[1] in the numerical simulations of Chapter 6, we restrict ourselves from now on to those. A casting of the original system, system (5.1.1),

[1] The extension to multiple dimensions is added to the list of further improvements in Chapter 8.

into the form[2]

$$\partial_t \mathbf{W} + \mathbf{A}(\mathbf{W}) \nabla \cdot \mathbf{W} = \mathbf{0}. \tag{5.1.5}$$

where

$$\mathbf{W} = \begin{pmatrix} \rho \\ u \\ p \\ \beta_1 \\ \alpha_1 \end{pmatrix}, \quad \mathbf{A}(\mathbf{W}) = \mathbf{B}(\mathbf{W}) + \mathbf{T}(\mathbf{W}), \quad \mathbf{T}(\mathbf{W}) = u\mathbf{I}_d, \tag{5.1.6}$$

and

$$\mathbf{B}(\mathbf{W}) = \begin{pmatrix} 0 & \rho & 0 & 0 & 0 \\ 0 & 0 & 1/\rho & 0 & 0 \\ 0 & \rho c^2 & 0 & 0 & 0 \\ 0 & 0 & 0 & 0 & 0 \\ 0 & \phi & 0 & 0 & 0 \end{pmatrix}, \tag{5.1.7}$$

reveals that the corresponding matrix $\mathbf{A}$ splits nicely into an acoustic part $\mathbf{B}$ and a transport part $\mathbf{T}$ [3]. The eigenvalues split into an acoustic part (a) and a transport part (t) as follows

$$\begin{aligned} &\lambda_1 = \lambda_1^a + \lambda_1^t, \quad \lambda_{2,3,4} = \lambda_{2,3,4}^a + \lambda_{2,3,4}^t, \quad \lambda_5 = \lambda_5^a + \lambda_5^t, \\ &\lambda_1^a = -c, \qquad \lambda_{2,3,4}^a = 0, \qquad \lambda_5^a = c, \\ &\lambda_1^t = u, \qquad \lambda_{2,3,4}^t = u, \qquad \lambda_5^t = u. \end{aligned} \tag{5.1.8}$$

The corresponding eigenvectors for the acoustic system, denoted as $\mathbf{r}_{1,2,3,4,5}^a$, remain the same as for the complete five-equation model: $\mathbf{r}_{1,2,3,4,5}^a = \mathbf{r}_{1,2,3,4,5}$, respectively. The eigenvectors $\mathbf{r}_{1,2,3,4,5}$ are given in Eq. (2.3.7).

Proposition 5.1.1. *Assume the stiffened gas (SG) equation of state (EOS). The characteristic fields associated with the wave $\lambda_{2,3,4}^a = 0$ are linearly degenerate. For the other two waves, associated with $\lambda_1^a = -c, \lambda_5^a = c$, the type is neither linearly degenerate nor genuinely nonlinear.*

Proof. It is trivial that characteristic fields associated with the wave $\lambda_{2,3,4}^a = 0$ are linearly degenerate. The second part of the proposition is more complicated. Since the current set of variables appears to be an inconvenient choice, we switch the set of variables. This does not change the mathematical structure of the model. We take a set of *entropic variables* denoted as $\mathbf{W}_e$. In this

[2]The derivation of the primitive equations of the acoustic scheme is straightforward and can be found in Appendix B.1.

[3]Formally, one might argue that the splitting turns out to be the following. In the primitive equations the transport part of the material derivative operator is put into the transport system and the remainder is put into the acoustic system.

set the variables s_1, s_2 are the specific entropies of the single phases. The acoustic system can be written as, see Appendix B.1 for the derivation,

$$\partial_t \mathbf{W}_e + \mathbf{A}_e(\mathbf{W}_e)\partial_x \mathbf{W}_e = 0, \tag{5.1.9}$$

where

$$\mathbf{W}_e = \begin{pmatrix} s_1 \\ s_2 \\ u \\ p \\ \beta_1 \end{pmatrix}, \quad \mathbf{A}_e = \begin{pmatrix} 0 & 0 & 0 & 0 & 0 \\ 0 & 0 & 0 & 0 & 0 \\ 0 & 0 & 0 & 1/\rho & 0 \\ 0 & 0 & \rho c^2 & 0 & 0 \\ 0 & 0 & 0 & 0 & 0 \end{pmatrix}. \tag{5.1.10}$$

The (right) eigenvectors of (5.1.9)-(5.1.10) can be chosen as

$$(\mathbf{r}_1^a)_e = \begin{bmatrix} 0 \\ 0 \\ c \\ -\rho c^2 \\ 0 \end{bmatrix}, \quad (\mathbf{r}_2^a)_e = \begin{bmatrix} 1 \\ 0 \\ 0 \\ 0 \\ 0 \end{bmatrix}, \quad (\mathbf{r}_3^a)_e = \begin{bmatrix} 0 \\ 1 \\ 0 \\ 0 \\ 0 \end{bmatrix}, \quad (\mathbf{r}_4^a)_e = \begin{bmatrix} 0 \\ 0 \\ 0 \\ 0 \\ 1 \end{bmatrix}, \quad (\mathbf{r}_5^a)_e = \begin{bmatrix} 0 \\ 0 \\ c \\ \rho c^2 \\ 0 \end{bmatrix}. \tag{5.1.11}$$

The speed of sound does not depend on the material velocity, for details we refer to Appendix A. Using that $\partial c/\partial u = 0$, one can deduce

$$(\nabla_{\mathbf{W}_e} \lambda_1^a(\mathbf{W}_e)) \cdot (\mathbf{r}_1^a)_e = (\nabla_{\mathbf{W}_e} \lambda_5^a(\mathbf{W}_e)) \cdot (\mathbf{r}_5^a)_e = \rho c^2 \frac{\partial c}{\partial p}. \tag{5.1.12}$$

The difficulty lies in calculating the derivative in (5.1.12). This derivative can be written by using elementary calculus as, see [27],

$$\frac{\partial c}{\partial p} = -c \left[\frac{(\rho c)^2}{2} \frac{\partial}{\partial p} \left(\frac{1}{(\rho c)^2} \right) - \rho \frac{\partial}{\partial p} \left(\frac{1}{\rho} \right) \right]. \tag{5.1.13}$$

Substitution of the mixture speed of sound, defined in (2.3.3), leads to

$$\frac{\partial c}{\partial p} = -c \left[\frac{(\rho c)^2}{2} \left(\beta_1 \frac{\partial}{\partial p} \left(\frac{1}{(\rho_1 c_1)^2} \right) + \beta_2 \frac{\partial}{\partial p} \left(\frac{1}{(\rho_2 c_2)^2} \right) \right) - \rho \left(\beta_1 \frac{\partial}{\partial p} \left(\frac{1}{\rho_1} \right) + \beta_2 \frac{\partial}{\partial p} \left(\frac{1}{\rho_2} \right) \right) \right]. \tag{5.1.14}$$

Using the SG EOS one can deduce

$$\frac{\partial}{\partial p} \left(\frac{1}{\rho_k} \right) = -\frac{1}{\rho_k^2 c_k^2}, \tag{5.1.15a}$$

$$\frac{\partial}{\partial p} \left(\frac{1}{(\rho_k c_k)^2} \right) = -\frac{2\gamma_k}{\rho_k^3 c_k^4}. \tag{5.1.15b}$$

Substitution gives after simplification

$$\frac{\partial c}{\partial p} = -c\left[\frac{\alpha_1}{\rho_1 c_1^2}\left(1 - \frac{\rho c^2 \gamma_1}{\rho_1 c_1^2}\right) + \frac{\alpha_2}{\rho_2 c_2^2}\left(1 - \frac{\rho c^2 \gamma_2}{\rho_2 c_2^2}\right)\right]. \tag{5.1.16}$$

In theory, this expression can equal zero, when e.g. both terms in the inner brackets vanish. Therefore, the characteristic fields associated with $\lambda_1^a = -c, \lambda_5^a = c$ are neither linearly degenerate nor genuinely nonlinear. However, in general this will not happen. In general the waves the characteristic fields associated with $\lambda_1^a = -c, \lambda_5^a = c$ are genuinely nonlinear. An alternative approach is as follows. When $\partial c/\partial p$ equals zero, the speed of sound does not depend on the pressure. This is in general not the case.

Let us denote the fluid state at time n by $\mathbf{Q}_j^n \equiv (\rho, \rho u, \rho E, \alpha_1\rho_1, \alpha_1)_j^n$, and an intermediate time level with $n+1-$. In the algorithm we alternate approximating the solutions of the two systems, i.e. one time step reads

1. Update $\mathbf{Q}_j^n$ to $\mathbf{Q}_j^{n+1-}$ using the acoustic system (5.1.3);
2. Update $\mathbf{Q}_j^{n+1-}$ to $\mathbf{Q}_j^{n+1}$ using the transport system (5.1.4).

5.2 Acoustic system

In this Section we consider the acoustic system. By taking $\{\tau, u, E, \beta_1, \alpha_1\}$ as set of independent variables, the acoustic system can be cast into the form

$$\partial_t \tau \; - \tau \partial_x u \quad = 0, \tag{5.2.1a}$$
$$\partial_t u \; + \tau \partial_x p \quad = 0, \tag{5.2.1b}$$
$$\partial_t E \; + \tau \partial_x (pu) = 0, \tag{5.2.1c}$$
$$\partial_t \beta_1 \qquad\quad = 0, \tag{5.2.1d}$$
$$\partial_t \alpha_1 + \rho\phi\tau \partial_x u = 0. \tag{5.2.1e}$$

Here $\tau = 1/\rho$ is the specific volume. The first three equations, Eq. (5.2.1a)-(5.2.1c), correspond to the gas dynamics equations, and the latter two contain the fraction variables which are specific for the five-equation two-phase flow model. In this formulation one notes the same form of each of the first three equations: The second term (flux-like term) here consists of a flux of velocity, pressure and momentum, respectively, multiplied by the specific volume. The latter two equations are formulated such that the flux-like term vanishes.

Note that the second term of each equation (except the fourth equation) contains the operator $\tau\partial_x$. The idea is to replace this operator. For $t \in [t^n, t^n + \Delta t]$ the operator $\tau(x,t)\partial_x$ is approximated by $\tau(x,t^n)\partial_x$. Hence, the acoustic system of time step n is approximated by

$$\partial_t \tau \; - \tau(x,t^n) \partial_x u \quad = 0, \tag{5.2.2a}$$
$$\partial_t u \; + \tau(x,t^n) \partial_x p \quad = 0, \tag{5.2.2b}$$
$$\partial_t E \; + \tau(x,t^n) \partial_x (pu) = 0, \tag{5.2.2c}$$
$$\partial_t \beta_1 \qquad\quad = 0, \tag{5.2.2d}$$
$$\partial_t \alpha_1 + \rho\phi\tau(x,t^n) \partial_x u = 0. \tag{5.2.2e}$$

We introduce the mass variable m defined by

$$m(x) = \int_0^x \rho(\breve{x}, t^n)\mathrm{d}\breve{x}. \tag{5.2.3}$$

Formally, we can write $\mathrm{d}m = \rho(x, t^n)\mathrm{d}x$. The change of variables: $\tau(x,\cdot) = \bar{\tau}(m,\cdot)$, $u(x,\cdot) = \bar{u}(m,\cdot)$, $E(x,\cdot) = \bar{E}(m,\cdot)$, $\beta_1(x,\cdot) = \bar{\beta_1}(m,\cdot)$, $\alpha_1(x,\cdot) = \bar{\alpha_1}(m,\cdot)$, $\rho(x,\cdot) = \bar{\rho}(m,\cdot)$, $\phi(x,\cdot) = \bar{\phi}(m,\cdot)$, is performed. This leads to the system:

$$\begin{aligned}
\partial_t\bar{\tau} \ -\partial_m\bar{u} \quad &= 0, && \text{(5.2.4a)}\\
\partial_t\bar{u} \ +\partial_m\bar{p} \quad &= 0, && \text{(5.2.4b)}\\
\partial_t\bar{E} \ +\partial_m(\bar{p}\bar{u}) &= 0, && \text{(5.2.4c)}\\
\partial_t\bar{\beta_1} \qquad &= 0, && \text{(5.2.4d)}\\
\partial_t\bar{\alpha_1}+\bar{\rho}\bar{\phi}\partial_m\bar{u} &= 0. && \text{(5.2.4e)}
\end{aligned}$$

The '-' symbols are now neglected and we arrive at the system:

$$\begin{aligned}
\partial_t\tau \ -\partial_m u \quad &= 0, && \text{(5.2.5a)}\\
\partial_t u \ +\partial_m p \quad &= 0, && \text{(5.2.5b)}\\
\partial_t E \ +\partial_m(pu) &= 0, && \text{(5.2.5c)}\\
\partial_t\beta_1 \qquad &= 0, && \text{(5.2.5d)}\\
\partial_t\alpha_1+\rho\phi\partial_m u &= 0. && \text{(5.2.5e)}
\end{aligned}$$

which can be written as

$$\partial_t\mathbf{Q}^{\text{LAG}} + \partial_m\mathcal{F}^{\text{LAG}}(\mathbf{Q}^{\text{LAG}}) + \mathcal{R}^{\text{LAG}}(\mathbf{Q}^{\text{LAG}}, \partial_m\mathbf{Q}^{\text{LAG}}) = \mathbf{0}, \tag{5.2.6}$$

where

$$\begin{aligned}
\mathbf{Q}^{\text{LAG}} &= (\tau, u, E, \beta_1, \alpha_1)^T && \text{(5.2.7a)}\\
\mathcal{F}^{\text{LAG}}(\mathbf{Q}^{\text{LAG}}) &= (-u, p, pu, 0, 0)^T, && \text{(5.2.7b)}\\
\mathcal{R}(\mathbf{Q}^{\text{LAG}}, \partial_m\mathbf{Q}^{\text{LAG}}) &= (0, 0, 0, 0, \rho\phi\partial_m u)^T. && \text{(5.2.7c)}
\end{aligned}$$

The superscript LAG refers to *Lagrangian* variables.

5.2.1 Relaxed system

Due to nonlinearities of the pressure, the Riemann problem associated with (5.2.6)-(5.2.7) is difficult to solve. This problem can be dealt with by using a *relaxation strategy*. The idea of this strategy is to deal with a larger but simpler system. The problems are caused by the pressure. The design principle is to consider the pressure as a new unknown, a so-called *surrogate pressure* which we denote as Π. We have chosen to use an HLLC-type solver for the relaxed system, where Chalons et al. use Godunov's method for their relaxed system. Godunov's method, developed by S. K. Godunov, is a conservative numerical scheme for solving PDEs. It is a finite-volume method which solves exact or approximate Riemann problems. The combination of using a relaxation approach and a Godunov solver on the relaxed system is common and known as a *Suliciu-type approximation*[31].

A Godunov method does not seem to be a natural choice for our relaxed system because in general no exact solution exists (due to the non-conservative term).

To proceed we first derive the relaxed system and its structure. In the next Subsection we present an HLLC-type solver for the relaxed system.

We refer to Appendix C for some background on obtaining the relaxed system. We introduce a surrogate pressure Π, which satisfies[4]

$$\partial_t \Pi + \tau a^2 \partial_x u = \mathfrak{y} \left(p - \Pi \right), \tag{5.2.8}$$

where a approximates the term ρc and $\mathfrak{y}$ is a relaxation parameter. The parameter a is constant. The exact choices will be specified later. The relaxed system is given by

$$\begin{aligned}
\partial_t \tau \; - \partial_m u \qquad\qquad &= 0, && \text{(5.2.9a)}\\
\partial_t u \; + \partial_m \Pi \qquad\qquad &= 0, && \text{(5.2.9b)}\\
\partial_t E \; + \partial_m (\Pi u) \qquad &= 0, && \text{(5.2.9c)}\\
\partial_t \beta_1 \qquad\qquad &= 0, && \text{(5.2.9d)}\\
\partial_t \alpha_1 + \rho\phi \partial_m u \qquad &= 0, && \text{(5.2.9e)}\\
\partial_t \Pi \; + a^2 \partial_m u \; &= \mathfrak{y} \left(p - \Pi \right). && \text{(5.2.9f)}
\end{aligned}$$

Note that we now have six equations. The numerical method is a *two step approach*:

- *Evolution* step: $\mathfrak{y} = 0$;
- *Source* step: $\mathfrak{y} \to +\infty$.

We alternate between the *evolution* and the *source* step with the parameter $\mathfrak{y}$. In the evolution step, i.e. $\mathfrak{y} = 0$, we obtain

$$\partial_t \mathbf{Q}_s^{\text{LAG}} + \partial_m \mathcal{F}_s^{\text{LAG}}(\mathbf{Q}_s^{\text{LAG}}) + \mathcal{R}_s^{\text{LAG}}(\mathbf{Q}_s^{\text{LAG}}, \partial_m \mathbf{Q}_s^{\text{LAG}}) = 0, \tag{5.2.10}$$

where the different terms are defined as:

$$\begin{aligned}
\mathbf{Q}_s^{\text{LAG}} &= (\tau, u, E, \beta_1, \alpha_1, \Pi)^T && \text{(5.2.11a)}\\
\mathcal{F}_s^{\text{LAG}}(\mathbf{Q}_s^{\text{LAG}}) &= (-u, \Pi, \Pi u, 0, 0, a^2 u)^T, && \text{(5.2.11b)}\\
\mathcal{R}(\mathbf{Q}_s^{\text{LAG}}, \partial_m \mathbf{Q}_s^{\text{LAG}}) &= (0, 0, 0, 0, \rho\phi \partial_m u, 0)^T. && \text{(5.2.11c)}
\end{aligned}$$

The subscript s refers to the relaxed system. After solving the evolution system from time level n to $n+1-$ we solve the source system, i.e. we let $\mathfrak{y} \to +\infty$ which enforces

$$\Pi = p^{\text{EOS}}(\tau, u, E, \beta_1, \alpha_1). \tag{5.2.12}$$

In order to determine the structure of the relaxed system, we use the following alternative form of the fifth equation

$$\partial_t \alpha_1 + \rho\phi \partial_m u = 0. \tag{5.2.13}$$

[4]This approximation is based on the primitive equation of the pressure, see Appendix B.1.

We write the full relaxed acoustic system as

$$\partial_t \mathbf{Q}_s^{\text{LAG}} + \mathbf{A}_s^{\text{LAG}}(\mathbf{Q}_s^{\text{LAG}})\partial_m \mathbf{Q}_s^{\text{LAG}} = \mathbf{0}. \tag{5.2.14}$$

with

$$\mathbf{Q}_s^{\text{LAG}} = \begin{pmatrix} \tau \\ u \\ E \\ \beta_1 \\ \alpha_1 \\ \Pi \end{pmatrix} \quad \mathbf{A}_s^{\text{LAG}}(\hat{\mathbf{Q}}_s^{\text{LAG}}) = \begin{pmatrix} 0 & -1 & 0 & 0 & 0 & 0 \\ 0 & 0 & 0 & 0 & 0 & 1 \\ 0 & \Pi & 0 & 0 & 0 & u \\ 0 & 0 & 0 & 0 & 0 & 0 \\ 0 & \rho\phi & 0 & 0 & 0 & 0 \\ 0 & a^2 & 0 & 0 & 0 & 0 \end{pmatrix}. \tag{5.2.15}$$

Hence, the system is hyperbolic with wave speeds

$$\lambda_1^{\text{LAG}} = -a, \quad \lambda_{2,3,4,5}^{\text{LAG}} = 0, \quad \lambda_6^{\text{LAG}} = a, \tag{5.2.16}$$

with corresponding (right) eigenvectors

$$\begin{aligned} \mathbf{r}_1^{\text{LAG}} &= \begin{bmatrix} 1 \\ a \\ au - \Pi \\ 0 \\ -\rho\phi \\ -a^2 \end{bmatrix}, \quad \mathbf{r}_2^{\text{LAG}} = \begin{bmatrix} 1 \\ 0 \\ 0 \\ 0 \\ 0 \\ 0 \end{bmatrix}, \quad \mathbf{r}_3^{\text{LAG}} = \begin{bmatrix} 0 \\ 0 \\ 1 \\ 0 \\ 0 \\ 0 \end{bmatrix}, \\ \mathbf{r}_4^{\text{LAG}} &= \begin{bmatrix} 0 \\ 0 \\ 0 \\ 1 \\ 0 \\ 0 \end{bmatrix}, \quad \mathbf{r}_5^{\text{LAG}} = \begin{bmatrix} 0 \\ 0 \\ 0 \\ 0 \\ 1 \\ 0 \end{bmatrix}, \quad \mathbf{r}_6^{\text{LAG}} = \begin{bmatrix} 1 \\ -a \\ -au - \Pi \\ 0 \\ -\rho\phi \\ -a^2 \end{bmatrix}. \end{aligned} \tag{5.2.17}$$

Proposition 5.2.1. *The characteristic fields associated with the waves $\lambda_1^{\text{LAG}}, ...\lambda_6^{\text{LAG}}$ are linearly degenerate.*

Proof. Since the waves speeds are all constant (the parameter a is constant), the computation is trivial

$$\nabla_{\mathbf{Q}_s^{\text{LAG}}} \lambda_k^{\text{LAG}} \cdot \mathbf{r}_k = \mathbf{0} \cdot \mathbf{r}_k = 0. \tag{5.2.18}$$

5.2.2 HLLC-type solver

In the Finite-volume approximation of the relaxed system (5.2.10)-(5.2.11) on cell C_i reads

$$\partial_t((\mathbf{Q}_s^{\text{LAG}})_i) + \frac{1}{\Delta m}\left((\boldsymbol{\phi}_s^{\text{LAG}})_{i+1/2}^{\text{HLLC}} - (\boldsymbol{\phi}_s^{\text{LAG}})_{i-1/2}^{\text{HLLC}}\right) + \int_{C_i} \mathcal{B}_s\left((\mathbf{Q}_s^{\text{LAG}})_i\right)\partial_m u \, \mathrm{d}C_i, \tag{5.2.19}$$

where the numerical flux approximates $\mathcal{F}_s^{\text{LAG}}\left((\mathbf{Q}_s^{\text{LAG}})\right)$ and

$$\mathcal{R}_s^{\text{LAG}}(\mathbf{Q}_s^{\text{LAG}}, \partial_m \mathbf{Q}_s^{\text{LAG}}) = \mathcal{B}_s\left(\mathbf{Q}_s^{\text{LAG}}\right)\partial_m u. \tag{5.2.20}$$

with $\mathcal{B}_s\left(\mathbf{Q}_s^{\text{LAG}}\right) = (0,0,0,0,\rho\phi,0)^T$. Note that a first order time integration method is used. Because the splitting approach is first order accurate in time, the overall scheme is at maximum first order in time. The objective is to obtain an approximation for the conservative contributions, i.e. the fluxes ϕ and for the non-conservative term which the rightmost term in Eq. (5.2.19).

Conservative terms

We use an HLLC-type solver to obtain approximation for the conservative part (acoustic system evolution step). For the following the reader is assumed to be familiar with HLLC-type schemes. If the reader is not familiar with this concept, we suggest to study Chapter 4 before proceeding with this Chapter. For a good introduction to HLLC-type schemes we also refer to the book of Toro [32]. In the HLLC solver we have four states separated by three waves. The HLLC approximate Riemann Solver, which has a very similar shape as the HLLC approximate Riemann Solver of the previous Chapter, is given by

$$\tilde{\mathbf{Q}}_s^{\text{LAG}}(m,t) = \begin{cases} (\mathbf{Q}_s^{\text{LAG}})_L & \text{if} \quad m/t \leq (\mathcal{S}_s^{\text{LAG}})_L, \\ (\mathbf{Q}_s^{\text{LAG}})_L^* & \text{if} \quad (\mathcal{S}_s^{\text{LAG}})_L \leq m/t < (\mathcal{S}_s^{\text{LAG}})_M, \\ (\mathbf{Q}_s^{\text{LAG}})_R^* & \text{if} \quad (\mathcal{S}_s^{\text{LAG}})_M \leq m/t < (\mathcal{S}_s^{\text{LAG}})_R, \\ (\mathbf{Q}_s^{\text{LAG}})_R & \text{if} \quad (\mathcal{S}_s^{\text{LAG}})_R \leq m/t. \end{cases} \tag{5.2.21}$$

This notation of the different states is:

$$\begin{aligned} (\mathbf{Q}_s^{\text{LAG}})_L &= (\tau_L, u_L, E_L, (\beta_1)_L, (\alpha_1)_L, \Pi_L)^T, \\ (\mathbf{Q}_s^{\text{LAG}})_L^* &= (\tau_L^*, u_L^*, E_L^*, (\beta_1)_L^*, (\alpha_1)_L^*, \Pi_L^*)^T, \\ (\mathbf{Q}_s^{\text{LAG}})_R^* &= (\tau_R^*, u_R^*, E_R^*, (\beta_1)_R^*, (\alpha_1)_R^*, \Pi_R^*)^T, \\ (\mathbf{Q}_s^{\text{LAG}})_R &= (\tau_R, u_R, E_R, (\beta_1)_R, (\alpha_1)_R, \Pi_R)^T. \end{aligned} \tag{5.2.22}$$

Here, $(\mathcal{S}_s^{\text{LAG}})_L, (\mathcal{S}_s^{\text{LAG}})_R$, corresponding to the wave speeds $\lambda_1^{\text{LAG}} = -a$ and $\lambda_6^{\text{LAG}} = a$, denote the slowest and fastest *mass signal speed* [5] respectively. The middle wave speed/mass signal speed $(\mathcal{S}_s^{\text{LAG}})_M$ corresponds to the multiple eigenvalue $\lambda_{2,3,4,5} = 0$. To determine the middle states $(\mathbf{Q}_s^{\text{LAG}})_K^*$ we again use the jump relations, similar as the previous Chapter:

$$\left(\boldsymbol{\phi}_s^{\text{LAG}}\right)_K^* = \left(\boldsymbol{\phi}_s^{\text{LAG}}\right)_K + (\mathcal{S}_s)_K\left(\left(\mathbf{Q}_s^{\text{LAG}}\right)_K^* - (\mathbf{Q}_s^{\text{LAG}})_K\right), \tag{5.2.23}$$

with $\left(\boldsymbol{\phi}_s^{\text{LAG}}\right)_K = \mathcal{F}_s^{\text{LAG}}\left((\boldsymbol{Q}_s^{\text{LAG}})_K\right)$ and $K = L, R$. As

$$\left(\nabla_{\mathbf{Q}_s^{\text{LAG}}}\, u\right) \cdot \mathbf{r}_{2,3,4,5}^{\text{LAG}} = 0, \tag{5.2.24a}$$

$$\left(\nabla_{\mathbf{Q}_s^{\text{LAG}}}\, \Pi\right) \cdot \mathbf{r}_{2,3,4,5}^{\text{LAG}} = 0, \tag{5.2.24b}$$

[5] The unit of these speeds-like quantities is $[\mathcal{S}_s^{\text{LAG}}] = [\rho][c]$

the velocity and pressure remain constant over the middle (contact) wave:

$$u_L^* = u_R^* \equiv u^*, \tag{5.2.25a}$$
$$\Pi_L^* = \Pi_R^* \equiv \Pi^*. \tag{5.2.25b}$$

To determine the components of $(\mathbf{Q}_s)_K^*$ we use Eq. (5.2.23). This is similar as in Chapter 4. A straightforward evaluation reveals that the states $(\mathbf{Q}_s)_K^*$ are given by

$$u^* = \frac{(\mathcal{S}_s^{\text{LAG}})_L u_L - (\mathcal{S}_s^{\text{LAG}})_R u_R + \Pi_R - \Pi_L}{(\mathcal{S}_s^{\text{LAG}})_L - (\mathcal{S}_s^{\text{LAG}})_R}, \tag{5.2.26a}$$
$$\Pi^* = \frac{\Pi_R(\mathcal{S}_s^{\text{LAG}})_L - \Pi_L(\mathcal{S}_s^{\text{LAG}})_R + (\mathcal{S}_s^{\text{LAG}})_L(\mathcal{S}_s^{\text{LAG}})_R(u_L - u_R)}{(\mathcal{S}_s^{\text{LAG}})_L - (\mathcal{S}_s^{\text{LAG}})_R}, \tag{5.2.26b}$$
$$\tau_K^* = \tau_K + \frac{u_K - u^*}{(\mathcal{S}_s^{\text{LAG}})_K}, \tag{5.2.26c}$$
$$E_K^* = E_K + \frac{\Pi^* u^* - \Pi_K u_K}{(\mathcal{S}_s^{\text{LAG}})_K}, \tag{5.2.26d}$$
$$(\beta_1)_K^* = (\beta_1)_K, \tag{5.2.26e}$$
$$(\alpha_1)_K^* = (\alpha_1)_K, \tag{5.2.26f}$$

for $K = L, R$. Note that the mass fraction is constant across the left and right wave, i.e. $(\beta_1)_K^* = (\beta_1)_K$. This is also obtained using the Riemann Invariants, see Section 2.3. Additionally, we obtain $(\mathcal{S}_s^{\text{LAG}})_K^2 = a^2$, for $K = L, R$. Since $(\mathcal{S}_s^{\text{LAG}})_L, (\mathcal{S}_s)_R^{\text{LAG}}$ and $(\mathcal{S}_s)_R^{\text{LAG}}$ correspond to $\lambda_1^{\text{LAG}} = -a, \lambda_6^{\text{LAG}} = a$ and $\lambda_{2,3,4,5}^{\text{LAG}} = 0$ respectively, we take the natural choice of

$$(\mathcal{S}_s^{\text{LAG}})_L = -a, \tag{5.2.27a}$$
$$(\mathcal{S}_s^{\text{LAG}})_M = 0, \tag{5.2.27b}$$
$$(\mathcal{S}_s^{\text{LAG}})_R = a. \tag{5.2.27c}$$

Then the expressions for u^*, Π^* reduce to

$$u^* = \frac{u_L + u_R}{2} + \frac{\Pi_L - \Pi_R}{2a}, \tag{5.2.28a}$$
$$\Pi^* = \frac{\Pi_L + \Pi_R}{2} + \frac{a}{2}(u_L - u_R). \tag{5.2.28b}$$

This result is also found by Chalons et al. [9] using the Godunov method. We approximate the left and right states at first order by $u_L = u_i, u_R = u_{i+1}, \Pi_L = \Pi_i, \Pi_R = \Pi_{i+1}$. Note that the sign of the mass signal speeds is fixed. Since $m/t > 0$ and $a > 0$ the left $((\mathbf{Q}_s^{\text{LAG}})_L)$ and right $((\mathbf{Q}_s^{\text{LAG}})_R)$ states can never be reached. Furthermore, in the fluxes of the middle states only velocity and pressure terms appear. Since the velocity and pressure terms are constant across the middle wave $(u_L^* = u_R^* = u^*, \Pi_L^* = \Pi_R^* = \Pi^*)$ connecting the middle states, the flux of both states, $\left(\boldsymbol{\phi}_s^{\text{LAG}}\right)_K^*$, is the same. Therefore, the corresponding HLLC flux vector consists of a single state:

$$\left(\boldsymbol{\phi}_s^{\text{LAG}}\right)_{i+1/2}^{\text{HLLC}} = \left(-u^*, \Pi^*, \Pi^* u^*, 0, 0, a^2 u^*\right)_{i+1/2}. \tag{5.2.29}$$

What remains is to specify the choice of the parameter a. We take the choice of Chalons et al.[6]:

$$a_M = H \max(\rho_L c_L, \rho_R c_R). \tag{5.2.30}$$

Here L, R denote the left and right interface of the corresponding cell, M the middle of the cell and $H > 1$. We take $H = 1.1$, this choice is arbitrary and we have not tested any other choice.

Non-conservative term

We now turn to the non-conservative part. This reads:

$$\mathcal{R}_s^{\text{LAG}}(\mathbf{Q}_s^{\text{LAG}}, \partial_m \mathbf{Q}_s^{\text{LAG}}) = \mathcal{B}_s\left(\mathbf{Q}_s^{\text{LAG}}\right) \partial_m u, \tag{5.2.31}$$

with $\mathcal{B}_s\left(\mathbf{Q}_s^{\text{LAG}}\right) = (0, 0, 0, 0, \rho\phi, 0)^T$. In the Finite volume approximation, we approximate the term $\mathcal{B}_s$ at first order, which leads to

$$\int_{C_i} \mathcal{B}_s\left(\left(\mathbf{Q}_s^{\text{LAG}}\right)_i\right) \partial_m u \, \mathrm{d}C_i \doteq \mathcal{B}_s\left(\left(\mathbf{Q}_s^{\text{LAG}}\right)_i\right) \int_{C_i} \partial_m u \, \mathrm{d}C_i, \tag{5.2.32}$$

where C_i denotes cell i. We propose to approximate the (volume) integral by

$$\int_{C_i} \partial_m u \mathrm{d}C_i = \int_{C_i} \tau \partial_x u \mathrm{d}C_i \doteq \tau_i \left(u^*_{i+1/2} - u^*_{i-1/2}\right). \tag{5.2.33}$$

Update formulae

Summarizing, the update formula for the discretized acoustic system (evolution step) reads:

$$\mathbf{Q}_i^{n+1-} = \mathbf{Q}_i^n - \frac{\Delta t}{(\rho)_i^n \Delta x}\left(\boldsymbol{\phi}^n_{i+1/2} - \boldsymbol{\phi}^n_{i-1/2}\right) - (\phi)_i^n \frac{\Delta t}{\Delta x}\left(\mathcal{H}^n_{i+1/2} - \mathcal{H}^n_{i-1/2}\right). \tag{5.2.34}$$

where

$$(\mathbf{Q}_i)^T = (\tau, u, E, \beta_1, \alpha_1, \Pi)_i, \tag{5.2.35a}$$

$$\left(\boldsymbol{\phi}^n_{i+1/2}\right)^T = (-u^*, \Pi^*, \Pi^* u^*, 0, 0, a^2 u^*)^n_{i+1/2}, \tag{5.2.35b}$$

$$\left(\mathcal{H}^n_{i+1/2}\right)^T = (0, 0, 0, 0, u^*, 0)^n_{i+1/2}. \tag{5.2.35c}$$

with

$$u^*_{i+1/2} = \frac{u_i + u_{i+1}}{2} + \frac{\Pi_i - \Pi_{i+1}}{2a}, \tag{5.2.36a}$$

$$\Pi^*_{i+1/2} = \frac{\Pi_i + \Pi_{i+1}}{2} + \frac{a}{2}(u_i - u_{i+1}), \tag{5.2.36b}$$

[6]The primitive equation of the pressure is given by

$$\partial_t p + \rho c^2 \partial_x u = \partial_t p + \tau(\rho c)^2 \partial_x u = \partial_t p + (\rho c)^2 \partial_m u = 0.$$

Hence, a approximates ρc.

5.2.3 Properties acoustic system

The update formulae for the discretized acoustic system in terms of conservative variables are given by (it follows from (5.2.34) and (5.1.3))

$$\rho_j^{n+1-} = K_j \rho_j^n, \tag{5.2.37a}$$

$$(\rho u)_j^{n+1-} = K_j \, (\rho u)_j^n - \frac{\Delta t}{\Delta x} \left(\Pi^*_{j+1/2} - \Pi^*_{j-1/2} \right), \tag{5.2.37b}$$

$$(\rho E)_j^{n+1-} = K_j \, (\rho E)_j^n - \frac{\Delta t}{\Delta x} \left(\Pi^*_{j+1/2} u^*_{j+1/2} - \Pi^*_{j-1/2} u^*_{j-1/2} \right), \tag{5.2.37c}$$

$$(\alpha_1 \rho_1)_j^{n+1-} = K_j \, (\alpha_1 \rho_1)_j^n \, , \tag{5.2.37d}$$

$$(\alpha_1)_j^{n+1-} = (\alpha_1)_j^n - (\phi)_j^n \frac{\Delta t}{\Delta x} \left(u^*_{j+1/2} - u^*_{j-1/2} \right), \tag{5.2.37e}$$

where K_j is given by

$$K_j = 1 - \frac{\Delta t}{\Delta x} \left(u^*_{j+1/2} - u^*_{j-1/2} \right). \tag{5.2.38}$$

For the acoustic scheme, i.e. (5.2.10)-(5.2.11), the stability requirement reads

$$\frac{\Delta t}{\Delta x} \max_j \left(\max(\tau_j^n, \tau_{j+1}^n) a_{j+1/2} \right) \leq 1. \tag{5.2.39}$$

This condition is the same as for the Euler equations and can be understood as follows. As we solve the system in lagrangian formulation, the CFL number for the acoustic system (5.2.10)-(5.2.11) is defined by

$$\mathcal{C}_a = \frac{\Delta t}{\Delta m} \max_j \left(|\lambda_j^{\text{LAG}}| \right), \tag{5.2.40}$$

with $\Delta m = \rho(x, t^n) \Delta x$. By noting that the (maximum) wave speed is $a_{j+1/2}$, we obtain the stability requirement (5.2.41). When dealing with two successive Riemann problems at the same cell, the stricter CFL restriction holds [9]:

$$\frac{\Delta t}{\Delta x} \max_j \left(\max(\tau_j^n, \tau_{j+1}^n) a_{j+1/2} \right) \leq 1/2. \tag{5.2.41}$$

This CFL restriction is linked to the *non-juxtaposition*. This means that the waves of the two Riemann problems may not interfere. This can be observed for severe cases. In the problems we have encountered, we use the limit (5.2.41).

5.3 Transport system

In this Section we present the solver for the transport system, which can be written as

$$\partial_t \mathbf{W} + \mathbf{T}(\mathbf{W}) \partial_x \mathbf{W} = \mathbf{0}, \tag{5.3.1}$$

with

$$\mathbf{T}(\mathbf{W}) = u\mathbf{I}_d. \tag{5.3.2}$$

Each single equation can be written in the form

$$\partial_t \upsilon = -\partial_x(\upsilon u) + \upsilon \partial_x u, \tag{5.3.3}$$

where $\upsilon \in \{\rho, \rho u, \rho E, \alpha_1\rho_1, \alpha_1\}$. This form is used in the Finite volume approximation. We approximate the velocity $u_{j+1/2}$ by actual velocity of the shock wave $u^*_{j+1/2}$ as defined in Eq. (5.2.28a). Furthermore, we use the upwind value to approximate the interface value $\upsilon_{j+1/2}$:

$$\upsilon^{n+1-}_{j+1/2} = \begin{cases} \upsilon^{n+1-}_{j}, & \text{if} \quad u^*_{j+1/2} \geq 0, \\ \upsilon^{n+1-}_{j+1}, & \text{if} \quad u^*_{j+1/2} < 0. \end{cases} \tag{5.3.4}$$

The Finite volume approximation reads:

$$\begin{aligned} \upsilon^{n+1}_j = \upsilon^{n+1-}_j \quad & -\frac{\Delta t}{\Delta x}\left(u^*_{j+1/2}\upsilon^{n+1-}_{j+1/2} - u^*_{j-1/2}\upsilon^{n+1-}_{j-1/2}\right) \\ & +\frac{\Delta t}{\Delta x}\upsilon^{n+1-}_j\left(u^*_{j+1/2} - u^*_{j-1/2}\right). \end{aligned} \tag{5.3.5}$$

Stability requirement

The wave speed of the transport system is $u^*_{j+1/2}$. Let us first assume that $u^*_{j-1/2}$ and $u^*_{j+1/2}$ have the same sign. In this case the CFL number is given by

$$\mathcal{C}_t = \frac{\Delta t}{\Delta x}\max_j |u^*_{j+1/2}|, \tag{5.3.6}$$

and the stability requirement reads

$$\mathcal{C}_t < 1. \tag{5.3.7}$$

In general, the stability requirement reads

$$\frac{\Delta t}{\Delta x}\max_j\left(\left(u^*_{j-1/2}\right)^+ - \left(u^*_{j+1/2}\right)^-\right) < 1, \tag{5.3.8}$$

where $b^\pm = (b \pm |b|)/2$. Note that we now have two stability requirements: One for the acoustic part and one for the transport part. We take the most severe of the two.

5.4 Behavior with respect to the Mach regime

In this Section we explore the behavior of the scheme consisting of both the acoustic and transport part as described in Sections 5.2, 5.3 respectively. In this analysis both the conservative part and

the non-conservative part are taken into account.

Let us introduce the non-dimensional quantities:

$$\begin{aligned} &\tilde{x} = \tfrac{x}{L}, \quad \tilde{t} = \tfrac{t}{T}, \qquad \tilde{u} = \tfrac{u}{u_0}, \quad \tilde{\rho} = \tfrac{\rho}{\rho_0}, \quad \tilde{p} = \tfrac{p}{p_0}, \quad \tilde{e} = \tfrac{e}{e_0}, \\ &\tilde{c} = \tfrac{c}{c_0}, \quad \tilde{\rho_1} = \tfrac{\rho_1}{(\rho_1)_0}. \end{aligned} \tag{5.4.1}$$

The parameters L, T denote the characteristic length and time and u_0, ρ_0, p_0, e_0 and c_0 are the characteristic velocity, density, pressure, internal energy and speed of sound for the bulk quantities. The parameters $(\rho_1)_0$ is the characteristic density. Note that a scaling of the volume fraction is useless. Furthermore, we set

$$u_0 = \frac{L}{T}, \quad e_0 = \frac{p_0}{\rho_0}, \quad c_0^2 = \frac{p_0}{\rho_0}. \tag{5.4.2}$$

The (bulk) *Mach number* is given by

$$M = \frac{u_0}{c_0}. \tag{5.4.3}$$

Furthermore, we introduce the scaled total internal energy

$$\tilde{E} = \tilde{e} + \frac{1}{2} M^2 \tilde{u}^2. \tag{5.4.4}$$

Rescaling the one-dimensional version of model (5.1.1) using the non dimensional quantities (5.4.1) leads to

$$\partial_{\tilde{t}}\tilde{\rho} + \partial_{\tilde{x}}(\tilde{\rho}\tilde{u}) = 0, \tag{5.4.5a}$$

$$\partial_{\tilde{t}}(\tilde{\rho}\tilde{u}) + \partial_{\tilde{x}}(\tilde{\rho}\tilde{u}^2) + \frac{1}{M^2}\partial_{\tilde{x}}\tilde{p} = 0, \tag{5.4.5b}$$

$$\partial_{\tilde{t}}(\tilde{\rho}\tilde{E}) + \partial_{\tilde{x}}(\tilde{\rho}\tilde{E}\tilde{u}) + \partial_{\tilde{x}}(\tilde{p}\tilde{u}) = 0, \tag{5.4.5c}$$

$$\partial_{\tilde{t}}(\alpha_1\tilde{\rho}_1) + \partial_{\tilde{x}}(\alpha_1\tilde{\rho}_1\tilde{u}) = 0, \tag{5.4.5d}$$

$$\partial_{\tilde{t}}(\alpha_1) + \partial_{\tilde{x}}(\alpha_1\tilde{u}) = 0. \tag{5.4.5e}$$

From now on, we consider the *low Mach regime*. We are in the low Mach regime if

- $\partial_{\tilde{x}}\tilde{p} = \mathcal{O}(M^2)$,
- $M << 1$.

The first condition means that all tilde variables remain of order 1. Let us denote with $\tilde{\Pi}$ the surrogate pressure corresponding to system (5.4.5), and with $\tilde{\beta}_1 = \tilde{\alpha}_1\tilde{\rho}_1/\tilde{\rho}$. In terms of rescaled variables Eq. (5.2.23) reads

$$-M\tilde{u}^* = -M\tilde{u}_K \mp \tilde{a}(\tilde{\tau}_K^* - \tilde{\tau}_K), \tag{5.4.6a}$$

$$\tilde{\Pi}^* = \tilde{\Pi}_K \mp \tilde{a}M(\tilde{u}^* - \tilde{u}_K), \tag{5.4.6b}$$

$$M\tilde{\Pi}_K^*\tilde{u}_K^* = M(\tilde{\Pi}\tilde{u})_K \mp \tilde{a}(\tilde{E}_K^* - \tilde{E}_K) \tag{5.4.6c}$$

$$0 = (\tilde{\beta}_1)_K^* - (\tilde{\beta}_1)_K, \tag{5.4.6d}$$

$$0 = (\tilde{\alpha}_1)_K^* - (\tilde{\alpha}_1)_K, \tag{5.4.6e}$$

$$M\tilde{a}^2\tilde{u}^* = M\tilde{a}^2\tilde{u}_K \mp \tilde{a}(\tilde{\Pi}^* - \tilde{\Pi}_K), \tag{5.4.6f}$$

where the $-$ sign is taken for $K = L$ and the $+$ sign for $K = R$. The expressions for $\tilde{u}^*$ and $\tilde{\Pi}^*$ reduce to

$$\tilde{u}^* = \frac{\tilde{u}_L + \tilde{u}_R}{2} + \frac{\tilde{\Pi}_L - \tilde{\Pi}_R}{2\tilde{a}M}, \tag{5.4.7a}$$

$$\tilde{\Pi}^* = \frac{\tilde{\Pi}_L + \tilde{\Pi}_R}{2} + \frac{\tilde{a}M}{2}(\tilde{u}_L - \tilde{u}_R). \tag{5.4.7b}$$

To study the behavior of the rescaled numerical scheme in the low Mach regime, we extend the approach of Chalons et al. [9] to our model. We consider smooth solutions of the rescaled system (5.4.5) and are interested in how the truncation error depends on the Mach number M.
By taking the left state $L = j$, right state $R = j + 1$ and the middle state $j + 1/2$, we get the expressions

$$\tilde{u}^*_{j+1/2} = \frac{\tilde{u}_j + \tilde{u}_{j+1}}{2} + \frac{\tilde{\Pi}_j - \tilde{\Pi}_{j+1}}{2(\tilde{a})_{j+1/2}M}, \tag{5.4.8a}$$

$$\tilde{\Pi}^*_{j+1/2} = \frac{\tilde{\Pi}_j + \tilde{\Pi}_{j+1}}{2} + \frac{(\tilde{a})_{j+1/2}M}{2}(\tilde{u}_j - \tilde{u}_{j+1}). \tag{5.4.8b}$$

The update formulae for the acoustic system in terms of rescaled variables are given by

$$\tilde{\rho}_j^{n+1-} = \tilde{K}_j \tilde{\rho}_j^n, \tag{5.4.9a}$$

$$(\tilde{\rho}\tilde{u})_j^{n+1-} = \tilde{K}_j \left(\tilde{\rho}\tilde{u}\right)_j^n - \frac{\Delta\tilde{t}}{M^2\Delta\tilde{x}}\left(\tilde{\Pi}^*_{j+1/2} - \tilde{\Pi}^*_{j-1/2}\right), \tag{5.4.9b}$$

$$\left(\tilde{\rho}\tilde{E}\right)_j^{n+1-} = \tilde{K}_j \left(\tilde{\rho}\tilde{E}\right)_j^n - \frac{\Delta\tilde{t}}{\Delta\tilde{x}}\left(\tilde{\Pi}^*_{j+1/2}\tilde{u}^*_{j+1/2} - \tilde{\Pi}^*_{j-1/2}\tilde{u}^*_{j-1/2}\right), \tag{5.4.9c}$$

$$(\alpha_1\tilde{\rho}_1)_j^{n+1-} = \tilde{K}_j \left(\alpha_1\tilde{\rho}_1\right)_j^n, \tag{5.4.9d}$$

$$(\alpha_1)_j^{n+1-} = (\alpha_1)_j^n - (\phi)_j^n \frac{\Delta t}{\Delta\tilde{x}}\left(\tilde{u}^*_{j+1/2} - \tilde{u}^*_{j-1/2}\right), \tag{5.4.9e}$$

$$\tilde{K}_j = 1 - \frac{\Delta\tilde{t}}{\Delta\tilde{x}}\left(\tilde{u}^*_{j+1/2} - \tilde{u}^*_{j-1/2}\right). \tag{5.4.9f}$$

Using Taylor series in Eq. (5.4.8) one finds that there exist smooth function $f_k, k = 1, 2$ of magnitude 1 with respect to M such that

$$\tilde{u}^*_{j+1/2} = \frac{\tilde{u}_j + \tilde{u}_{j+1}}{2} + M\Delta\tilde{x}f_1(x_{j+1/2}, t^n) + \mathcal{O}\left(M\Delta\tilde{x}^2\right), \tag{5.4.10a}$$

$$\tilde{\Pi}^*_{j+1/2} = \frac{\tilde{\Pi}_j + \tilde{\Pi}_{j+1}}{2} + M\Delta\tilde{x}f_2(x_{j+1/2}, t^n) + \mathcal{O}\left(M\Delta\tilde{x}^2\right). \tag{5.4.10b}$$

From (5.4.10) it can easily be deduced that there exists a smooth function f_3 of magnitude 1 with respect to M such that

$$\tilde{u}^*_{j+1/2}\tilde{\Pi}^*_{j+1/2} = \frac{\tilde{u}_j + \tilde{u}_{j+1}}{2}\frac{\tilde{\Pi}_j + \tilde{\Pi}_{j+1}}{2} + M\Delta\tilde{x}f_3(x_{j+1/2}, t^n) + \mathcal{O}\left(M\Delta\tilde{x}^2\right). \tag{5.4.11}$$

Substitution of (5.4.10), (5.4.11) into (5.4.9) gives

$$\tilde{\rho}_j^{n+1-} = \tilde{K}_j \tilde{\rho}_j^n, \tag{5.4.12a}$$

$$(\tilde{\rho}\tilde{u})_j^{n+1-} = \tilde{K}_j \left(\tilde{\rho}\tilde{u}\right)_j^n - \frac{\Delta\tilde{t}}{M^2}\frac{\tilde{\Pi}_{j+1} - \tilde{\Pi}_{j-1}}{2\Delta\tilde{x}} + \mathcal{O}\left(\frac{\Delta\tilde{x}\Delta\tilde{t}}{M}\right), \tag{5.4.12b}$$

$$\begin{aligned}\left(\tilde{\rho}\tilde{E}\right)_j^{n+1-} &= \tilde{K}_j \left(\tilde{\rho}\tilde{E}\right)_j^n \\ &\quad - \frac{\Delta\tilde{t}}{\Delta\tilde{x}}\left(\frac{\tilde{u}_j + \tilde{u}_{j+1}}{2}\frac{\tilde{\Pi}_j + \tilde{\Pi}_{j+1}}{2} - \frac{\tilde{u}_{j-1} + \tilde{u}_j}{2}\frac{\tilde{\Pi}_{j-1} + \tilde{\Pi}_j}{2}\right) \\ &\quad + \mathcal{O}\left(\Delta\tilde{x}\Delta\tilde{t}M\right),\end{aligned} \tag{5.4.12c}$$

$$(\alpha_1\tilde{\rho}_1)_j^{n+1-} = \tilde{K}_j \left(\alpha_1\tilde{\rho}_1\right)_j^n, \tag{5.4.12d}$$

$$(\alpha_1)_j^{n+1-} = (\alpha_1)_j^n - (\phi)_j^n \Delta\tilde{t}\frac{\tilde{u}_{j+1} - \tilde{u}_{j-1}}{2\Delta\tilde{x}} + \mathcal{O}\left(M\Delta\tilde{x}\Delta\tilde{t}\right), \tag{5.4.12e}$$

$$\tilde{K}_j = 1 - \Delta\tilde{t}\frac{\tilde{u}_{j+1} - \tilde{u}_{j-1}}{2\Delta\tilde{x}} + \mathcal{O}\left(M\Delta\tilde{x}\Delta\tilde{t}\right), \tag{5.4.12f}$$

yielding [7]

$$\tilde{\rho}_j^{n+1-} = \tilde{K}_j \tilde{\rho}_j^n, \tag{5.4.13a}$$

$$(\tilde{\rho}\tilde{u})_j^{n+1-} = \tilde{K}_j \left(\tilde{\rho}\tilde{u}\right)_j^n - \frac{\Delta\tilde{t}}{M^2}\partial_{\tilde{x}}\tilde{p} + \mathcal{O}\left(\frac{\Delta\tilde{x}\Delta\tilde{t}}{M}\right) + \mathcal{O}\left(\Delta\tilde{x}^2\Delta\tilde{t}\right), \tag{5.4.13b}$$

$$\left(\tilde{\rho}\tilde{E}\right)_j^{n+1-} = \tilde{K}_j \left(\tilde{\rho}\tilde{E}\right)_j^n - \Delta\tilde{t}\partial_{\tilde{x}}(\tilde{p}\tilde{u}) + \mathcal{O}\left(\Delta\tilde{x}\Delta\tilde{t}M\right), \tag{5.4.13c}$$

$$(\alpha_1\tilde{\rho}_1)_j^{n+1-} = \tilde{K}_j \left(\alpha_1\tilde{\rho}_1\right)_j^n, \tag{5.4.13d}$$

$$(\alpha_1)_j^{n+1-} = (\alpha_1)_j^n - \phi\Delta\tilde{t}\partial_{\tilde{x}}(\tilde{u}) + \mathcal{O}\left(M\Delta\tilde{x}\Delta\tilde{t}\right) + \mathcal{O}\left(\Delta\tilde{x}^2\Delta\tilde{t}\right), \tag{5.4.13e}$$

$$\tilde{K}_j = 1 - \Delta\tilde{t}\partial_{\tilde{x}}\tilde{u} + \mathcal{O}\left(M\Delta\tilde{x}\Delta\tilde{t}\right) + \mathcal{O}\left(\Delta\tilde{x}^2\Delta\tilde{t}\right). \tag{5.4.13f}$$

This is consistent with

$$\partial_{\tilde{t}}\tilde{\tau} - \tilde{\tau}\partial_{\tilde{x}}\tilde{u} = \mathcal{O}\left(\Delta\tilde{t}\right) + \mathcal{O}\left(M\Delta\tilde{x}\right), \tag{5.4.14a}$$

$$\partial_{\tilde{t}}u + \tilde{\tau}\partial_{\tilde{x}}\tilde{p} = \mathcal{O}\left(\Delta\tilde{t}\right) + \mathcal{O}\left(\frac{\Delta\tilde{x}}{M}\right), \tag{5.4.14b}$$

$$\partial_{\tilde{t}}E + \tilde{\tau}\partial_{\tilde{x}}(\tilde{p}\tilde{u}) = \mathcal{O}\left(\Delta\tilde{t}\right) + \mathcal{O}\left(M\Delta\tilde{x}\right), \tag{5.4.14c}$$

$$\partial_{\tilde{t}}\tilde{\beta}_1 = \mathcal{O}\left(\Delta\tilde{t}\right), \tag{5.4.14d}$$

$$\partial_{\tilde{t}}(\tilde{\alpha}_1) + \phi\partial_{\tilde{x}}(\tilde{u}) = \mathcal{O}\left(\Delta\tilde{t}\right) + \mathcal{O}\left(M\Delta\tilde{x}\right) + \mathcal{O}\left(\Delta\tilde{x}^2\right). \tag{5.4.14e}$$

We are interested in the behavior of the entire system with respect to the Mach regime, i.e. the transport system has to be solved now. The rescaled transport system reads

$$\begin{aligned}&\frac{1}{\Delta\tilde{t}}(\tilde{v}_j^{n+1} - \tilde{L}_j\tilde{v}_j^{n+1-}) + \frac{1}{\Delta\tilde{x}}\left(\tilde{v}_{j+1/2}^{n+1-}\frac{\tilde{u}_j + \tilde{u}_{j+1}}{2} - \tilde{v}_{j-1/2}^{n+1-}\frac{\tilde{u}_{j-1} + \tilde{u}_j}{2}\right) \\ &= \mathcal{O}\left(\Delta\tilde{x}\right) + \mathcal{O}\left(M\Delta\tilde{x}\right),\end{aligned} \tag{5.4.15}$$

[7] Following [9], the term $\mathcal{O}\left(\Delta\tilde{x}^2\Delta\tilde{t}\right)$ is obtained by using $\partial_{\tilde{x}\tilde{x}}\tilde{p} = \mathcal{O}(M^2)$, which holds for the low Mach regime.

with

$$\tilde{L}_j = 1 + \frac{\Delta\tilde{t}}{\Delta\tilde{x}}\left(\tilde{u}^*_{j+1/2} - \tilde{u}^*_{j-1/2}\right). \tag{5.4.16}$$

Here we have used $\tilde{\Pi}^n_{j+1} = \tilde{\Pi}^n_j + \mathcal{O}\left(M^2\Delta\tilde{x}\right)$. This reduces to, by recognizing the second term as a derivative:

$$\frac{1}{\Delta\tilde{t}}(\tilde{v}^{n+1}_j - \tilde{L}_j\tilde{v}^{n+1-}_j) + \partial_{\tilde{x}}(\tilde{v}\tilde{u}) = \mathcal{O}\left(\Delta\tilde{x}\right) + \mathcal{O}\left(M\Delta\tilde{x}\right). \tag{5.4.17}$$

Hence, the behavior of the transport system with respect to the Mach regime is given by

$$\partial_{\tilde{t}}\tilde{v} + \tilde{u}\partial_{\tilde{x}}\tilde{v} = \mathcal{O}\left(\Delta\tilde{t}\right) + \mathcal{O}\left(\Delta\tilde{x}\right) + \mathcal{O}\left(M\Delta\tilde{x}\right). \tag{5.4.18}$$

To find the behavior of the entire system (i.e. acoustic and transport part) with respect to the Mach regime we substitute (5.4.13) into (5.4.17) and obtain

$$\partial_{\tilde{t}}\tilde{\rho} + \partial_{\tilde{x}}(\tilde{\rho}\tilde{u}) = \mathcal{O}\left(\Delta\tilde{t}\right) + \mathcal{O}\left(\Delta\tilde{x}\right) + \mathcal{O}\left(M\Delta\tilde{x}\right), \tag{5.4.19a}$$

$$\partial_{\tilde{t}}(\tilde{\rho}\tilde{u}) + \partial_{\tilde{x}}(\tilde{\rho}\tilde{u}^2) + \frac{1}{M^2}\partial_{\tilde{x}}\tilde{p} = \mathcal{O}\left(\Delta\tilde{t}\right) + \mathcal{O}\left(\Delta\tilde{x}\right) + \mathcal{O}\left(M\Delta\tilde{x}\right) + \mathcal{O}\left(\frac{\Delta\tilde{x}}{M}\right), \tag{5.4.19b}$$

$$\partial_{\tilde{t}}(\tilde{\rho}\tilde{E}) + \partial_{\tilde{x}}(\tilde{\rho}\tilde{E}\tilde{u}) + \partial_{\tilde{x}}(\tilde{p}\tilde{u}) = \mathcal{O}\left(\Delta\tilde{t}\right) + \mathcal{O}\left(\Delta\tilde{x}\right) + \mathcal{O}\left(M\Delta\tilde{x}\right), \tag{5.4.19c}$$

$$\partial_{\tilde{t}}(\alpha_1\tilde{\rho}_1) + \partial_{\tilde{x}}(\alpha_1\tilde{\rho}_1\tilde{u}) = \mathcal{O}\left(\Delta\tilde{t}\right) + \mathcal{O}\left(\Delta\tilde{x}\right) + \mathcal{O}\left(M\Delta\tilde{x}\right), \tag{5.4.19d}$$

$$\partial_{\tilde{t}}(\tilde{\alpha}_1) + \tilde{u}\partial_{\tilde{t}}\alpha_1 + \phi\partial_{\tilde{x}}(\tilde{u}) = \mathcal{O}\left(\Delta\tilde{t}\right) + \mathcal{O}\left(\Delta\tilde{x}\right) + \mathcal{O}\left(M\Delta\tilde{x}\right). \tag{5.4.19e}$$

5.5 The low Mach regime correction

The term $\mathcal{O}(\Delta\tilde{x}/M)$ causes trouble in the low Mach regime. To deal with this, we modify the scheme slightly. Therefore, we use a correction factor [9]. Introduce a parameter δ and replace Π^* by

$$\Pi^{*,\delta} = \frac{\Pi_L + \Pi_R}{2} + \delta\frac{a}{2}(u_L - u_R), \tag{5.5.1}$$

or in terms of scaled quantities

$$\tilde{\Pi}^{*,\delta} = \frac{\tilde{\Pi}_L + \tilde{\Pi}_R}{2} + \delta\frac{\tilde{a}M}{2}(\tilde{u}_L - \tilde{u}_R). \tag{5.5.2}$$

The other parameters do not change. Considering the equations for the rescaled variables, Eq. (5.4.6b) (or Eq. (5.4.6f)) changes to

$$\tilde{\Pi}^{*,\delta} = \tilde{\Pi}_K \mp \tilde{a}\left(\tilde{u}^* \mp \frac{1}{2}(\delta-1)(\tilde{u}_L - \tilde{u}_R) - \tilde{u}_K\right) = \tilde{\Pi}_K \mp \tilde{a}\left(\tilde{u}^{*,\delta}_K - \tilde{u}_K\right). \tag{5.5.3}$$

where

$$\tilde{u}^{*,\delta}_K = \tilde{u}^* \mp \frac{1}{2}(\delta-1)(\tilde{u}_L - \tilde{u}_R). \tag{5.5.4}$$

Again the $-$ sign is taken for $K = L$ and the $+$ sign for $K = R$. The equations for the rescaled variables change to

$$-M\tilde{u}^* = -M\tilde{u}_K \mp \tilde{a}(\tilde{\tau}_K^{*,\delta} - \tilde{\tau}_K), \tag{5.5.5a}$$
$$\tilde{\Pi}^{*,\delta} = \Pi_K \mp \tilde{a}M(\tilde{u}_K^{*,\delta} - \tilde{u}_K), \tag{5.5.5b}$$
$$M\tilde{\Pi}^{*,\delta}\tilde{u}^* = M(\tilde{\Pi u})_K \mp \tilde{a}(\tilde{E}_K^{*,\delta} - \tilde{E}_K) \tag{5.5.5c}$$
$$0 = (\tilde{\beta}_1)_K^{*,\delta} - (\tilde{\beta}_1)_K, \tag{5.5.5d}$$
$$0 = (\alpha_1)_K^{*,\delta} - (\alpha_1)_K, \tag{5.5.5e}$$
$$M\tilde{a}^2\tilde{u}_K^* = M\tilde{a}^2\tilde{u}_K \mp \tilde{a}(\tilde{\Pi}^{*,\delta} - \tilde{\Pi}_K), \tag{5.5.5f}$$

Again, we take the left state $L = j$, right state $R = j + 1$ and the middle state $j + 1/2$, and get

$$\tilde{u}_{j+1/2}^* = \frac{\tilde{u}_j + \tilde{u}_{j+1}}{2} + \frac{\tilde{\Pi}_j - \tilde{\Pi}_{j+1}}{2\tilde{a}_{j+1/2}M}, \tag{5.5.6a}$$
$$\tilde{\Pi}_{j+1/2}^{*,\delta} = \frac{\tilde{\Pi}_j + \tilde{\Pi}_{j+1}}{2} + \delta_{j+1/2}\frac{\tilde{a}_{j+1/2}M}{2}(\tilde{u}_j - \tilde{u}_{j+1}). \tag{5.5.6b}$$

The update formulae for the acoustic system are now given by, compare with (5.4.9):

$$\tilde{\rho}_j^{n+1-} = \tilde{K}_j\tilde{\rho}_j^{n+1-}, \tag{5.5.7a}$$
$$(\tilde{\rho}\tilde{u})_j^{n+1-} = \tilde{K}_j\,(\tilde{\rho}\tilde{u})_j^{n+1-} - \frac{\Delta\tilde{t}}{M^2\Delta\tilde{x}}\left(\tilde{\Pi}_{j+1/2}^{*,\delta} - \tilde{\Pi}_{j-1/2}^{*,\delta}\right), \tag{5.5.7b}$$
$$\left(\tilde{\rho}\tilde{E}\right)_j^{n+1-} = \tilde{K}_j\left(\tilde{\rho}\tilde{E}\right)_j^{n+1-} - \frac{\Delta\tilde{t}}{\Delta\tilde{x}}\left(\tilde{\Pi}_{j+1/2}^{*,\delta}\tilde{u}_{j+1/2}^* - \tilde{\Pi}_{j-1/2}^{*,\delta}\tilde{u}_{j-1/2}^*\right), \tag{5.5.7c}$$
$$(\alpha_1\tilde{\rho}_1)_j^{n+1-} = \tilde{K}_j\,(\alpha_1\tilde{\rho}_1)_j^{n+1-}, \tag{5.5.7d}$$
$$(\alpha_1)_j^{n+1-} = (\alpha_1)_j^{n+1-} - (\phi)_j^n\frac{\Delta t}{\Delta x}\left(\tilde{u}_{j+1/2}^* - \tilde{u}_{j-1/2}^*\right), \tag{5.5.7e}$$
$$\tilde{K}_j = 1 - \frac{\Delta\tilde{t}}{\Delta\tilde{x}}\left(\tilde{u}_{j+1/2}^* - \tilde{u}_{j-1/2}^*\right). \tag{5.5.7f}$$

Analogously, using Taylor series one finds that there exist smooth functions $f_k^\delta, k = 1, 2$ of magnitude 1 with respect to M such that

$$\tilde{u}_{j+1/2}^* = \frac{\tilde{u}_j + \tilde{u}_{j+1}}{2} + M\Delta\tilde{x}f_1^\delta(x_{j+1/2}, t^n) + \mathcal{O}\left(M\Delta\tilde{x}^2\right), \tag{5.5.8a}$$
$$\tilde{\Pi}_{j+1/2}^{*,\delta} = \frac{\tilde{\Pi}_j + \tilde{\Pi}_{j+1}}{2} + \delta_{j+1/2}M\Delta\tilde{x}f_2^\delta(x_{j+1/2}, t^n) + \mathcal{O}\left(M\Delta\tilde{x}^2\right). \tag{5.5.8b}$$

From (5.5.8) it can easily be deduced that there exist smooth functions $f_k, k = 3, 4$ of magnitude 1 with respect to M such that

$$\tilde{u}_{j+1/2}^*\tilde{\Pi}_{j+1/2}^* = \frac{\tilde{u}_j + \tilde{u}_{j+1}}{2}\frac{\tilde{\Pi}_j + \tilde{\Pi}_{j+1}}{2} + M\Delta\tilde{x}f_4^\delta(x_{j+1/2}, t^n)$$
$$+ \delta_{j+1/2}M\Delta\tilde{x}f_5^\delta(x_{j+1/2}, t^n) + \mathcal{O}\left(M\Delta\tilde{x}^2\right). \tag{5.5.9a}$$

Substitution of (5.5.8), (5.5.9) into (5.5.7) gives

$$\tilde{\rho}_j^{n+1-} = \tilde{K}_j \tilde{\rho}_j^{n+1-}, \tag{5.5.10a}$$

$$(\tilde{\rho}\tilde{u})_j^{n+1-} = \tilde{K}_j \left(\tilde{\rho}\tilde{u}\right)_j^{n+1-} - \frac{\Delta\tilde{t}}{M^2}\frac{\tilde{\Pi}_{j+1} - \tilde{\Pi}_{j-1}}{2\Delta\tilde{x}} + \mathcal{O}\left(\frac{\delta\Delta\tilde{x}\Delta\tilde{t}}{M}\right), \tag{5.5.10b}$$

$$\begin{aligned}\left(\tilde{\rho}\tilde{E}\right)_j^{n+1-} &= \tilde{K}_j \left(\tilde{\rho}\tilde{E}\right)_j^{n+1-} \\ &\quad - \Delta\tilde{t}\left(\frac{\tilde{u}_j + \tilde{u}_{j+1}}{2}\frac{\tilde{\Pi}_j + \tilde{\Pi}_{j+1}}{2} - \frac{\tilde{u}_{j-1} + \tilde{u}_j}{2}\frac{\tilde{\Pi}_{j-1} + \tilde{\Pi}_j}{2}\right) \\ &\quad + \mathcal{O}\left(M\Delta\tilde{x}\Delta\tilde{t}\right) + \mathcal{O}\left(M\delta\Delta\tilde{x}\Delta\tilde{t}\right),\end{aligned} \tag{5.5.10c}$$

$$(\alpha_1\tilde{\rho}_1)_j^{n+1-} = \tilde{K}_j \left(\alpha_1\tilde{\rho}_1\right)_j^{n+1-}, \tag{5.5.10d}$$

$$(\alpha_1)_j^{n+1-} = \tilde{K}_j \left(\alpha_1\right)_j^{n+1-} - (\phi)_j^n \Delta\tilde{t}\frac{\tilde{u}_{j+1} - \tilde{u}_{j-1}}{2\Delta\tilde{x}} + \mathcal{O}\left(M\Delta\tilde{x}\Delta\tilde{t}\right), \tag{5.5.10e}$$

$$\tilde{K}_j = 1 - \Delta\tilde{t}\frac{\tilde{u}_{j+1} - \tilde{u}_{j-1}}{2\Delta\tilde{x}} + \mathcal{O}\left(M\Delta\tilde{x}\Delta\tilde{t}\right), \tag{5.5.10f}$$

yielding

$$\tilde{\rho}_j^{n+1-} = \tilde{K}_j \tilde{\rho}_j^{n+1-}, \tag{5.5.11a}$$

$$(\tilde{\rho}\tilde{u})_j^{n+1-} = \tilde{K}_j \left(\tilde{\rho}\tilde{u}\right)_j^{n+1-} - \frac{\Delta\tilde{t}}{M^2}\partial_{\tilde{x}}\tilde{p} + \mathcal{O}\left(\frac{\delta\Delta\tilde{x}\Delta\tilde{t}}{M}\right) + \mathcal{O}\left(\Delta\tilde{x}^2\Delta\tilde{t}\right), \tag{5.5.11b}$$

$$\begin{aligned}\left(\tilde{\rho}\tilde{E}\right)_j^{n+1-} &= \tilde{K}_j \left(\tilde{\rho}\tilde{E}\right)_j^{n+1-} - \Delta\tilde{t}\partial_{\tilde{x}}(\tilde{p}\tilde{u}) + \mathcal{O}\left(\Delta\tilde{x}^2\Delta\tilde{t}\right) \\ &\quad + \mathcal{O}\left(M\Delta\tilde{x}\Delta\tilde{t}\right) + \mathcal{O}\left(M\delta\Delta\tilde{x}\Delta\tilde{t}\right),\end{aligned} \tag{5.5.11c}$$

$$(\alpha_1\tilde{\rho}_1)_j^{n+1-} = \tilde{K}_j \left(\alpha_1\tilde{\rho}_1\right)_j^{n+1-}, \tag{5.5.11d}$$

$$(\alpha_1)_j^{n+1-} = \tilde{K}_j \left(\alpha_1\right)_j^{n+1-} - \phi\Delta\tilde{t}\partial_{\tilde{x}}(\tilde{u}) + \mathcal{O}\left(M\Delta\tilde{x}\Delta\tilde{t}\right) + \mathcal{O}\left(\Delta\tilde{x}^2\Delta\tilde{t}\right), \tag{5.5.11e}$$

$$\tilde{K}_j = 1 - \Delta\tilde{t}\partial_{\tilde{x}}\tilde{u} + \mathcal{O}\left(M\Delta\tilde{x}\Delta\tilde{t}\right) + \mathcal{O}\left(\Delta\tilde{x}^2\Delta\tilde{t}\right). \tag{5.5.11f}$$

Note the additional δ in comparison with (5.4.13). This reveals the effect of the correction factor δ: The term $\mathcal{O}\left(\delta\Delta\tilde{x}/M\right)$ can be tuned by an appropriate choice of the parameter δ. The latter system is consistent with

$$\partial_{\tilde{t}}\tilde{\tau} - \tilde{\tau}\partial_{\tilde{x}}\tilde{u} = \mathcal{O}\left(\Delta\tilde{t}\right) + \mathcal{O}\left(M\Delta\tilde{x}\right), \tag{5.5.12a}$$

$$\partial_{\tilde{t}}u + \tilde{\tau}\partial_{\tilde{x}}\tilde{p} = \mathcal{O}\left(\Delta\tilde{t}\right) + \mathcal{O}\left(\frac{\delta\Delta\tilde{x}}{M}\right), \tag{5.5.12b}$$

$$\partial_{\tilde{t}}E + \tilde{\tau}\partial_{\tilde{x}}(\tilde{p}\tilde{u}) = \mathcal{O}\left(\Delta\tilde{t}\right) + \mathcal{O}\left(M\Delta\tilde{x}\right) + \mathcal{O}\left(\delta M\Delta\tilde{x}\right), \tag{5.5.12c}$$

$$\partial_{\tilde{t}}\tilde{\beta}_1 = \mathcal{O}\left(\Delta\tilde{t}\right), \tag{5.5.12d}$$

$$\partial_{\tilde{t}}(\tilde{\alpha}_1) + \phi\partial_{\tilde{x}}(\tilde{u}) = \mathcal{O}\left(\Delta\tilde{t}\right) + \mathcal{O}\left(M\Delta\tilde{x}\right) + \mathcal{O}\left(\Delta\tilde{x}^2\right). \tag{5.5.12e}$$

The transport system does not change. We substitute (5.5.11) into (5.4.17) to obtain the behavior with respect to the Mach regime. This yields:

$$\partial_{\tilde{t}}\tilde{\rho} + \partial_{\tilde{x}}(\tilde{\rho}\tilde{u}) = \mathcal{O}\left(\Delta\tilde{t}\right) + \mathcal{O}\left(\Delta\tilde{x}\right) + \mathcal{O}\left(M\Delta\tilde{x}\right), \tag{5.5.13a}$$

$$\partial_{\tilde{t}}(\tilde{\rho}\tilde{u}) + \partial_{\tilde{x}}(\tilde{\rho}\tilde{u}^2) + \frac{1}{M^2}\partial_{\tilde{x}}\tilde{p} = \mathcal{O}\left(\Delta\tilde{t}\right) + \mathcal{O}\left(\Delta\tilde{x}\right) + \mathcal{O}\left(M\Delta\tilde{x}\right) + \mathcal{O}\left(\frac{\delta\Delta\tilde{x}}{M}\right), \tag{5.5.13b}$$

$$\partial_{\tilde{t}}(\tilde{\rho}\tilde{E}) + \partial_{\tilde{x}}(\tilde{\rho}\tilde{E}\tilde{u}) + \partial_{\tilde{x}}(\tilde{p}\tilde{u}) = \mathcal{O}\left(\Delta\tilde{t}\right) + \mathcal{O}\left(\Delta\tilde{x}\right) + \mathcal{O}\left(M\Delta\tilde{x}\right) + \mathcal{O}\left(M\delta\Delta\tilde{x}\right), \tag{5.5.13c}$$

$$\partial_{\tilde{t}}(\alpha_1\tilde{\rho}_1) + \partial_{\tilde{x}}(\alpha_1\tilde{\rho}_1\tilde{u}) = \mathcal{O}\left(\Delta\tilde{t}\right) + \mathcal{O}\left(\Delta\tilde{x}\right) + \mathcal{O}\left(M\Delta\tilde{x}\right), \tag{5.5.13d}$$

$$\partial_{\tilde{t}}(\alpha_1) + \partial_{\tilde{x}}(\alpha_1\tilde{u}) = \mathcal{O}\left(\Delta\tilde{t}\right) + \mathcal{O}\left(\Delta\tilde{x}\right) + \mathcal{O}\left(M\Delta\tilde{x}\right). \tag{5.5.13e}$$

By choosing the correction factor $\delta = \mathcal{O}(M)$ the term $\mathcal{O}(\delta\Delta\tilde{x}/M)$ vanishes. We conclude that the analysis of Chalons et al. [9] can be extended to the five-equation model of Kapila et al.

5.6 Modified scheme

The new scheme taking the low Mach number correction into account is referred to as the *modified scheme*. The modification in comparison with the scheme of Sections 5.1-5.3 is very small.

Acoustic scheme conservative part

The HLLC flux vector (again consisting of a single state) of the modified scheme reads:

$$\left(\boldsymbol{\phi}_s^{\text{LAG},\delta}\right)^{\text{HLLC}} = \left(-u^*, \Pi^{*,\delta}, \Pi^{*,\delta}u^*, 0, 0, a^2u^*\right). \tag{5.6.1}$$

Acoustic scheme non-conservative part

This remains unchanged.

Transport scheme

This remains unchanged.

6

Shock tube problems & Numerical results

In this Chapter we test the numerical schemes of the previous Chapters on several shock tube problems. In these problems a horizontally placed shock tube is divided into a left part and a right part. These parts are separated by a membrane. To model the interaction of the fluids, the membrane is removed at time $t = 0$. The situation is visualized in Figure 6.1. All tests are performed in one dimension, with first order accuracy in space (unless stated differently) and time. A high CFL number is used to show the robustness of the schemes. To reduce the temporal errors, higher order time integration methods can be used. These methods may lead to oscillations. A higher order time integration method can not be used for the scheme of Chapter 5 (due to the first order temporal accuracy of the splitting method). For a good comparison of the schemes first order temporal accuracy is used for all schemes. Positive higher order spatial accuracy can be obtained by using flux limiters, see Chapter 2. These flux limiters are not used for the comparison of the different schemes. In a further research, see Chapter 8, higher order methods can be used.

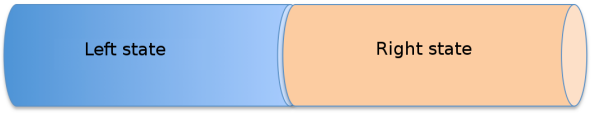

Figure 6.1: A schematic view of a shock tube composed with two fluids.

In this Chapter we first perform the tests with the PG EOS: Sod's shock tube, a pressure jump problem and a difficult test case: the no-reflection problem. Next, we perform two SG EOS test cases: A strong pressure jump problem and a water-air mixture problem. In this last problem both of the states are composed with a mixture of the fluids.

6.1 Sod's shock Tube

The first test we perform is the well-known Sod's shock tube. This test is often used for testing the accuracy of computational fluid codes and is investigated by and named after G.A. Sod [30]. This test consists of a shock tube filled with one gas at rest. Both the density and the pressure in the left state are higher than in the right state.

The initial values are given in Table 6.1. As this test is developed for the Euler equations of gas

	ρ	u	p	β_1	α_1
Left state	1.0	0.0	1.0	0.0	0.0
Right state	0.125	0.0	0.1	0.0	0.0

Table 6.1: Initial values Sod's shock tube.

dynamics, the last two equations of the five-equation model add no new information ($\beta_1 = 0, \alpha_1 = 0$). We perform this test as a preliminary test for the gas dynamic equations. The thermodynamic constants for the SG gas EOS (which is here PG EOS) are given in Table 6.2. Numerical results are performed for the five schemes: (i) The Osher-type scheme for Kapila's model (ii) The Osher-type scheme for Kreeft and Koren's model (iii) The HLLC-type scheme for Kapila's model (iv) The HLLC-type scheme for Kreeft and Koren's model (v) The Lagrange-Projection like scheme for Kapila's model without correction [a] with correction [b]. The results are obtained at time $t = 0.2$ with $N = 400$ cells. Furthermore, the CFL number is taken to be 0.95 for all schemes (i)-(v). The results are visualized in Figure 6.2.

adiabatic index	SG-pressure	SG-internal energy
$\gamma_1 = 1.6$	$\Pi_1 = 0.0$	$q_1 = 0.0$
$\gamma_2 = 1.4$	$\Pi_2 = 0.0$	$q_2 = 0.0$

Table 6.2: Thermodynamic constants for the SG EOS for Sod's shock tube.

We see that all schemes accurately capture the different waves. Both the mass fraction as well as the volume fraction remain at height zero for all schemes, as they should be. The schemes (i)-(iv) result in almost exactly the same profiles and the pairs (i) and (iii) (Kapila's model) and (ii) and (iv) (Kreeft and Koren's model) seem to be at the exact same location. The only scheme that results in slightly different profiles is the Lagrange-Project like scheme (v). The location of the rightmost shock wave is for Lagrange-Project like scheme the a little bit of. We have not tested whether this error vanishes on a finer grid. On the other hand, the rarefaction wave on the left is captured best with the scheme (v) [b]. We show a zoom of the density and pressure profile in these zones in Figure 6.3.

Here we see that the shock wave is captured by three cells only for schemes (i)-(iv), and five cells for scheme (v). Furthermore, we note that, for all the schemes, there are no oscillations visible and there is no overshoot visible.

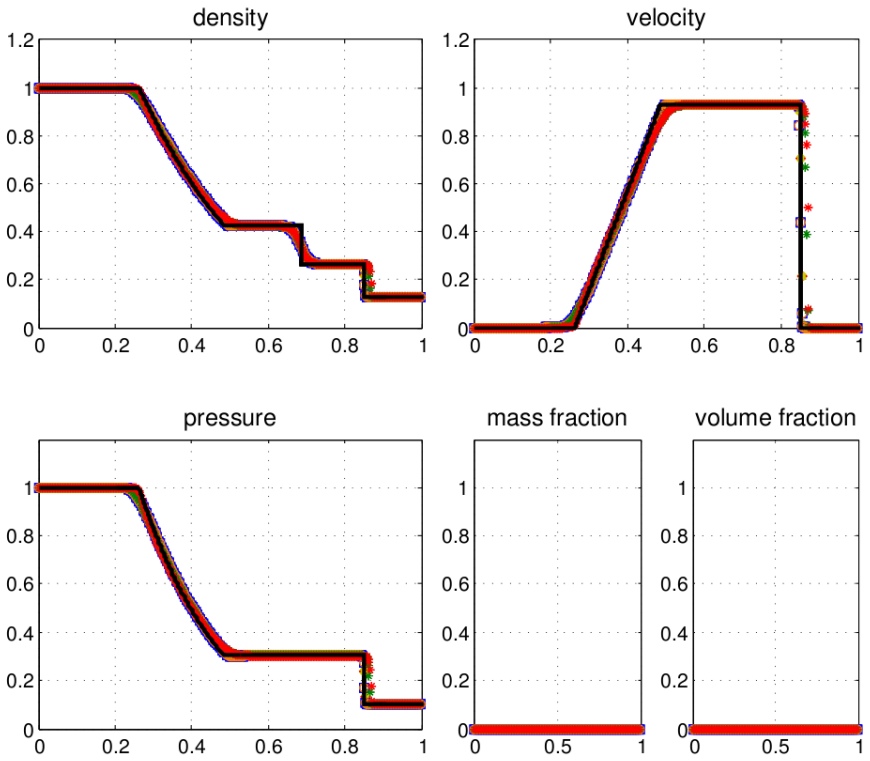

Figure 6.2: Numerical results of Sod's shock tube at time $t = 0.2$, number of grid cells $N = 400$ and CFL$= 0.95$ for (i)-(v). The various schemes are visualized by the symbols (i): $\times$, (ii): $\diamond$, (iii): $\circ$, (iv): $\square$, (v) [a]: $*$ (v) [b]: $*$. The black line displays the exact solution.

6.2 Pressure jump problem

In this test case, proposed by Barberon al. [4] and used by e.g. [11], a shock tube is filled with two gases with different density. The pressures of both sides are slightly different. The interface is located at $x = 0.5$. Due to the pressure difference, a pressure shock will propagate rightwards.
The initial values are given Table 6.3. The thermodynamic constants for the SG EOS (which is here

	ρ	u	p	β_1	α_1
Left state	10	50.0	1.1×10^5	1.0	1.0
Right state	1.0	50.0	1.0×10^5	0.0	0.0

Table 6.3: Initial values pressure jump problem.

PG EOS) are given in Table 6.4. Numerical results are obtained for the schemes: (i), (ii), (iii), (v) [a], (v) [b]. The HLLC-type scheme for Kreeft and Koren's model, scheme (iv), can not deal with the pressure jump. Apparently, the treatment of the conservative part is not robust enough. The results are obtained at time $t = 1.0 \times 10^{-3}$ with $N = 400$ cells. Furthermore, the CFL number is taken to be 0.95 for every scheme. The results are visualized in Figure 6.4.

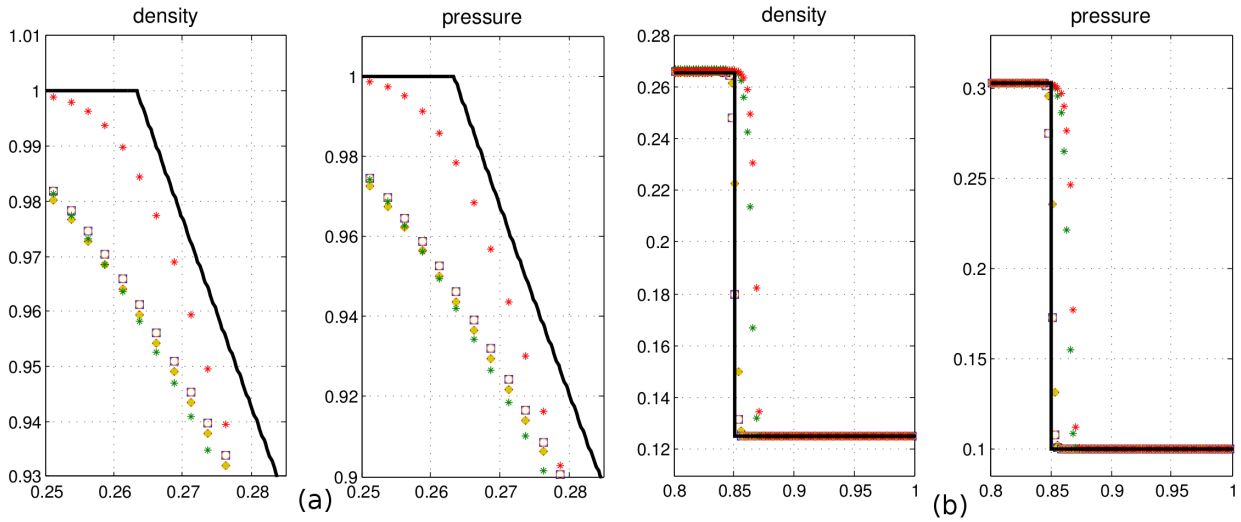

Figure 6.3: Numerical results of Sod's shock tube at time $t = 0.2$, number of grid cells $N = 400$ and CFL$= 0.95$ for (i)-(v). The various schemes are visualized by the symbols (i): $\times$, (ii): $\diamond$, (iii): $\circ$, (iv): $\square$, (v) [a]: $*$ (v) [b]: $*$. The black line displays the exact solution. This Figure shows a zoom for the density and pressure profiles of (a) the rarefaction wave left (b) the rightmost shock wave.

adiabatic index	SG-pressure	SG-internal energy
$\gamma_1 = 1.4$	$\Pi_1 = 0.0$	$q_1 = 0.0$
$\gamma_2 = 7.0$	$\Pi_2 = 3.0 \times 10^9$	$q_2 = 0.0$

Table 6.4: Thermodynamic constants for the SG EOS for pressure jump problem.

We see that all schemes capture the several waves accurately. The schemes almost give the same profiles. The height of the velocity and the pressure profile is for scheme (ii) a little off. This test case shows that all the schemes, except for (iv), can simulate flows with high pressure jumps. Furthermore, we note that, for all the schemes, there are no oscillations visible and there is no overshoot visible.

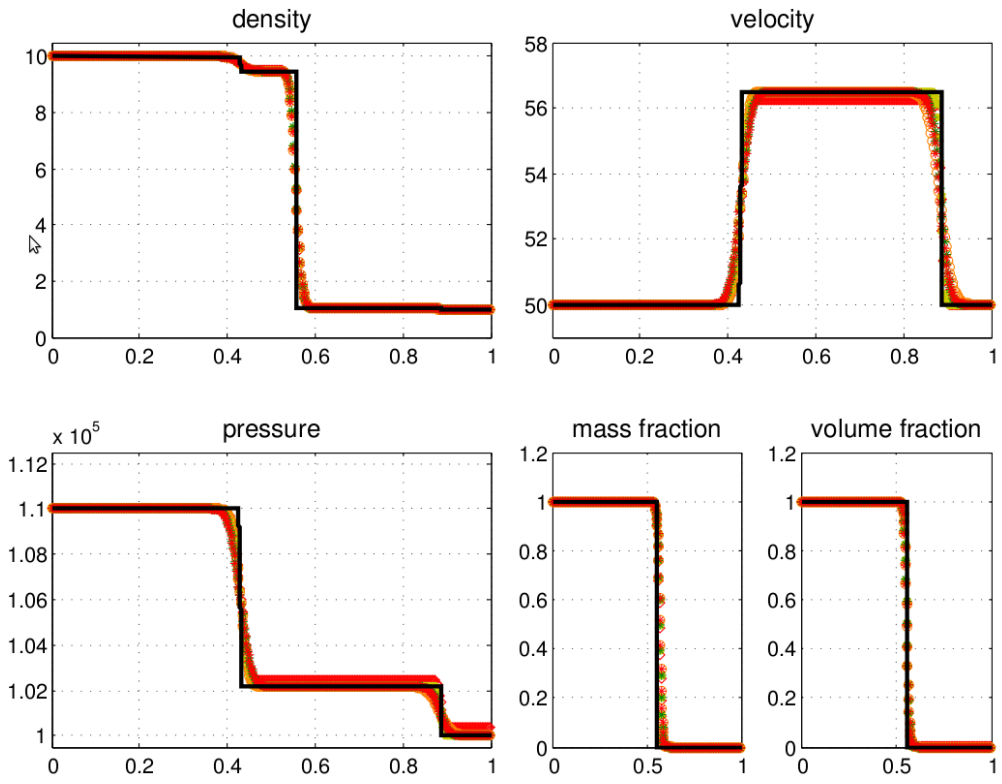

Figure 6.4: Numerical results of the strong pressure jump problem at time $t = 1.5 \times 10^{-4}$, number of grid cells $N = 400$ and CFL$= 0.95$ for (i): $\times$, (ii): $\diamond$, (iii): $\circ$, (v) [a]: $*$ (v) [b]: $*$. The black line displays the exact solution.

6.3 No-reflection problem

The third PG EOS test we perform is the so-called no-reflection problem. This problem has been studied in [22]. In this test case, consisting of a shock tube filled with two fluids, the right state is initially at rest and the left state moves towards the right state. The density and especially the pressure of the left state are high compared to the right state. This will cause the two-fluid interface and the shockwave to move rightwards. The initial conditions are chosen such that no reflection wave occurs.
The initial values are given Table 6.5. The thermodynamic constants for the SG EOS (which is here

	ρ	u	p	β_1	α_1
Left state	3.1748	9.4350	100	1.0	1.0
Right state	1.0	0.0	1.0	0.0	0.0

Table 6.5: Initial values no-reflection problem.

PG EOS) are given in Table 6.6.

adiabatic index	SG-pressure	SG-internal energy
$\gamma_1 = 1.6667$	$\Pi_1 = 0.0$	$q_1 = 0.0$
$\gamma_2 = 1.2$	$\Pi_2 = 0.0$	$q_2 = 0.0$

Table 6.6: Thermodynamic constants for the SG EOS for the no-reflection problem.

Numerical results are performed for all five schemes (i)-(v). The results are obtained at time $t = 0.02$ with $N = 400$ cells. Furthermore, the CFL number is taken to be 0.95 for all schemes (i)-(v). The results are visualized in Figure 6.5. There appear to be some differences at both the contact discontinuity (located at around $[0.05]$) and the shock wave (located at around $[0.2]$). We show a zoom of these zones in Figures 6.6 and 6.7. In Figure 6.6 we see that the schemes (ii) and (iv) do not capture the shock waves accurately. The position of shock in the velocity and pressure profile is wrong. Furthermore, in the density profile both its height and its position is wrong. In Figure 6.7 we see a small 'bump' in the profiles which is not in the exact solution. The bumps are for the two different models in the opposite direction. The 'width' of the bumps is larger for the schemes (ii) and (iv). Furthermore, the 'height' of the bumps is of the same order. It is not tested whether the results improve for a finer grid. For all the schemes, there are no oscillations visible and there is no overshoot visible.

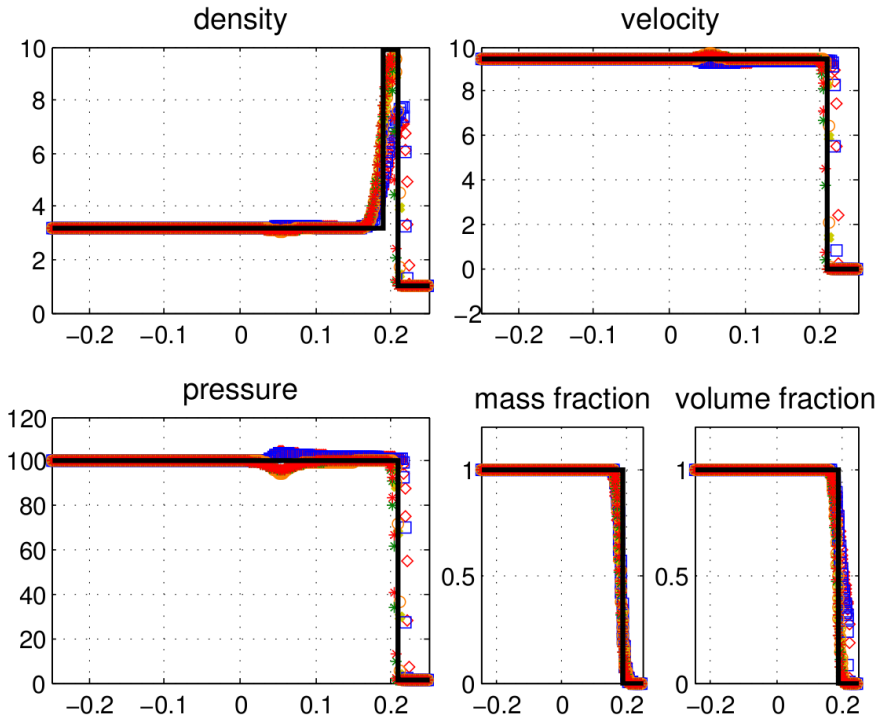

Figure 6.5: Numerical results of the no-reflection problem at time $t = 0.2$, number of grid cells $N = 400$ and CFL$= 0.95$ for (i)-(v). The various schemes are visualized by the symbols (i): $\times$ (ii): $\diamond$ (iii): $\circ$ (iv): $\square$ (v) [a]: $*$ (v) [b]: $*$. The black line displays the exact solution.

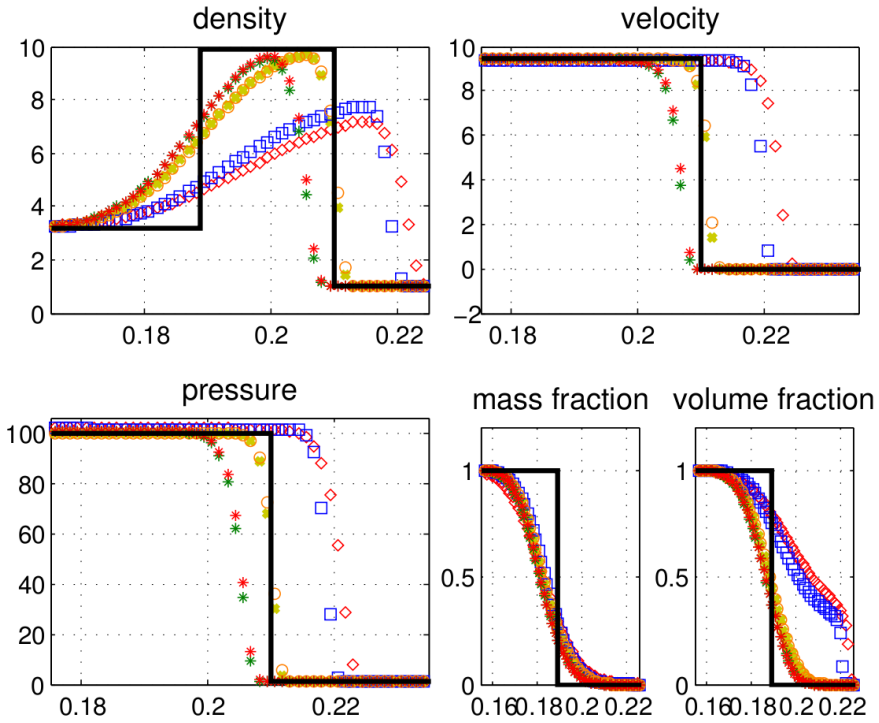

Figure 6.6: Numerical results of the no-reflection problem at time $t = 0.2$, number of grid cells $N = 400$ and CFL$= 0.95$ for (i)-(v). The various schemes are visualized by the symbols (i): $\times$ (ii): $\diamond$ (iii): $\circ$ (iv): $\square$ (v) [a]: $*$ (v) [b]: $*$. The black line displays the exact solution.

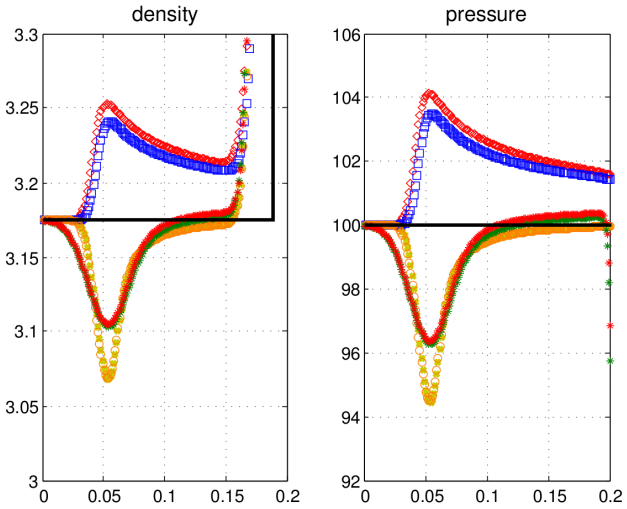

Figure 6.7: Numerical results of the no-reflection problem at time $t = 0.2$, number of grid cells $N = 400$ and CFL$= 0.95$ for (i)-(v). The various schemes are visualized by the symbols (i): $\times$, (ii): $\diamond$, (iii): $\circ$, (iv): $\square$, (v) [a]: $*$ (v) [b]: $*$. The black line displays the exact solution. This Figure shows a zoom of the rightmost shock wave for the density and pressure profiles.

This test case is apparently the hardest test case so far. None of the schemes is able to capture the shock wave in the density profile accurately. We now show the power of using a limiter for the higher order spatial accuracy. We have equipped the schemes (i) and (iii) with the Koren limiter. The spatial reconstruction is done for the primitive variables. We show the results in Figure 6.8.

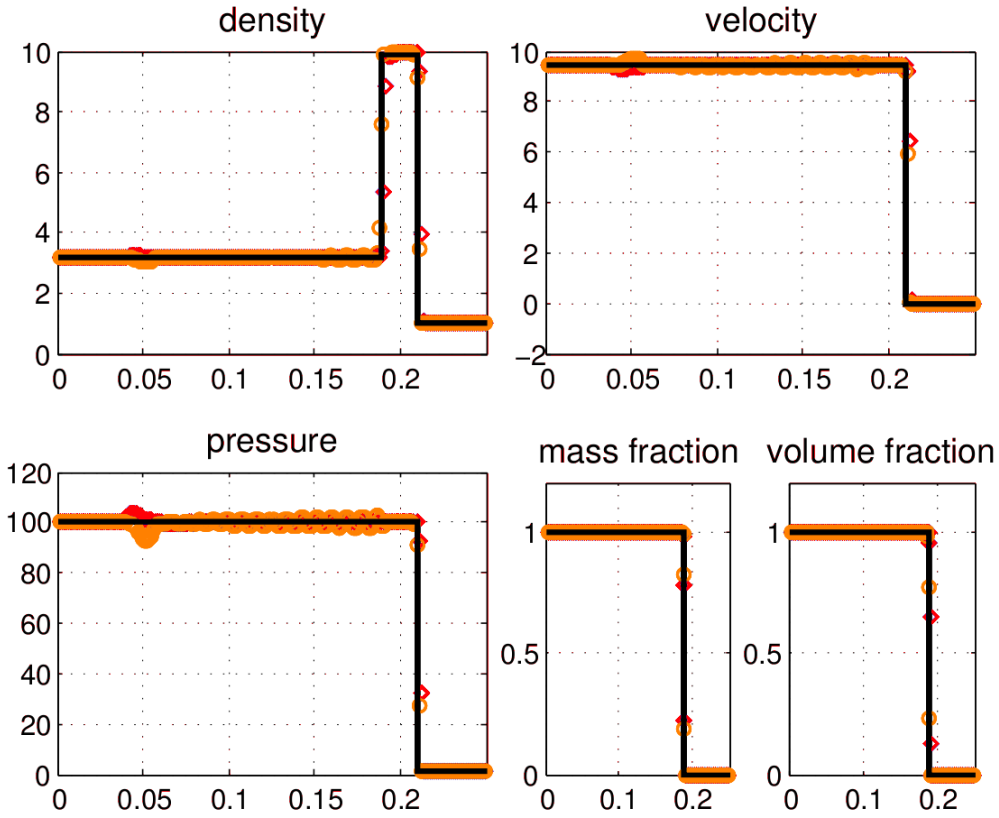

Figure 6.8: Numerical results of the no-reflection problem at time $t = 0.2$, number of grid cells $N = 400$ and CFL$= 0.45$ for (ii), (iii). The Koren limiter is used. The various schemes are visualized by the symbols (ii): $\diamond$, (iii): $\circ$. The black line displays the exact solution.

Both of the schemes capture the waves very accurately. The cost of this is that the CFL number has to be reduced to 0.45 to obtain stability and some oscillations appear. These oscillations for the density and pressure profile are shown in Figure 6.9. We see that scheme (iii) shows a lot of oscillations compared to scheme (ii). We have not tested whether this difference also appears for other shock tube problems.

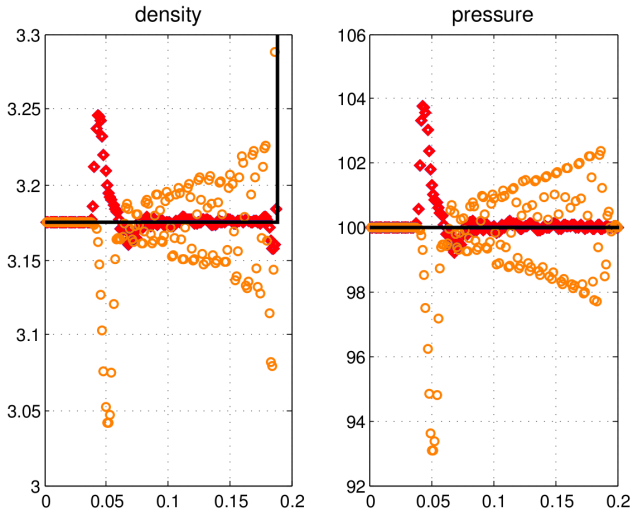

Figure 6.9: Numerical results of the no-reflection problem at time $t = 0.2$, number of grid cells $N = 400$ and CFL$= 0.45$ for (ii), (iii). The Koren limiter is used. The various schemes are visualized by the symbols (ii): $\diamond$, (iii): $\circ$. The black line displays the exact solution.

6.4 Strong pressure jump problem

In this test case, proposed by Luo et al. [24] and used in e.g. [11], a shock tube of length 100 is filled with a high-pressure gas on the left side and a low-pressure liquid on the right side. The densities of both sides are similar. The interface is located at $x = 50$. Due to the pressure difference, a strong pressure shock will propagate rightwards.

	ρ	u	p	β_1	α_1
Left state	1.271	0.0	9.119252×10^9	1.0	1.0
Right state	0.9999	0.0	1.01325×10^6	0.0	0.0

Table 6.7: Initial values strong pressure jump problem.

The initial values are given in Table 6.7. The thermodynamic constants for the SG EOS are given in Table 6.8. Numerical results are performed for the schemes: (i) The HLLC-type scheme for Kapila's model (v) The Lagrange-Projection like scheme for Kapila's model [a] without correction [b] with low Mach correction. We have chosen for these schemes because these are the best candidates for the PG EOS test cases. The results are obtained at time $t = 1.5 \times 10^{-4}$ with $N = 400$ cells. Furthermore, the CFL number is taken to be 0.95 for (iii), (v) [a] and (v) [b]. The results are visualized in Figure 6.10[1].

[1]The exact solution of the velocity profile is not shown here since it was unfortunately not available.

adiabatic index	SG-pressure	SG-internal energy
$\gamma_1 = 1.4$	$\Pi_1 = 0.0$	$q_1 = 0.0$
$\gamma_2 = 7.0$	$\Pi_2 = 3.0 \times 10^9$	$q_2 = 0.0$

Table 6.8: Thermodynamic constants for the SG EOS for the strong pressure jump problem.

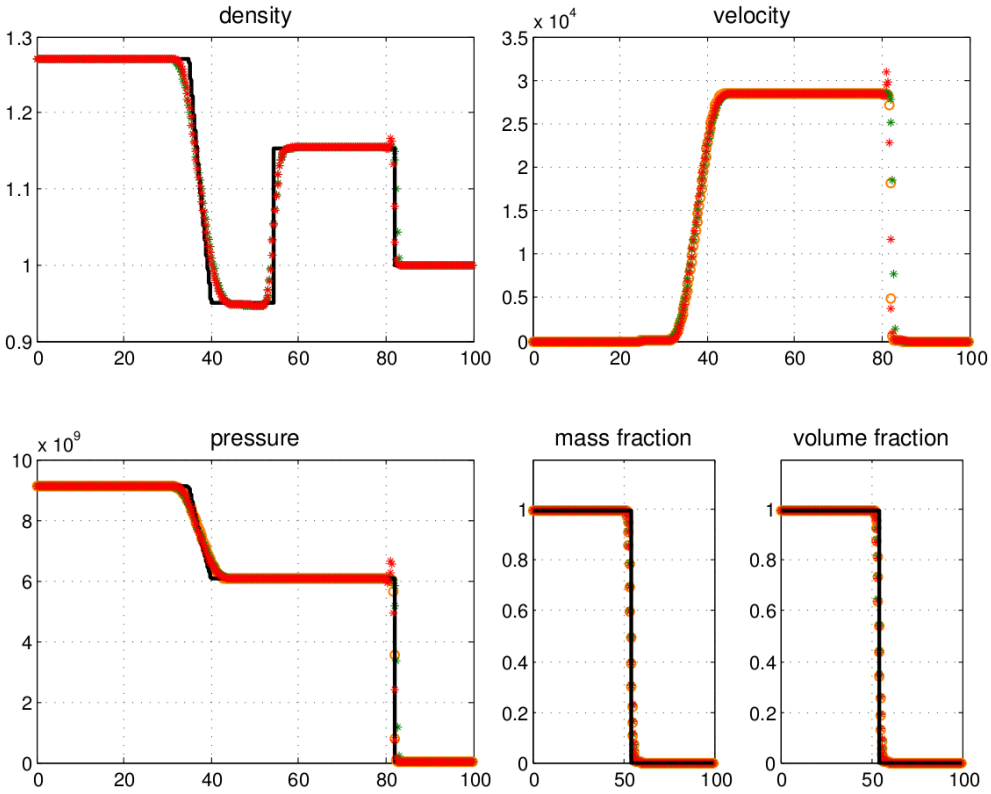

Figure 6.10: Numerical results of the strong pressure jump problem at time $t = 1.5 \times 10^{-4}$, number of grid cells $N = 400$ and CFL$= 0.95$, for (iii), (v) [a] and (v) [b]. The various schemes are visualized by the symbols (iii): $\circ$, (v) [a]: $*$, (v) [b]: $*$. The black line displays the exact solution.

We see that all schemes capture the several waves accurately. The schemes almost give the same profiles. The scheme (v) [b] shows some overshooting at the right shock wave, for which we do not have an explanation. This vanishes completely when the CFL number is reduced. No oscillations are visible. This test case shows that the schemes (iii), (v) [a], and (v) [b] can deal with the SG EOS and can simulate flows with high pressure jumps.

6.5 Water-air mixture problem

In this shock tube test we consider a water-air mixture problem. This test case have been considered by Murrone and Guillard [27] (2005) and by Kreeft and Koren [22] (2010). In contrast to all previous test cases, the shock tube is now filled with a mixture of water and air ($0 < \beta, \alpha < 1$). Both mixture states are initially at rest. The pressure of left state is 10^4 times as high as it is in the right state. The initial values are given Table in 6.9. The thermodynamic constants for the stiffened gas

	ρ	u	p	β_1	α_1
Fluid 1	525	0.0	10^9	0.0476	0.5
Fluid 2	525	0.0	10^5	0.9524	0.5

Table 6.9: Initial values water-air mixture problem.

EOS are given in Table 6.10. Numerical results are performed for the schemes: (i) The HLLC-type scheme for Kapila's model (v) The Lagrange-Projection like scheme for Kapila's model [a] without correction [b] with low Mach correction. The results are obtained at time $t = 2.0 \times 10^{-4}$ with $N = 400$ cells. Furthermore, the CFL number is taken to be 0.95 for (iii), (v) [a] and (v) [b]. The results are visualized in Figure 6.11

adiabatic index	SG-pressure	SG-internal energy
$\gamma_1 = 1.4$	$\Pi_1 = 0.0$	$q_1 = 0.0$
$\gamma_2 = 4.4$	$\Pi_2 = 6.0 \times 10^8$	$q_2 = 0.0$

Table 6.10: Thermodynamic constants for the SG EOS for the water-air mixture problem.

We see that all schemes result in almost the same profiles. The shock waves are captured very accurately as only three cells are required here. These results are in agreement with Murrone and Guillard [27] and Kreeft and Koren [22]. They also need just three cells to capture the waves. Murrone and Guillard have used a so-called VFRoe-ncv scheme (1000 cells) [7]. This scheme is an alternative (Finite Volume) Roe scheme, where 'ncv' refers to *non-conservative variables*. Kreeft and Koren have used, as discussed, the Osher-type scheme (also 400 cells). However, they make use of a second order (limiter) approximation. In contrast our results are obtained at first order. Furthermore, for all the schemes there are no oscillations visible and there is no overshoot visible.

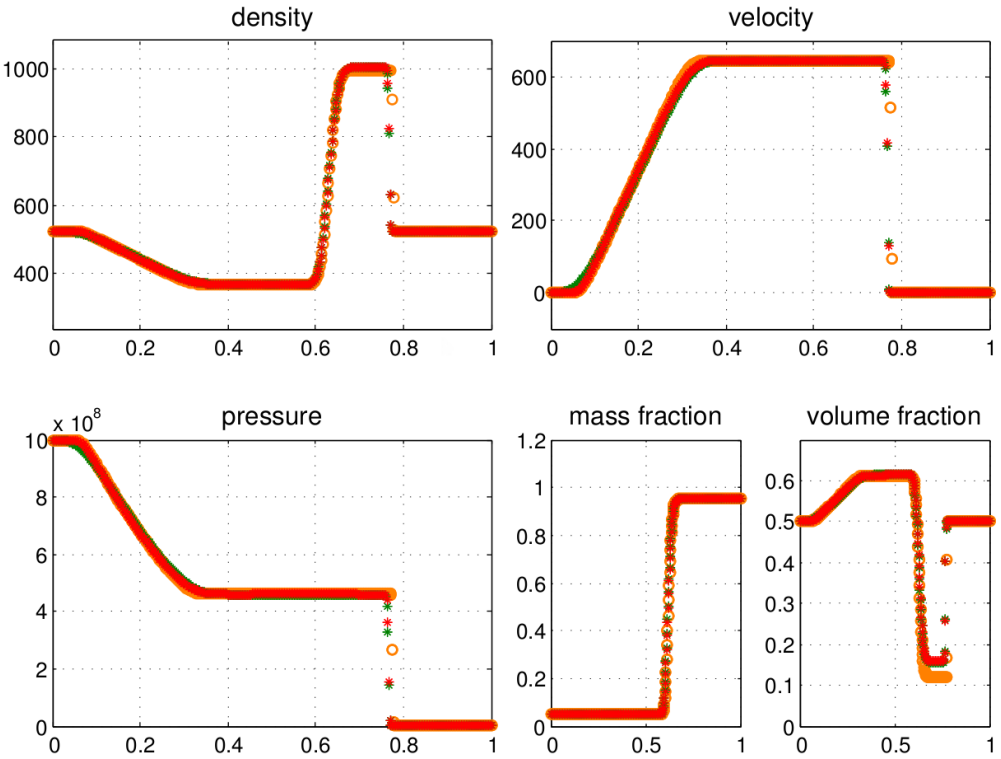

Figure 6.11: Numerical results of the water-air mixture problem at time $t = 2.0 \times 10^{-4}$, number of grid cells $N = 400$ and CFL$= 0.95$, for (iii), (v) [a] and (v) [b]. The various schemes are visualized by the symbols (iii): $\circ$, (v) [a]: $*$, (v) [b]: $*$.

By taking a closer look at the results, some small differences between the schemes (iii), (v) [a] and (v) [b] can be found. First, we see a difference in the volume fraction profile at around $[0.65, 0, 78]$. Secondly, there are some small differences at the rarefaction wave on the left at around $[0, 0.1]$. We show a zoom of the pressure and volume fraction profile in the zone of the rightmost shock wave in Figure 6.12. Interestingly, (iii) and (v) [a] show almost the exact same profile for the pressure here. Scheme (v) [b] shows a little sharper profile here, this is in better agreement with [27] and [22], see Figure 6.13. For the considered zone of the volume fraction, the profiles of (v) [a] and (v) [b] are a little higher than the profile of scheme (iii). The slightly lower profile is in better agreement with [27] and [22].

6.6 Summary and Conclusions

We have performed the PG EOS test cases for all schemes. For Sod's shock tube no major differences are found for the schemes (i)-(iv). Schemes (v)[a], (v)[b] however, shows some slightly different results. The position of the shockwave is a little bit off. On the other hand, scheme (v)[b] (Lagrange-Projection like scheme with low Mach number correction) captures the rarefaction wave on the left the best. For the pressure jump problem scheme (iv) fails, for the other schemes no visible differences are obtained. The no-reflection problem appears to be the hardest test case. The schemes for the model of Kreeft and Koren, i.e. (ii) and (iv), do not perform well here. Again the

position of the shockwave is a little bit off for schemes (v)[a] and (v)[b]. The 'bump' in the profiles is the smallest for the schemes (v)[a] and (v)[b].

Next, we have tested the schemes (iii), (v)[a], (v)[b] for two SG EOS test cases, since these schemes performed the best for the PG EOS test cases. For the strong pressure jump problem no visible differences are observed. For the water-air mixture problem the only visible difference is for the volume fraction profile, for which scheme (iii) is in better agreement with [27] and [22].

Based on these shock tube tests, we would advice to use scheme (iii). Keep in mind that schemes (v)[a] and (v)[b] are not developed for shock tube tests, but for the low Mach regime. This has to be tested still, see Chapter 8.

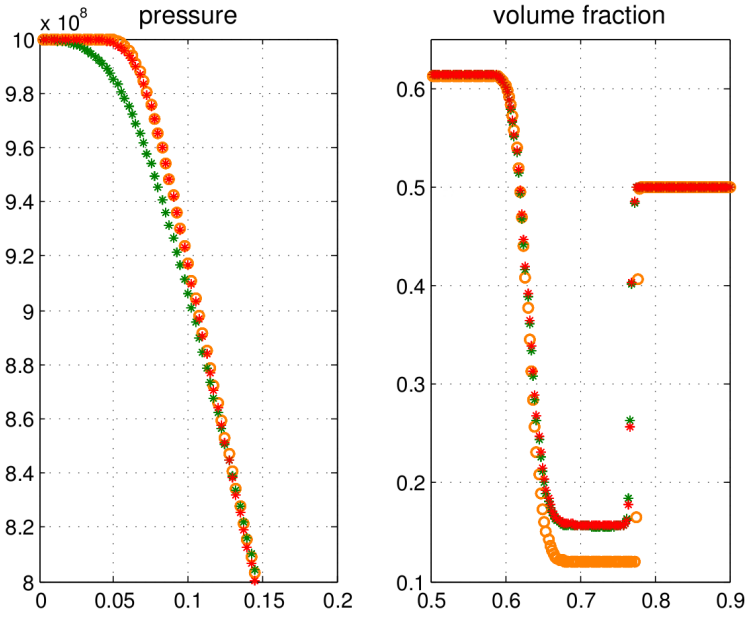

Figure 6.12: Numerical results of the water-air mixture problem at time $t = 2.0 \times 10^{-4}$, number of grid cells $N = 400$ and CFL$= 0.95$, for (iii), (v) [a] and (v) [b]. The various schemes are visualized by the symbols (iii): $\circ$, (v) [a]: $*$, (v) [b]: $*$. This Figure shows a zoom of the rightmost shock wave for the density and pressure profiles.

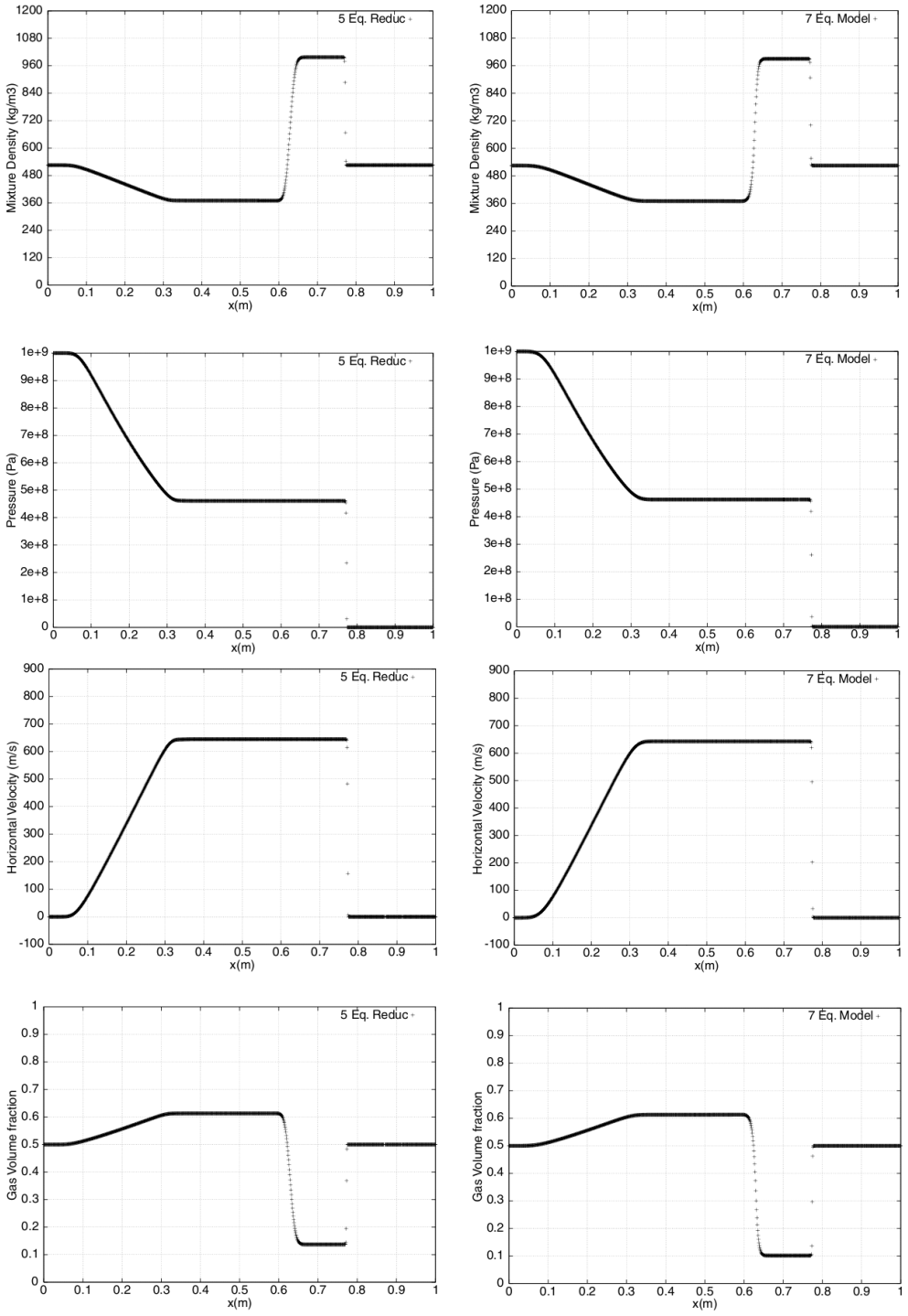

Figure 6.13: Numerical results of the water-air mixture problem by Murrone et al. On the left side the results of the five-equation model are visualized and on the right side the results of the seven-equation model are visualized. The solutions are computed with 1000 cells.

Part II

Source terms

This part describes the mass and heat transfer modeling: So-called source terms are added to the model.

7

Mass and Heat flux extension of the model

The goal of this Chapter is to derive a new five-equation model by adding mass and heat transfer to the model. There exist a few different five-equation models taking mass and heat transfer into account, e.g. [11, 29]. The convective part of these models is equal to the convective part of Kapila's model, i.e. the only difference consists of the source terms. Unlike these existing models, mass and heat transfer between the two fluids is not taken into account in the model of Kreeft and Koren.
We divide our extension into two parts (i) an isentropic mass flux extension and (ii) a non-isentropic mass and heat flux extension. The first part should be considered as a first step towards the eventual extension. In this part use is made of simple isentropic compressibility relations and no heat transfer is considered. In part (ii) this simplification is not used. The more complete non-isentropic extension should be used for numerical experiments. Furthermore, we show that our extension satisfies the second law of thermodynamics.
This Chapter is organised as follows. First, in Section 7.1 we derive the isentropic mass transfer. Next, in Section 7.2 we derive the non-isentropic mass and heat flux extension and show that the second law of thermodynamics for the non-isentropic extension is satisfied.

7.1 Isentropic mass flux extension

Let us repeat the five-equation model for convenience. The first four equations read:

$$\partial_t \rho + \nabla \cdot (\rho \mathbf{u}) = 0, \tag{7.1.1a}$$
$$\partial_t (\rho \mathbf{u}) + \nabla \cdot (\rho \mathbf{u} \otimes \mathbf{u}) + \nabla p = \mathbf{0}, \tag{7.1.1b}$$
$$\partial_t (\rho E) + \nabla \cdot (\rho E \mathbf{u}) + \nabla \cdot (p \mathbf{u}) = 0, \tag{7.1.1c}$$
$$\partial_t (\alpha_1 \rho_1) + \nabla \cdot (\alpha_1 \rho_1 \mathbf{u}) = 0, \tag{7.1.1d}$$

and for the fifth equation we have one of the following:

$$\partial_t \alpha_1 + \mathbf{u} \cdot \nabla \alpha_1 + \phi \nabla \cdot \mathbf{u} = 0, \tag{7.1.2a}$$
$$\partial_t (\alpha_1 \rho_1 E_1) + \nabla \cdot (\alpha_1 \rho_1 E_1 \mathbf{u}) + \nabla \cdot (\alpha_1 p \mathbf{u}) = p \mathbf{u} \cdot \nabla \alpha_1 + (\alpha_1 - \beta) \mathbf{u} \cdot \nabla p + p \phi \nabla \cdot \mathbf{u}. \tag{7.1.2b}$$

We assume there to be a mass flux $\dot{m}$ from fluid 2 to fluid 1 (and of course we also have the mass flux $-\dot{m}$ from fluid 1 to fluid 2). The equations for mass change to [1]

$$\partial_t(\alpha_1\rho_1) + \nabla \cdot (\alpha_1\rho_1\mathbf{u}) = \dot{m}, \tag{7.1.3a}$$
$$\partial_t(\alpha_2\rho_2) + \nabla \cdot (\alpha_2\rho_2\mathbf{u}) = -\dot{m}, \tag{7.1.3b}$$
$$\partial_t\rho + \nabla \cdot (\rho\mathbf{u}) = 0. \tag{7.1.3c}$$

The equation for the mass of fluid 2, Eq. (7.1.3b), is written to show that no mass is lost, i.e. the mass leaving fluid 2 indeed enters fluid 1. Of course, this equation can be neglected since it is obtained by subtracting (7.1.3a) from (7.1.3c).

We proceed by deriving new expressions for the mechanical rate-of-work $\tilde{\dot{W}}_M$ and thermodynamical rate-of-work $\tilde{\dot{W}}_T$ from Eq. 7.1.2b.

7.1.1 Mechanical work

The mechanical rate-of-work term is derived by combining equations for mass and momentum. The momentum equation of fluid 1 reads:

$$\partial_t(\alpha_1\rho_1\mathbf{u}) + \nabla \cdot (\alpha_1\rho_1\mathbf{u} \otimes \mathbf{u}) + \nabla(\alpha_1 p) = \mathbf{F}. \tag{7.1.4}$$

Our goal is now to derive a new expression for the force $\mathbf{F}$. By subsequently taking the inner product of $\mathbf{F}$ with $\mathbf{u}$ we get the mechanical rate-of-work term. We start off by rewriting Eq. (7.1.4):

$$\alpha_1\rho_1\partial_t\mathbf{u} + \mathbf{u}\left[\partial_t(\alpha_1\rho_1) + \nabla \cdot (\alpha_1\rho_1\mathbf{u})\right] + \alpha_1\rho_1\mathbf{u}\nabla \cdot \mathbf{u} + \nabla(\alpha_1 p) = \mathbf{F}. \tag{7.1.5}$$

By substituting the Eq. for mass of fluid 1 (7.1.3a) we arrive at

$$\alpha_1\rho_1\frac{\mathrm{D}\mathbf{u}}{\mathrm{D}t} + \dot{m}\mathbf{u} + \nabla(\alpha_1 p) = \mathbf{F}. \tag{7.1.6}$$

Next, we repeat the primitive equation of the velocity (given in Section 2.3)

$$\frac{\mathrm{D}\mathbf{u}}{\mathrm{D}t} + \frac{1}{\rho}\nabla p = \mathbf{0}. \tag{7.1.7}$$

Eliminating $\frac{\mathrm{D}\mathbf{u}}{\mathrm{D}t}$ from (7.1.6) and (7.1.7), we obtain

$$\mathbf{F} = p\nabla\alpha_1 + (\alpha_1 - \beta)\nabla p + \dot{m}\mathbf{u}, \tag{7.1.8}$$

An interpretation of the first two terms is given in [22]. The additional term $\dot{m}\mathbf{u}$ can be interpreted easily: The change of momentum due to the mass flux is the amount of mass that flows to fluid 1 at speed u. The rate of energy exchange due to mechanical work changes to

$$\tilde{\dot{W}}_M = \mathbf{F} \cdot \mathbf{u} = p\mathbf{u} \cdot \nabla\alpha_1 + (\alpha_1 - \beta)\mathbf{u} \cdot \nabla p + \dot{m}\mathbf{u} \cdot \mathbf{u} = \dot{W}_M + \dot{m}\mathbf{u} \cdot \mathbf{u}. \tag{7.1.9}$$

Note that the additional term in the mechanical rate-of-work term is a change in the kinetic energy.

[1] For a formal derivation one could follow the derivation of Section 2.2 with a slight modification.

7.1.2 Thermodynamical work

Primitive equations

Next, we derive some primitive equations, similar to [22]. The primitive equation for the bulk energy,

$$\frac{\mathrm{D}e}{\mathrm{D}t} + \frac{p}{\rho}\nabla \cdot \mathbf{u} = 0, \tag{7.1.10}$$

is still valid since its derivation only includes bulk density, bulk energy, and Eq. (7.1.7), in which the phase transfer terms do not appear. For the densities ρ_1 and ρ_2, the primitive equations change to

$$\frac{\mathrm{D}\rho_1}{\mathrm{D}t} + \frac{\rho_1}{\alpha_1}\frac{\mathrm{D}\alpha_1}{\mathrm{D}t} + \rho_1\nabla \cdot \mathbf{u} = \frac{\dot{m}}{\alpha_1}, \tag{7.1.11a}$$

$$\frac{\mathrm{D}\rho_2}{\mathrm{D}t} - \frac{\rho_2}{\alpha_2}\frac{\mathrm{D}\alpha_1}{\mathrm{D}t} + \rho_2\nabla \cdot \mathbf{u} = -\frac{\dot{m}}{\alpha_2}. \tag{7.1.11b}$$

The change of the density of fluid k is the scaled amount of mass that enters into fluid k. The primitive equation for the mass fraction β changes to:

$$\frac{\mathrm{D}\beta}{\mathrm{D}t} = \frac{1}{\rho}\left[\partial_t(\alpha_1\rho_1) + \nabla \cdot (\alpha_1\rho_1\mathbf{u})\right] - \frac{\beta}{\rho}\left[\partial_t\rho + \nabla \cdot (\rho\mathbf{u})\right] = \frac{\dot{m}}{\rho}. \tag{7.1.12}$$

The primitive equation of the internal energy e_1 can be found by combining Eq. (7.1.2b), (7.1.11a) and (7.1.7), this results in

$$\frac{\mathrm{D}e_1}{\mathrm{D}t} + \frac{p}{\rho_1}\nabla \cdot \mathbf{u} + \frac{\dot{m}}{\alpha_1\rho_1}(e_1 - \frac{1}{2}\mathbf{u} \cdot \mathbf{u}) = \frac{\tilde{\dot{W}}_T}{\alpha_1\rho_1}. \tag{7.1.13}$$

Similarly, for fluid 2 we find:

$$\frac{\mathrm{D}e_2}{\mathrm{D}t} + \frac{p}{\rho_2}\nabla \cdot \mathbf{u} - \frac{\dot{m}}{\alpha_2\rho_2}(e_2 - \frac{1}{2}\mathbf{u} \cdot \mathbf{u}) = -\frac{\tilde{\dot{W}}_T}{\alpha_2\rho_2}. \tag{7.1.14}$$

As a consistency check of the new primitive equations, one can express the material derivative of ρe by using the obtained primitive equations (7.1.11), (7.1.13) and (7.1.14) into bulk variables again, i.e. one should obtain:

$$\frac{\mathrm{D}(\rho e)}{\mathrm{D}t} = \rho\frac{\mathrm{D}e}{\mathrm{D}t} + e\frac{\mathrm{D}\rho}{\mathrm{D}t}. \tag{7.1.15}$$

By using isentropic compressibility relations, one can derive primitive equations for the volume fraction and the pressure. We only consider mass transfer. No heat is added to the flow and there is no viscosity or heat conduction. Furthermore, assume the mass transfer process is isentropic. Hence, there are no non-adiabatic processes and therefore the entropies of both fluids are constant:

$$\frac{\mathrm{D}s_1}{\mathrm{D}t} = 0, \tag{7.1.16a}$$

$$\frac{\mathrm{D}s_2}{\mathrm{D}t} = 0. \tag{7.1.16b}$$

Using these isentropic compressibility relations, we can express, for both fluids, the material derivative of the pressure into thermodynamical variables as:

$$\frac{\mathrm{D}p}{\mathrm{D}t} = \left(\frac{\partial p}{\partial \rho_1}\right)_{s_1} \frac{\mathrm{D}\rho_1}{\mathrm{D}t} + \left(\frac{\partial p}{\partial s_1}\right)_{\rho_1} \frac{\mathrm{D}s_1}{\mathrm{D}t} = c_1^2 \frac{\mathrm{D}\rho_1}{\mathrm{D}t}, \tag{7.1.17a}$$

$$\frac{\mathrm{D}p}{\mathrm{D}t} = \left(\frac{\partial p}{\partial \rho_2}\right)_{s_2} \frac{\mathrm{D}\rho_2}{\mathrm{D}t} + \left(\frac{\partial p}{\partial s_2}\right)_{\rho_2} \frac{\mathrm{D}s_2}{\mathrm{D}t} = c_2^2 \frac{\mathrm{D}\rho_2}{\mathrm{D}t}, \tag{7.1.17b}$$

where c_1, c_2 denote the speeds of sound of the fluids. By substituting the primitive equations for the densities (7.1.11), Eq. (7.1.17) can be written as:

$$\frac{\mathrm{D}p}{\mathrm{D}t} + \rho_1 c_1^2 \left(\frac{1}{\alpha_1}\frac{\mathrm{D}\alpha_1}{\mathrm{D}t} + \nabla \cdot \mathbf{u}\right) - c_1^2 \frac{\dot{m}}{\alpha_1} = 0, \tag{7.1.18a}$$

$$\frac{\mathrm{D}p}{\mathrm{D}t} + \rho_2 c_2^2 \left(-\frac{1}{\alpha_2}\frac{\mathrm{D}\alpha_1}{\mathrm{D}t} + \nabla \cdot \mathbf{u}\right) + c_2^2 \frac{\dot{m}}{\alpha_2} = 0. \tag{7.1.18b}$$

Eliminating the material derivative of the pressure from Eq. (7.1.18) yields an equation for the volume fraction

$$\frac{\mathrm{D}\alpha_1}{\mathrm{D}t} + \phi \nabla \cdot \mathbf{u} = \frac{\dot{m}}{\rho_I}, \quad \phi = \alpha_1 \alpha_2 \frac{\frac{1}{\rho_2 c_2^2} - \frac{1}{\rho_1 c_1^2}}{\frac{\alpha_1}{\rho_1 c_1^2} + \frac{\alpha_2}{\rho_2 c_2^2}}, \quad \rho_I = \frac{\frac{\rho_1 c_1^2}{\alpha_1} + \frac{\rho_2 c_2^2}{\alpha_2}}{\frac{c_1^2}{\alpha} + \frac{c_2^2}{\alpha_2}}. \tag{7.1.19}$$

Here ρ_I can be seen as an interfacial density; it is a weighted average of the densities ρ_1, ρ_2. It is interesting to see that this result has also been obtained by Saurel et al. [29]. Although their derivation is different, they have also assumed an isentropic mass transfer process. Note that for equal densities of the fluids the interfacial density reduces to the bulk density, which one expects initially. If we also have equal speed of sound of the both phases, the part of divergence of the velocity vanishes ($\phi = 0$), i.e. the equation for the volume fraction reduces to

$$\frac{\mathrm{D}\alpha_1}{\mathrm{D}t} = \frac{\dot{m}}{\rho}, \tag{7.1.20}$$

which is a simple advection equation. The primitive equation of the pressure follows by eliminating the volume fraction from Eq. (7.1.18):

$$\frac{\mathrm{D}p}{\mathrm{D}t} + \frac{1}{\tau}\left(\nabla \cdot \mathbf{u} + \frac{\dot{m}}{\rho_2} - \frac{\dot{m}}{\rho_1}\right) = \frac{\mathrm{D}p}{\mathrm{D}t} + \rho c^2 \left(\nabla \cdot \mathbf{u} + \frac{\dot{m}}{\rho_2} - \frac{\dot{m}}{\rho_1}\right) = 0. \tag{7.1.21}$$

Here, the bulk isentropic compressibility τ is defined as

$$\tau = \alpha \tau_1 + \alpha_2 \tau_2, \quad \tau_1 = \frac{1}{\rho_1 c_1^2}, \quad \tau_2 = \frac{1}{\rho_2 c_2^2}, \tag{7.1.22}$$

with τ_1, τ_2 the isentropic compressibilities of both fluids. Apparently, the primitive equation of the pressure is not influenced by the mass flux if the densities ρ_1, ρ_2 are equal.

7.1.3 Thermodynamic work relations

We derive the thermal rate-of-work term $\tilde{\dot{W}}_T$. Let us express the pressure in terms of density and internal energy of both fluids: $p = p(e_1, \rho_1), p = p(e_2, \rho_2)$. By taking the material derivative of the pressure, we get:

$$\frac{\mathrm{D}p}{\mathrm{D}t}(e_1, \rho_1) = \frac{\mathrm{D}p}{\mathrm{D}t}(e_2, \rho_2). \tag{7.1.23}$$

By expanding the derivatives into thermodynamical variables, one finds

$$\left(\frac{\partial p}{\partial e_1}\right)_{\rho_1} \frac{\mathrm{D}e_1}{\mathrm{D}t} + \left(\frac{\partial p}{\partial \rho_1}\right)_{e_1} \frac{\mathrm{D}\rho_1}{\mathrm{D}t} = \left(\frac{\partial p}{\partial e_2}\right)_{\rho_2} \frac{\mathrm{D}e_2}{\mathrm{D}t} + \left(\frac{\partial p}{\partial \rho_2}\right)_{e_2} \frac{\mathrm{D}\rho_2}{\mathrm{D}t}. \tag{7.1.24}$$

Substitution of (7.1.11), (7.1.13) and (7.1.14) into (7.1.24) gives

$$\begin{aligned}
\tilde{\dot{W}}_T \Bigg[&\frac{1}{\alpha_1\rho_1}\left(\frac{\partial p}{\partial e_1}\right)_{\rho_1} + \frac{1}{\alpha_2\rho_2}\left(\frac{\partial p}{\partial e_2}\right)_{\rho_2}\Bigg] = \\
&\frac{\mathrm{D}\alpha_1}{\mathrm{D}t}\left[\frac{\rho_1}{\alpha_1}\left(\frac{\partial p}{\partial \rho_1}\right)_{e_1} + \frac{\rho_2}{\alpha_2}\left(\frac{\partial p}{\partial \rho_2}\right)_{e_2}\right] \\
&+ \left[\rho_1\left(\frac{\partial p}{\partial \rho_1}\right)_{e_1} + \frac{p}{\rho_1}\left(\frac{\partial p}{\partial e_1}\right)_{\rho_1} - \rho_2\left(\frac{\partial p}{\partial \rho_2}\right)_{e_2} - \frac{p}{\rho_2}\left(\frac{\partial p}{\partial e_2}\right)_{\rho_2}\right] \nabla \cdot \mathbf{u} \\
&+ \frac{\dot{m}}{\alpha_1\rho_1}(e_1 - \tfrac{1}{2}\mathbf{u}\cdot\mathbf{u})\left(\frac{\partial p}{\partial e_1}\right)_{\rho_1} + \frac{\dot{m}}{\alpha_2\rho_2}(e_2 - \tfrac{1}{2}\mathbf{u}\cdot\mathbf{u})\left(\frac{\partial p}{\partial e_2}\right)_{\rho_2} \\
&- \frac{\dot{m}}{\alpha_1}\left(\frac{\partial p}{\partial \rho_1}\right)_{e_1} - \frac{\dot{m}}{\alpha_2}\left(\frac{\partial p}{\partial \rho_2}\right)_{e_2}.
\end{aligned} \tag{7.1.25}$$

Next, we make use of the speed of sound of the fluids written in thermodynamical variables:

$$\begin{aligned}
c_1^2 &= \left(\frac{\partial p}{\partial \rho_1}\right)_{s_1} = \left(\frac{\partial p}{\partial \rho_1}\right)_{e_1} + \frac{p}{\rho_1^2}\left(\frac{\partial p}{\partial e_1}\right)_{\rho_1}, \\
c_2^2 &= \left(\frac{\partial p}{\partial \rho_2}\right)_{s_2} = \left(\frac{\partial p}{\partial \rho_2}\right)_{e_2} + \frac{p}{\rho_2^2}\left(\frac{\partial p}{\partial e_2}\right)_{\rho_2}.
\end{aligned} \tag{7.1.26}$$

Substituting (7.1.19) and (7.1.26) gives an expression for the thermodynamical rate-of-work term $\dot{W}_T$:

$$\begin{aligned}
\tilde{\dot{W}}_T \Bigg[&\frac{1}{\alpha_1\rho_1}\left(\frac{\partial p}{\partial e_1}\right)_{\rho_1} + \frac{1}{\alpha_2\rho_2}\left(\frac{\partial p}{\partial e_2}\right)_{\rho_2}\Bigg] = \\
&\left(-\phi\nabla\cdot\mathbf{u} + \frac{\dot{m}}{\rho_I}\right)\left[\frac{\rho_1}{\alpha_1}\left(\frac{\partial p}{\partial \rho_1}\right)_{e_1} + \frac{\rho_2}{\alpha_2}\left(\frac{\partial p}{\partial \rho_2}\right)_{e_2}\right] \\
&+ \left(\rho_1 c_1^2 - \rho_2 c_2^2\right)\nabla\cdot\mathbf{u} \\
&+ \frac{\dot{m}}{\alpha_1\rho_1}(e_1 - \tfrac{1}{2}\mathbf{u}\cdot\mathbf{u})\left(\frac{\partial p}{\partial e_1}\right)_{\rho_1} + \frac{\dot{m}}{\alpha_2\rho_2}(e_2 - \tfrac{1}{2}\mathbf{u}\cdot\mathbf{u})\left(\frac{\partial p}{\partial e_2}\right)_{\rho_2} \\
&- \frac{\dot{m}}{\alpha_1}\left(\frac{\partial p}{\partial \rho_1}\right)_{e_1} - \frac{\dot{m}}{\alpha_2}\left(\frac{\partial p}{\partial \rho_2}\right)_{e_2}.
\end{aligned} \tag{7.1.27}$$

The thermodynamical work rate $\tilde{\dot{W}}_T$ is the superposition of a part for the divergence of the velocity, denoted as $\tilde{\dot{W}}_{T,D}$, and the mass transfer part, denoted as $\tilde{\dot{W}}_{T,m}$:

$$\tilde{\dot{W}}_T = \tilde{\dot{W}}_{T,D} + \tilde{\dot{W}}_{T,m}. \tag{7.1.28}$$

In the following derivations we will need the *Grüneisen coefficient*, denoted as Γ_k with k the number of each phase, given by

$$\Gamma_k = \frac{1}{\rho_k}\left(\frac{\partial p}{\partial e_k}\right)_{\rho_k}. \tag{7.1.29}$$

Let us introduce some notation for simplicity. The *bulk Grüneisen coefficient* Γ is defined as

$$\Gamma = \frac{\Gamma_1}{\alpha_1} + \frac{\Gamma_2}{\alpha_2}. \tag{7.1.30}$$

Furthermore, we denote

$$\begin{aligned} \sigma &= \frac{\rho_1 c_1^2}{\alpha_1} + \frac{\rho_2 c_2^2}{\alpha_2}, \\ \varsigma &= \frac{c_1^2}{\alpha_1} + \frac{c_2^2}{\alpha_2}, \end{aligned} \tag{7.1.31}$$

hence $\rho_I = \sigma/\varsigma$. Consider the terms of the divergence of the velocity. Rewriting the term in the third line of (7.1.27) yields

$$\rho_1 c_1^2 - \rho_2 c_2^2 = \phi\sigma. \tag{7.1.32}$$

By again using (7.1.26) for the first term in the right-hand side of (7.1.27), we can write

$$\begin{aligned} &-\phi\left[\frac{\rho_1}{\alpha_1}\left(\frac{\partial p}{\partial \rho_1}\right)_{e_1} + \frac{\rho_2}{\alpha_2}\left(\frac{\partial p}{\partial \rho_2}\right)_{e_2}\right] - \rho_1 c_1^2 - \rho_2 c_2^2 \\ &= -\phi\left(\sigma - p\Gamma\right) + \phi\sigma \\ &= p\phi\Gamma. \end{aligned} \tag{7.1.33}$$

This means that we get for the contribution of the divergence of the velocity part to the thermodynamic rate-of-work:

$$\tilde{\dot{W}}_{T,D} = p\phi\nabla\cdot\mathbf{u}. \tag{7.1.34}$$

Next, we consider the contribution of the mass transfer part. The speed of sound (7.1.26) is also used to simplify the following terms:

$$\begin{aligned} &\frac{1}{\rho_I}\left[\frac{\rho_1}{\alpha_1}\left(\frac{\partial p}{\partial \rho_1}\right)_{e_1} + \frac{\rho_2}{\alpha_2}\left(\frac{\partial p}{\partial \rho_2}\right)_{e_2}\right] - \frac{1}{\alpha_1}\left(\frac{\partial p}{\partial \rho_1}\right)_{e_1} - \frac{1}{\alpha_2}\left(\frac{\partial p}{\partial \rho_2}\right)_{e_2} \\ &= \frac{1}{\rho_I}\left[\sigma - p\Gamma\right] + \frac{p}{\alpha_1\rho_1^2}\left(\frac{\partial p}{\partial e_1}\right)_{\rho_1} + \frac{p}{\alpha_2\rho_2^2}\left(\frac{\partial p}{\partial e_2}\right)_{\rho_2} - \varsigma \\ &= p\left[\frac{1}{\alpha_1\rho_1^2}\left(\frac{\partial p}{\partial e_1}\right)_{\rho_1} + \frac{1}{\alpha_2\rho_2^2}\left(\frac{\partial p}{\partial e_2}\right)_{\rho_2}\right] - \frac{p\Gamma}{\rho_I}. \end{aligned} \tag{7.1.35}$$

Combining (7.1.27) and (7.1.35) gives the contribution of the mass transfer part:

$$\tilde{\dot{W}}_{T,\dot{m}} = -\frac{p}{\rho_I}\dot{m} + \frac{\dot{m}}{\Gamma}\left[\frac{\Gamma_1}{\alpha_1}\left((e_1 - \frac{1}{2}\mathbf{u}\cdot\mathbf{u}) + \frac{p}{\rho_1}\right) + \frac{\Gamma_2}{\alpha_2}\left((e_2 - \frac{1}{2}\mathbf{u}\cdot\mathbf{u}) + \frac{p}{\rho_2}\right)\right]. \tag{7.1.36}$$

7.1.4 Isentropic mass flux extension model

The equations (7.1.9), (7.1.28), (7.1.34) and (7.1.36) give us the total rate of energy exchange per unit volume between fluid 2 and fluid 1:

$$\begin{aligned}\tilde{\dot{W}} = \quad & p\mathbf{u}\cdot\nabla\alpha_1 + (\alpha_1 - \beta)\mathbf{u}\cdot\nabla p + p\phi\nabla\cdot\mathbf{u} \\ & + \dot{m}\tfrac{1}{2}\mathbf{u}\cdot\mathbf{u} - \dot{m}\frac{p}{\rho_I} + \frac{\dot{m}}{\Gamma}\left[\frac{\Gamma_1}{\alpha_1}\left(e_1 + \frac{p}{\rho_1}\right) + \frac{\Gamma_2}{\alpha_2}\left(e_2 + \frac{p}{\rho_2}\right)\right].\end{aligned} \tag{7.1.37}$$

The term $\dot{m}\frac{1}{2}\mathbf{u}\cdot\mathbf{u}$ represents the change in kinetic energy. An interpretation of the term $-p\mathrm{D}\alpha_1/\mathrm{D}t$ is given in [22]. The latter two terms represent the mass rate in interfacial energy $\dot{m}e_I$, where the interfacial energy is given by

$$e_I = \frac{1}{\Gamma}\left[\frac{\Gamma_1}{\alpha_1}\left(e_1 + \frac{p}{\rho_1}\right) + \frac{\Gamma_2}{\alpha_2}\left(e_2 + \frac{p}{\rho_2}\right)\right] - \frac{p}{\rho_I}. \tag{7.1.38}$$

The isentropic model with mass transfer reads:

$$\partial_t\rho + \nabla\cdot(\rho\mathbf{u}) = 0, \tag{7.1.39a}$$
$$\partial_t(\rho\mathbf{u}) + \nabla\cdot(\rho\mathbf{u}\otimes\mathbf{u}) + \nabla p = \mathbf{0}, \tag{7.1.39b}$$
$$\partial_t(\rho E) + \nabla\cdot(\rho E\mathbf{u}) + \nabla(p\mathbf{u}) = \mathbf{0}, \tag{7.1.39c}$$
$$\partial_t(\alpha_1\rho_1) + \nabla\cdot(\alpha_1\rho_1\mathbf{u}) = \dot{m}, \tag{7.1.39d}$$

with for the fifth equation one of the following:

$$\partial_t(\alpha_1\rho_1 E_1) + \nabla\cdot(\alpha_1\rho_1 E_1\mathbf{u}) + \nabla\cdot(\alpha_1 p\mathbf{u}) = \dot{W} + \dot{m}\left(e_I + \frac{1}{2}\mathbf{u}\cdot\mathbf{u}\right) \tag{7.1.40a}$$
$$\partial_t\alpha_1 + \mathbf{u}\cdot\nabla\alpha_1 + \phi\nabla\cdot\mathbf{u} = \frac{\dot{m}}{\rho_I}, \tag{7.1.40b}$$

with $\dot{W}$ defined in Chapter 2.

7.2 Non-isentropic mass and heat flux extension

In this Section we extend the model further by modelling both mass and heat transfer. An important aspect here, in contrast to the previous Section, is that we do not assume an isentropic process. As a result, the derivations are more involved.
The heat transfer term, denoted as Q, appears in the energy equations of the single fluids. Consider the model equations in Section 7.1.4. The equations for mass, Eq. (7.2.28a) and Eq. (7.2.28d), momentum, Eq. (7.2.28b) and bulk energy, Eq. (7.2.28c), do not change. The fifth equation, Eq.

(7.1.40), however, has to be updated. We assume that the equation of the volume fraction can be written as:

$$\frac{\mathrm{D}\alpha_1}{\mathrm{D}t} + \phi\nabla\cdot\mathbf{u} = \frac{\dot{m}}{\tilde{\rho}_I} + \frac{Q}{\chi}, \tag{7.2.1}$$

where $\tilde{\rho}_I$ and χ have to be determined. Hence, we assume that the mass and heat transfer terms have no influence on the convective part of the model. Furthermore, we have assumed that the mass and heat transfer terms are modelled separately. This means that it is possible to have only mass transfer or only heat transfer. The form of the equation is in agreement with [11, 29].
By a straightforward derivation, given in Appendix B.3, an expression for the thermodynamical rate-of-work term (in terms of the material derivative of the volume fraction) can be found:

$$\begin{aligned}\frac{\mathrm{D}\alpha_1}{\mathrm{D}t}(\sigma - p\Gamma) = {} & \nabla\cdot\mathbf{u}\phi\sigma + \dot{m}\varsigma + \tilde{\dot{W}}_T\Gamma \\ & -\dot{m}\left(e_1 - \frac{1}{2}\mathbf{u}\cdot\mathbf{u} + \frac{p}{\rho_1}\right)\frac{\Gamma_1}{\alpha_1} \\ & -\dot{m}\left(e_2 - \frac{1}{2}\mathbf{u}\cdot\mathbf{u} + \frac{p}{\rho_2}\right)\frac{\Gamma_2}{\alpha_2}.\end{aligned} \tag{7.2.2}$$

Substitution of (7.2.1) into this relation, Eq. (7.2.2), the expression for the thermodynamical rate-of-work term is obtained

$$\begin{aligned}\tilde{\dot{W}}_T\Gamma = {} & p\Gamma\nabla\cdot\mathbf{u} + \\ & \dot{m}(e_1 - \tfrac{1}{2}\mathbf{u}\cdot\mathbf{u} + \frac{p}{\rho_1})\frac{\Gamma_1}{\alpha_1} + \dot{m}(e_2 - \tfrac{1}{2}\mathbf{u}\cdot\mathbf{u} + \frac{p}{\rho_2})\frac{\Gamma_2}{\alpha_2} \\ & +\dot{m}\left(\frac{\sigma - p\Gamma}{\tilde{\rho}_I} - \varsigma\right) + Q\frac{\sigma - p\Gamma}{\chi}\end{aligned} \tag{7.2.3}$$

The equations (7.1.9) and (7.2.3) give us the total rate of energy exchange per unit volume between fluid 2 and fluid 1:

$$\begin{aligned}\tilde{\dot{W}} = {} & \dot{W} \\ & +\frac{\dot{m}}{\Gamma}\left[(e_1 + \frac{p}{\rho_1})\frac{\Gamma_1}{\alpha_1} + \dot{m}(e_2 + \frac{p}{\rho_2})\frac{\Gamma_2}{\alpha_2}\right] - \dot{m}\frac{p}{\tilde{\rho}_I} + \dot{m}\tfrac{1}{2}\mathbf{u}\cdot\mathbf{u} + \frac{\dot{m}\sigma}{\Gamma}\left(\frac{1}{\tilde{\rho}_I} - \frac{\varsigma}{\sigma}\right) \\ & +\frac{Q}{\chi}\left(\frac{\sigma}{\Gamma} - p\right).\end{aligned} \tag{7.2.4}$$

The first line of Eq. (7.2.4) consists of the convective part, the second line of the mass transfer part and the third line of the heat transfer part. Consider the heat flux term. Starting at the volume fraction, Eq. (7.2.1), the heat transfer term is multiplied with $\sigma/\Gamma - p$. Since Q is the heat flux in the equation of the internal energy, we require $\chi = \sigma/\Gamma - p$. Consider the mass transfer terms. Except for the additional term $\frac{\dot{m}\sigma}{\Gamma}\left(\frac{1}{\tilde{\rho}_I} - \frac{\varsigma}{\sigma}\right)$ the mass transfer is the same as for the isentropic model. For $\tilde{\rho}_I = \sigma/\varsigma = \rho_I$ this additional term vanishes.

7.2.1 Determination $\tilde{\rho_I}$

In this Subsection we determine the term $\tilde{\rho_I}$. The derivation is similar to [36], however they consider a seven-equation model where we consider a five-equation model. Let us consider the equations concerning mechanical relaxation for fluid 1:

$$\partial_t \alpha_1 = \dot{m}/\tilde{\rho_I}, \tag{7.2.5a}$$
$$\partial_t \alpha_1 \rho_1 = \dot{m}, \tag{7.2.5b}$$
$$\partial_t (\rho \mathbf{u}) = \mathbf{0}, \tag{7.2.5c}$$
$$\partial_t (\alpha_1 \rho_1 E_1) = \left(\tilde{e}_I + \frac{1}{2} \mathbf{u} \cdot \mathbf{u} \right) \dot{m}, \tag{7.2.5d}$$

where $\tilde{e}_I = \tilde{e}_I(\tilde{\rho}_I)$ defined in (7.1.38) in which ρ_I is replaced by $\tilde{\rho}_I$. From Eq. (7.2.5b) and (7.2.5d) it follows:

$$\alpha_1 \rho_1 \partial_t (e_1) = \dot{m} \left(\tilde{e}_I - e_1 \right). \tag{7.2.6}$$

The internal energy of fluid 1, e_1, can be expressed in terms of pressure p and density of fluid 1 ρ_1: $e_1 = e_1(p, \rho_1)$ [33]. Differentiate (7.2.21) with respect to t to find

$$\alpha_1 \rho_1 \left(\frac{\partial e_1}{\partial p} \right)_{\rho_1} \frac{\partial p}{\partial t} + \alpha_1 \rho_1 \left(\frac{\partial e_1}{\partial \rho_1} \right)_p \frac{\partial \rho_1}{\partial t} = \tilde{\rho_I} \left(\tilde{e}_I - e_1 \right) \partial_t \alpha_1. \tag{7.2.7}$$

From (7.2.5a), (7.2.5b) we get

$$\alpha_1 \partial_t \rho_1 = \left(\tilde{\rho_I} - \rho_1 \right) \partial_t \alpha_1 \tag{7.2.8}$$

By substituting (7.2.8) into (7.2.7) we obtain

$$\alpha_1 \rho_1 \left(\frac{\partial e_1}{\partial p} \right)_{\rho_1} \frac{\partial p}{\partial t} + \rho_1 (\tilde{\rho_I} - \rho_1) \left(\frac{\partial e_1}{\partial \rho_1} \right)_p \frac{\partial \alpha_1}{\partial t} = \tilde{\rho_I} \left(\tilde{e}_I - e_1 \right) \partial_t \alpha_1. \tag{7.2.9}$$

We can now express the pressure in terms of variables of fluid 1:

$$\frac{\partial p}{\partial t} = \frac{\Gamma_1}{\alpha_1} \left(-\rho_1 (\tilde{\rho_I} - \rho_1) \left(\frac{\partial e_1}{\partial \rho_1} \right)_p + \tilde{\rho_I} \left(\tilde{e}_I - e_1 \right) \right) \partial_t \alpha_1. \tag{7.2.10}$$

Similarly, by using the equations of fluid 2 we obtain

$$\frac{\partial p}{\partial t} = -\frac{\Gamma_2}{\alpha_2} \left(-\rho_2 (\tilde{\rho_I} - \rho_2) \left(\frac{\partial e_2}{\partial \rho_2} \right)_p + \tilde{\rho_I} \left(\tilde{e}_I - e_2 \right) \right) \partial_t \alpha_1. \tag{7.2.11}$$

Combining (7.1.38), (7.2.10) and (7.2.11) we arrive at

$$\begin{aligned} &\frac{\Gamma_1}{\alpha_1} \left(-\rho_1 (\tilde{\rho_I} - \rho_1) \left(\frac{\partial e_1}{\partial \rho_1} \right)_p + \tilde{\rho_I} \left(\left(\frac{1}{\Gamma} \left[\frac{\Gamma_1}{\alpha_1} \left(e_1 + \frac{p}{\rho_1} \right) + \frac{\Gamma_2}{\alpha_2} \left(e_2 + \frac{p}{\rho_2} \right) \right] - \frac{p}{\tilde{\rho_I}} \right) - e_1 \right) \right) \\ &= -\frac{\Gamma_2}{\alpha_2} \left(-\rho_2 (\tilde{\rho_I} - \rho_2) \left(\frac{\partial e_2}{\partial \rho_2} \right)_p + \tilde{\rho_I} \left(\left(\frac{1}{\Gamma} \left[\frac{\Gamma_1}{\alpha_1} \left(e_1 + \frac{p}{\rho_1} \right) + \frac{\Gamma_2}{\alpha_2} \left(e_2 + \frac{p}{\rho_2} \right) \right] - \frac{p}{\tilde{\rho_I}} \right) - e_2 \right) \right), \end{aligned}$$

(7.2.12)

which can be simplified to

$$\begin{aligned}&\tilde{\rho_I}\left[\frac{\Gamma_1}{\alpha_1}\left(-\rho_1\left(\frac{\partial e_1}{\partial \rho_1}\right)_p+\frac{p}{\rho_1}\right)+\frac{\Gamma_2}{\alpha_2}\left(-\rho_2\left(\frac{\partial e_2}{\partial \rho_2}\right)_p+\frac{p}{\rho_2}\right)\right]= \\ &-\frac{\Gamma_1}{\alpha_1}\rho_1^2\left(\frac{\partial e_1}{\partial \rho_1}\right)_p-\frac{\Gamma_2}{\alpha_2}\rho_2^2\left(\frac{\partial e_2}{\partial \rho_2}\right)_p+p\Gamma.\end{aligned} \tag{7.2.13}$$

Since our goal is to find an expression for the interfacial density. This means that we only need to simplify (7.2.13). The speed of sound is given by

$$\rho_k c_k^2=\left(\frac{p}{\rho_k^2}-\left(\frac{\partial e_k}{\partial \rho_k}\right)_p\right)\left(\frac{\partial e_k}{\partial p}\right)_{\rho_k}^{-1}. \tag{7.2.14}$$

From this we can deduce:

$$\left(\frac{\partial e_k}{\partial \rho_k}\right)_p=\frac{p}{\rho_k^2}-c_k^2\left(\frac{\partial e_k}{\partial p}\right)_{\rho_k}=\frac{p}{\rho_k^2}-\frac{c_k^2}{\Gamma_k\rho_k}. \tag{7.2.15}$$

Substituting gives

$$\begin{aligned}&\tilde{\rho_I}\left[\frac{\Gamma_1}{\alpha_1}\left(-\rho_1\left(\frac{p}{\rho_1^2}-\frac{c_1^2}{\Gamma_1\rho_1}\right)+\frac{p}{\rho_1}\right)+\frac{\Gamma_2}{\alpha_2}\left(-\rho_2\left(\frac{p}{\rho_2^2}-\frac{c_2^2}{\Gamma_2\rho_2}\right)+\frac{p}{\rho_2}\right)\right]= \\ &-\frac{\Gamma_1}{\alpha_1}\rho_1^2\left(\frac{p}{\rho_1^2}-\frac{c_1^2}{\Gamma_1\rho_1}\right)-\frac{\Gamma_2}{\alpha_2}\rho_2^2\left(\frac{p}{\rho_2^2}-\frac{c_2^2}{\Gamma_2\rho_2}\right)+p\Gamma,\end{aligned} \tag{7.2.16}$$

which simplifies to

$$\tilde{\rho_I}=\frac{\frac{\rho_1 c_1^2}{\alpha_1}+\frac{\rho_2 c_2^2}{\alpha_2}}{\frac{c_1^2}{\alpha}+\frac{c_2^2}{\alpha_2}}=\frac{\sigma}{\varsigma}=\rho_I. \tag{7.2.17}$$

This is an interesting result; apparently the contribution of the mass flow to the rate-of-work term is the same for isentropic and non-isentropic flow.

7.2.2 Determination χ

In this Subsection we derive the parameter χ. Again, the derivation is similar to [36], Let us consider the equations concerning temperature relaxation for fluid 1:

$$\partial_t \alpha_1 = Q/\chi, \tag{7.2.18a}$$
$$\partial_t \alpha_1\rho_1 = 0, \tag{7.2.18b}$$
$$\partial_t (\rho \mathbf{u}) = \mathbf{0}, \tag{7.2.18c}$$
$$\partial_t (\alpha_1\rho_1 E_1) = Q. \tag{7.2.18d}$$

From Eq. (7.2.18a) and (7.2.18d) it follows:

$$\partial_t(\alpha_1\rho_1 E_1) = \chi\partial_t\alpha_1. \tag{7.2.19}$$

Next, we can write

$$\partial_t(\alpha_1\rho_1 E_1) = E_1\partial_t(\alpha_1\rho_1) + \alpha_1\rho_1\partial_t e_1 + \mathbf{u}\left[\partial_t(\alpha_1\rho_1\mathbf{u}) - \mathbf{u}\partial_t(\alpha_1\rho_1)\right]. \tag{7.2.20}$$

By using (7.2.18b), (7.2.19), (7.2.18c) we obtain

$$\partial_t(\alpha_1\rho_1 E_1) = \alpha_1\rho_1\partial_t e_1 = \chi\partial_t\alpha_1. \tag{7.2.21}$$

The internal energy of fluid 1, e_1, can be expressed in terms of pressure p and density of fluid 1 ρ_1: $e_1 = e_1(p, \rho_1)$ [33]. Differentiate (7.2.21) with respect to t to find

$$\alpha_1\rho_1\left(\frac{\partial e_1}{\partial p}\right)_{\rho_1}\frac{\partial p}{\partial t} + \alpha_1\rho_1\left(\frac{\partial e_1}{\partial \rho_1}\right)_{p}\frac{\partial \rho_1}{\partial t} = \chi\partial_t\alpha_1. \tag{7.2.22}$$

Substitute (7.2.18b) into (7.2.22), this yields

$$\alpha_1\rho_1\left(\frac{\partial e_1}{\partial p}\right)_{\rho_1}\frac{\partial p}{\partial t} - \rho_1^2\left(\frac{\partial e_1}{\partial \rho_1}\right)_{p}\frac{\partial \alpha_1}{\partial t} = \chi\partial_t\alpha_1. \tag{7.2.23}$$

We can now express the pressure in terms of variables of fluid 1:

$$\partial_t p = \frac{\chi + \rho_1^2\left(\frac{\partial e_1}{\partial \rho_1}\right)_p}{\alpha_1\rho_1\left(\frac{\partial e_1}{\partial p}\right)_{\rho_1}}\partial_t\alpha_1. \tag{7.2.24}$$

Similarly, by using the equations of fluid 2 we obtain

$$\frac{\partial p}{\partial t} = -\frac{\chi + \rho_2^2\left(\frac{\partial e_2}{\partial \rho_2}\right)_p}{\alpha_2\rho_2\left(\frac{\partial e_2}{\partial p}\right)_{\rho_2}}\partial_t\alpha_1. \tag{7.2.25}$$

Combining (7.2.24) and (7.2.25) we arrive at the expression of χ

$$\chi = \frac{\frac{\rho_1 c_1^2}{\alpha_1} + \frac{\rho_2 c_2^2}{\alpha_2}}{\frac{\Gamma_1}{\alpha_1} + \frac{\Gamma_2}{\alpha_2}} - p = \frac{\sigma}{\Gamma} - p. \tag{7.2.26}$$

7.2.3 Non-isentropic mass and heat flux extension model

By using the expression for $\chi, \tilde{\rho_I}$ as obtained in the Sections (7.2.1) and (7.2.2), the total rate of energy exchange per unit volume between fluid 2 and fluid 1 is:

$$\tilde{\dot{W}} = \dot{W} + \dot{m}\left(e_I + \frac{1}{2}\mathbf{u}\cdot\mathbf{u}\right) + Q. \tag{7.2.27}$$

The non-isentropic model with mass and heat flux extensions reads:

$$\partial_t \rho + \nabla \cdot (\rho \mathbf{u}) = 0, \tag{7.2.28a}$$
$$\partial_t (\rho \mathbf{u}) + \nabla \cdot (\rho \mathbf{u} \otimes \mathbf{u}) + \nabla p = \mathbf{0}, \tag{7.2.28b}$$
$$\partial_t (\rho E) + \nabla \cdot (\rho E \mathbf{u}) + \nabla \cdot (p \mathbf{u}) = 0, \tag{7.2.28c}$$
$$\partial_t (\alpha_1 \rho_1) + \nabla \cdot (\alpha_1 \rho_1 \mathbf{u}) = \dot{m}. \tag{7.2.28d}$$

For the fifth equation we have one of the following:

$$\partial_t \alpha_1 + \mathbf{u} \cdot \nabla \alpha_1 + \phi \nabla \cdot \mathbf{u} = \frac{\dot{m}}{\rho_I} + \frac{Q}{\chi}, \tag{7.2.29a}$$
$$\partial_t (\alpha_1 \rho_1 E_1) + \nabla \cdot (\alpha_1 \rho_1 E_1 \mathbf{u}) + \nabla \cdot (\alpha_1 p \mathbf{u}) = \dot{W} + \dot{m} \left(e_I + \frac{1}{2} \mathbf{u} \cdot \mathbf{u} \right) + Q. \tag{7.2.29b}$$

7.2.4 Derivation mixture entropy

The goal of this Subsection is to derive an equation for the mixture entropy. We start off by substituting (7.2.29a) and (7.2.3) into the entropy equations of both fluids (B.2.4):

$$\begin{aligned} \alpha_1 \rho_1 T_1 \frac{\mathrm{D}s_1}{\mathrm{D}t} = \; & \tfrac{\dot{m}}{\Gamma} \left[\tfrac{\Gamma_1}{\alpha_1} \left[e_1 + \tfrac{p}{\rho_1} \right] + \tfrac{\Gamma_2}{\alpha_2} \left[e_2 + \tfrac{p}{\rho_2} \right] \right] \\ & - \dot{m} \left[e_1 + \tfrac{p}{\rho_1} \right] + Q \left(\tfrac{p}{\chi} + 1 \right), \end{aligned} \tag{7.2.30}$$

where the kinetic energy terms cancel. And similarly, for fluid 2 we get:

$$\begin{aligned} \alpha_2 \rho_2 T_2 \frac{\mathrm{D}s_2}{\mathrm{D}t} = \; & - \tfrac{\dot{m}}{\Gamma} \left[\tfrac{\Gamma_1}{\alpha_1} \left[e_1 + \tfrac{p}{\rho_1} \right] + \tfrac{\Gamma_2}{\alpha_2} \left[e_2 + \tfrac{p}{\rho_2} \right] \right] \\ & + \dot{m} \left[e_2 + \tfrac{p}{\rho_2} \right] - Q \left(\tfrac{p}{\chi} + 1 \right) \end{aligned} \tag{7.2.31}$$

Combining (7.2.30) and (7.2.31) gives

$$\begin{aligned} \partial_t (\rho s) + \nabla \cdot (\rho s \mathbf{u}) = \; & Q \left(\frac{T_2 - T_1}{T_1 T_2} \right) \left(\frac{p}{\chi} + 1 \right) \\ & + \frac{\dot{m}}{\Gamma} \left(\frac{T_2 - T_1}{T_1 T_2} \right) \left(e_I + \tfrac{p}{\rho_I} \right) + \dot{m} \left(\frac{g_2}{T_2} - \frac{g_1}{T_1} \right). \end{aligned} \tag{7.2.32}$$

where the Gibbs free quantities are given by

$$g_k = e_k + \frac{p}{\rho_k} - T_k s_k, \tag{7.2.33}$$

and the mixture entropy is defined by

$$\rho s = \alpha_1 \rho_1 s_1 + \alpha_2 \rho_2 s_2. \tag{7.2.34}$$

We model mass and heat transfer terms as

$$\begin{aligned} \dot{m} \; &= \nu (g_2 - g_1), \\ Q \; &= \theta (T_2 - T_1). \end{aligned} \tag{7.2.35}$$

with ν, θ relaxation parameters. The ODE system of the source terms is first solved for the temperature relaxation and then for the Gibbs free energy relaxation, similar to [36]. We assume that the temperature remains in equilibrium during the Gibbs free energy relaxation.
Let us consider the heat transfer part first. Eq. (7.2.32) reduces to

$$\partial_t(\rho s) + \nabla \cdot (\rho s \mathbf{u}) = \theta \left(\frac{(T_2 - T_1)^2}{T_1 T_2} \right) \left(\frac{p}{\chi} + 1 \right) \geq 0. \tag{7.2.36}$$

Hence, for the heat transfer part the mixture entropy satisfies the second law of thermodynamics. Next, we consider the mass transfer part. Eq. (7.2.32) reduces to

$$\partial_t(\rho s) + \nabla \cdot (\rho s \mathbf{u}) = \frac{\nu}{T_{eq}} (g_2 - g_1)^2 \geq 0, \tag{7.2.37}$$

with $T_{eq} = T_1 = T_2$ the equilibrium temperature, and again the second law of thermodynamics is satisfied.

8 Wrapping up

8.1 Conclusions and recommendations

For the five-equation model various formulations exist. We have decided to compare two possible candidates: (i) The original formulation of Kapila et al. and (ii) a new formulation proposed by Kreeft and Koren. For the model of Kapila et al. an HLLC-type solver has been proposed by Daude et al. [11]. On the other hand, an Osher-type solver has been proposed by Kreeft and Koren [22] for their model. To be able to have a good comparison, we have developed a new Osher-type scheme for Kapila's model and a new HLLC-type scheme for Kreeft and Koren's model.

The main contribution of this thesis is the development of a new Lagrange-projection like scheme for the five-equation two-phase flow model. The key idea here was to split the different physical effects into two submodels and to develop different numerical schemes for the submodels. This approach lends itself perfectly for a low Mach number analysis. An improvement of the scheme in the low Mach regime, similar to Chalons et al. [9], can be made and implemented easily.

We have made a comparison of the different models and schemes on several shock tube test cases. In this comparison we have used first order spatial and temporal accuracy as higher order methods may cause problems related to robustness. This revealed that Kapila's model is the better model to use. The main reason therefore lies in the computation of the non-conservative terms. This is more complicated for the formulation of Kreeft and Koren. One has to make use of Riemann invariants which slows the computation down. For the numerical method we would recommend to use the HLLC-type scheme. The Osher-type scheme for Kapila's model performs equally well, in terms of accuracy. However, the Osher-type scheme is more costly due to the computation of the Riemann invariants. The new developed Lagrange-projection like scheme also performs well in the test cases. For the two test cases (No-reflection problem, Sod's shock tube), the position of the shock wave is a little bit off. The low Mach number correction shows some first improvements for the water-air mixture problem. The actual low Mach problems have to be tested for this method.

On top of this, we have derived a mass and heat flux extension of the model. The formulation of the model of Kreeft and Koren brings results here. To determine the heat transfer terms this formulation is required.

8.2 Further work

Of course, there are many things to do still. We give a list of further improvements below.

Comparison of the different schemes

- Obviously, more (shock tube) problems should be tested to draw more evidence for our conclusions. We have equipped only the best schemes on the perfect gas test cases with the stiffened gas equation of state. This can be done for the other schemes also, to have a better comparison.
- Convergence of the numerical schemes (to the exact solutions when available) has to be tested.
- Explore more about using a limiter for obtaining higher order accuracy for the different schemes. How about the oscillations?

Lagrange-projection like scheme

- The main objective here, is to further test the low Mach regime extension of the scheme. We have now only considered problems in one-dimension. To our knowledge, the low Mach number problems are not common when considering one dimensional problems. It is however possible by taking the area of the pipe into account, see e.g. [25].
- An extension of the scheme for multi dimensional problems (2 or 3 dimensions) has to be made. This is done for the Euler equations of gas dynamics by Chalons et al. [9].
- In this thesis we did not test the scheme with a limiter for the spatial reconstruction and a higher order time integration method (e.g. a Runge-Kutta method) for the temporal accuracy. This can be done in some further work.
- An extension to moving grids can be made for fluid structure interaction.

Mass and Heat flux extension of the model

- The main challenge here lies in the development of a robust treatment of the source terms. The approach of Zein [36] for the treatment of the source terms has been applied by Daude et al. [11] for different source terms. This approach appeared not to be robust for the five-equation model, since the CFL number had to be reduced, for the stability, to $\mathcal{C} = 0.1$. We expect that this problem does not simply disappear when using other source terms. This has not been tested.
- For the source terms both temperature and mechanical relaxation are used. In most, if not all, two-phase flow models, to our knowledge, these relaxation processes are instantaneous. A new and more physical approach, is to consider a non-instantaneous relaxation, see (for the seven equation model) [10].

Bibliography

[1] Anderson J.D., Fundamentals of Aerodynamics, McGraw-Hill, (1991).

[2] Bunn A.R., Carson P.A., Explosion at the Sayono-Shushenskaya hydro-electricity power station, in IChemE, Loss Prevention Bulletin 228, 4-8 (2012).

[3] Baer M.R., Nunziato J.W., A two-phase mixture theory for the deflagration-todetonation transition (ddt) in reactive granular materials. Int J Multiphase Flow 12, 861–89 (1986).

[4] Barberon T., Helluy P., Rouy S.. Practical computation of axisymmetrical multifluid flows. Int J Finite Volumes 1, 1–36 (2004).

[5] Batten P., Clarke N., Lambert C., Causon D.M., On the choice of wavespeeds for the HLLC Riemann Solver. Shock Waves 4, 25-34 (1994).

[6] Box G.E.P., Science and Statistics, Journal of the American Statistical Association 71, 791–799 (1976).

[7] Buffard T., Gallouët T., Hérrard J.M., A sequel to a rough Godunov scheme: application to real gases, Comput Fluids 29, 813-847, (2000).

[8] Castro E.C., High Order ADER FV/DG Numerical Methods for Hyperbolic Equations, Monographs of the School of Doctoral Studies in Environmental Engineering, Università Degli Studi Di Trento (2007).

[9] Chalons C., Girardin M., Kokh S., An all-regime Lagrange-Projection like scheme for the gas dynamics equations on unstructured meshes, Hal 01007622v2 (2014).

[10] Crouzet F., Daude F., Galon P., Hérard J.M., Hurisse O., Liu Y., Validation of a two-fluid model on unsteady liquid–vapor water flows, Comput Fluids 119, 131-142, (2015).

[11] Daude F., Galon P., Gao Z., Blaud E. Numerical experiments using a HLLC-type scheme with ALE formulation for compressible two-phase flows five-equation models with phase transition, Comput Fluids 94, 112-138, (2014).

[12] Davis S.F., Simplified Second-Order Godunov-Type Methods. SIAM J. Sci Stat Comput 9, 445-473 (1982).

[13] Harten A., Lax P.D., Van Leer B., On Upstream Differencing and Godunov-Type Schemes for Hyperbolic Conservation Laws. SIAM Review 25, 35-61 (1983).

[14] Hemker P.W., Spekreijse S.P., Multiple grid and Osher's scheme for the efficient solution of the steady Euler equations. Appl Num Math 2, 475-493 (1986).

[15] Jacobs T., The New Pathways of Multiphase Flow Modeling, Journal of Petroleum Technology February 2015, 62-67 (2015).

[16] Jeffrey A., Quasilinear Hyperbolic Systems and Waves, Pitman (1976).

[17] Johnson E., Colonius T., Implementation of WENO schemes in compressible multicomponent flow problems. J Comput Phys 219, 715-32 (2006).

[18] Kapila A.K., Menikoff R., BDzil J.B., Son S.F., Stewart DS. Two-phase modeling of deflagration-to-detonation transition in granular materials: reduced equations. Phys Fluids, 13, 3002-25 (2001).

[19] Kirsner, W., Condensation induced water hammer. Heating/Piping/Air Conditioning Magazine (1999). Available from www.kirsner.org/kce/media/pdfs/KirsnerHammer.pdf [last viewed 29 July 2015]

[20] Koren, B. A robust upwind discretization method for advection, diffusion and source terms. In C.B. Vreugdenhil & B. Koren (Eds.), Numerical Methods for Advection-Diffusion Problems, 117-138 (1993), Braunschweig/Wiesbaden: Vieweg.

[21] Kreeft J.J., Unsteady compressible two-fluid flow model for interface capturing. On the dynamics of a shock-bubble interaction, MSc thesis, Centrum voor Wiskunde en Informatica (2007).

[22] Kreeft J.J., Koren B., A new formulation of Kapila's five-equation model for compressible two-fluid flow, and its numerical treatment, J Comput Phys, 229, 6220-6242 (2010).

[23] Liu T.P., Hyperbolic conservation laws with relaxation, Comm. Math. Phys. 108, 153-75 (1987).

[24] Luo H., Baum J.D., Lohner R., On the computation of multi-material flows using ALE formulation. J Comput Phys, 194, 206-27 (2004).

[25] LeMartelot S., Nkonga B., Saurel R., Liquid and liquid-gas flows at all speed. J. Comput. Phys. 255, 53–82 (2013).

[26] Le Métayer O., Massoni J., Saurel R.. Elaborating equations of state of a liquid and its vapor for two-phase flow models. Int J Thermal Sci, 43, 265-276 (2004).

[27] Murrone A., Guillard H., A five equation reduced model for compressible two phase flow problems, J Comput Phys 202, 664-698 (2005).

[28] Osher S., Solomon F., Upwind difference schemes for hyperbolic systems of conservation laws. Math of Comput 38, 339–374 (1982).

[29] Saurel R., Petitpas F., Abgrall R., Modelling phase transition in metastable liquids: application to cavitating and flashing flows. J Fluid Mech, 607, 313-50 (2008).

[30] Sod G. A., A survey of several finite difference methods for systems of nonlinear hyperbolic conservation laws. J Comput Phys 27, 1–31 (1978).

[31] Suliciu I., On modelling phase transition by means of rate-type constitutive equations, shock wave structure, Int. J. Ing. Sci. 28, 827-841 (1990).

[32] Toro E.F., Riemann Solvers and Numerical Methods for Fluid Dynamics, A Practical Introduction - 3rd edition, Springer (2009).

[33] Toro E.F., Spruce M., Speares W., Restoration of the contact surface in the HLL-Riemann solver. Shock Waves 4, 25-34 (1994).

[34] Whitham G.B., Linear and Nonlinear Waves, Wiley, New York (1974).

[35] Wood, A.B., A textbook of Sound, London: G. Bell and Sons Ltd (1930).

[36] Zein A., Hantke M., Warnecke G., Modeling phase transition for compressible two-phase flows applied to metastable liquids. J Comput Phys 229, 2964-2998 (2010).

[37] Zein A., Numerical methods for multiphase mixture conservation laws with phase transition. PhD thesis Fakultät für Mathematik der Otto-von-Guericke-Universität Magdeburg (2010).

Appendices

A

Implementation issues

In this Appendix we discuss the implementation issues. For the implementation of the various solvers a MATLAB-code has been written by the author.

A.1 Equation of State

To complete the model an additional equation relating the state variables is required: An Equation of State (EOS). For both fluids we use the generalized stiffened gas (SG) EOS which reads:

$$p = \rho_k(e_k - q_k)(\gamma_k - 1) - \gamma_k \pi_k, \tag{A.1.1}$$

where γ_k, π_k and q_k are characteristic constants of the thermodynamic behaviour of the fluid, $k = 1, 2$. Since we have not implemented mass and heat transfer, the terms q_k are zero. The speed of sound for the SG EOS is given by

$$c_k^2 = \left[\frac{p}{\rho_k^2} - \partial_{\rho_k} e_k\right](\partial_p e_k)^{-1} = \gamma_k \frac{p + \pi_k}{\rho_k}. \tag{A.1.2}$$

The bulk internal energy satisfies

$$\rho e = p\left(\frac{\alpha_1}{\gamma_1 - 1} + \frac{\alpha_2}{\gamma_2 - 1}\right) + \alpha_1\rho_1 q_1 + \alpha_2\rho_2 q_2 + \alpha_1 \frac{\gamma_1}{\gamma_1 - 1}\pi_1 + \alpha_2 \frac{\gamma_2}{\gamma_2 - 1}\pi_2. \tag{A.1.3}$$

A.2 Switch various variable sets

To switch from one set of variables to another, the EOS has to be used. We only use the Lagrangian variables (in the relaxed system) for Kapila's model, therefore we do not give the switches for the

Lagrangian variables for the model of Kreeft and Koren. The vectors of conservative, primitive and Lagrangian variables (in the relaxed system) are respectively:

$$\mathbf{Q} = \begin{pmatrix} \rho \\ \rho u \\ \rho E \\ \alpha_1 \rho_1 \\ \mathbf{Q}_5 \end{pmatrix}, \quad \mathbf{W} = \begin{pmatrix} \rho \\ u \\ p \\ \beta \\ \alpha_1 \end{pmatrix}, \quad \mathbf{Q}_s^{\text{LAG}} = \begin{pmatrix} \tau \\ u \\ E \\ \beta_1 \\ \alpha_1 \\ \Pi \end{pmatrix} \tag{A.2.1}$$

with $\mathbf{Q}_5 = \alpha_1, \alpha_1 \rho_1 E_1$ for Kapila's model and Kreeft and Koren's model respectively.

A.2.1 Primitive to Conservative variables

The switch from primitive to conservative variables turns out to be:

$$\mathbf{Q} = \begin{pmatrix} \rho \\ \rho u \\ \rho E \\ \alpha_1 \rho_1 \\ \mathbf{Q}_5 \end{pmatrix} = \begin{pmatrix} W_1 \\ W_1 W_2 \\ W_4 \frac{W_3 + \gamma_1 \pi_1}{\gamma_1 - 1} + W_1 W_5 q_1 + (1 - W_4) \frac{W_3 + \gamma_2 \pi_2}{\gamma_2 - 1} + W_1 (1 - W_5) q_2 + \frac{1}{2} W_1 W_2^2 \\ W_1 W_4 \\ W_4 \frac{W_3 + \gamma_1 \pi_1}{\gamma_1 - 1} + W_1 W_5 q_1 + \frac{1}{2} W_1 W_2^2 \end{pmatrix}, \tag{A.2.2}$$

with $\mathbf{Q}_5(\mathbf{W}) = W_5, W_4 \frac{W_3 + \gamma_1 \pi_1}{\gamma_1 - 1} + W_1 W_5 q_1 + \frac{1}{2} W_1 W_2^2$ for Kapila's model and Kreeft and Koren's model respectively.

A.2.2 Conservative to Primitive variables

For Kapila's model the switch is given by:

$$\mathbf{W} = \begin{pmatrix} \rho \\ u \\ p \\ \beta \\ \alpha_1 \end{pmatrix} = \begin{pmatrix} Q_1 \\ Q_2/Q_1 \\ p_{KP}(\mathbf{Q}) \\ Q_4/Q_1 \\ Q_5 \end{pmatrix}, \tag{A.2.3}$$

with

$$\begin{aligned} p_{KP}(\mathbf{Q}) = \; & \left[Q_3 - Q_2^2/(2Q_1) - Q_4 q_1 - (Q_1 - Q_4)q_2 - Q_5 \tfrac{\gamma_1\pi_1}{\gamma_1 - 1} - (Q_1 - Q_5)\tfrac{\gamma_2\pi_2}{\gamma_2 - 1}\right] \\ & \times \left[\tfrac{Q_5}{\gamma_1 - 1} + \tfrac{1 - Q_5}{\gamma_2 - 1}\right]^{-1}. \end{aligned} \tag{A.2.4}$$

The switch from conservative variables to primitive variables for the Kreeft and Koren model is a little bit more involved. Finding an expression for the variables p and α in terms of $\mathbf{Q}$ is done as follows. We use the EOS for both fluids to obtain

$$p = \alpha_1 \left(\rho_1(e_1 - q_1)(\gamma_1 - 1) - \gamma_1\pi_1\right) + \alpha_2 \left(\rho_2(e_2 - q_2)(\gamma_2 - 1) - \gamma_2\pi_2\right), \tag{A.2.5}$$

and write the EOS for fluid 1 as

$$\alpha_1 = \left[p + \gamma_1\pi_1\right]^{-1} \left[\alpha_1\rho_1 e_1(\gamma_1 - 1) - \alpha_1\rho_1 q_1(\gamma_1 - 1)\right]. \tag{A.2.6}$$

Substitution of (A.2.6) into (A.2.5) yields

$$p^2 + D_1 p + D_2 = 0 \tag{A.2.7}$$

with

$$\begin{aligned} D_1 = \; & \gamma_1\pi_1 - \alpha_1\rho_1 e_1(\gamma_1 - 1) + \alpha_1\rho_1 q_1(\gamma_1 - 1) \\ & + \gamma_2\pi_2 - \alpha_2\rho_2 e_2(\gamma_2 - 1) + \alpha_2\rho_2 q_2(\gamma_2 - 1), \\ D_2 = \; & (\gamma_1\pi_1 - \gamma_2\pi_2)\left[\alpha_1\rho_1 e_1(\gamma_1 - 1) - \alpha_1\rho_1 q_1(\gamma_1 - 1)\right] \\ & - \gamma_1\pi_1\left[\alpha_1\rho_1 e_1(\gamma_1 - 1) - \alpha_1\rho_1 q_1(\gamma_1 - 1)\right. \\ & \left. + \alpha_2\rho_2 e_2(\gamma_2 - 1) - \alpha_2\rho_2 q_2(\gamma_2 - 1) - \gamma_2\pi_2\right]. \end{aligned} \tag{A.2.8}$$

or in terms of $\mathbf{Q}$:

$$\begin{aligned} D_1 = \; & \gamma_1\pi_1 - \left(Q_5 - Q_4\tfrac{Q_2^2}{Q_1^2}\right)(\gamma_1 - 1) + Q_4 q_1(\gamma_1 - 1) \\ & + \gamma_2\pi_2 - \left(Q_3 - Q_5 - Q_4\tfrac{Q_2^2}{Q_1^2}\right)(\gamma_2 - 1) + (Q_1 - Q_4)q_2(\gamma_2 - 1), \\ D_2 = \; & (\gamma_1\pi_1 - \gamma_2\pi_2)\left[\left(Q_5 - Q_4\tfrac{Q_2^2}{Q_1^2}\right)(\gamma_1 - 1) - Q_4 q_1(\gamma_1 - 1)\right] \\ & - \gamma_1\pi_1\left[\left(Q_5 - Q_4\tfrac{Q_2^2}{Q_1^2}\right)(\gamma_1 - 1) - Q_4 q_1(\gamma_1 - 1)\right. \\ & \left. + \left(Q_3 - Q_5 - Q_4\tfrac{Q_2^2}{Q_1^2}\right)(\gamma_2 - 1) - (Q_1 - Q_4)q_2(\gamma_2 - 1) - \gamma_2\pi_2\right]. \end{aligned} \tag{A.2.9}$$

The switch from conservative to primitive variables turns out to be:

$$\mathbf{W} = \begin{pmatrix} \rho \\ u \\ p \\ \beta \\ \alpha_1 \end{pmatrix} = \begin{pmatrix} Q_1 \\ Q_2/Q_1 \\ p_{KK} \\ Q_4/Q_1 \\ [p_{KK} + \gamma_1 \pi_1]^{-1} \left[\left(Q_5 - Q_4 \frac{Q_2^2}{Q_1^2} \right) (\gamma_1 - 1) - Q_4 q_1 (\gamma_1 - 1) \right] \end{pmatrix}, \tag{A.2.10}$$

where $p_{KK} = p_{KK}(\mathbf{Q})$ is the solution of (A.2.7).

A.2.3 Conservative to Lagrangian variables

The switch from conservative to Lagrangian variables is given by:

$$\mathbf{Q}_s^{\text{LAG}} = \begin{pmatrix} \tau \\ u \\ E \\ \beta_1 \\ \alpha_1 \\ \Pi \end{pmatrix} = \begin{pmatrix} 1/Q_1 \\ Q_2/Q_1 \\ Q_3/Q_1 \\ Q_4/Q_1 \\ Q_5 \\ p \end{pmatrix}. \tag{A.2.11}$$

As this switch is applied in the first step we can take the pressure $p = W_3$ from the primitive variables.

A.2.4 Lagrangian to Conservative variables

The switch from Lagrangian to conservative variables is given by:

$$\mathbf{Q} = \begin{pmatrix} \rho \\ \rho u \\ \rho E \\ \alpha_1 \rho_1 \\ Q_5 \end{pmatrix} = \begin{pmatrix} 1/Q_1^L \\ Q_2^L/Q_1^L \\ Q_3^L/Q_1^L \\ Q_4^L/Q_1^L \\ Q_5^L \end{pmatrix}, \tag{A.2.12}$$

with $\mathbf{Q}_s^{\text{LAG}} = (Q_j^L), j = 1, ..., 6$.

B
Some derivations

In this Appendix we give some derivations which are not shown in the first two parts of this thesis.

B.1 Primitive equations acoustic scheme

The derivation of the primitive equations for the acoustic scheme (5.1.3) is presented here. Basically, the derivation is the same as for the complete five-equation model, see e.g. [22], but one has to replace the material derivative by single time derivatives.
Substituting (5.1.3a) into (5.1.3b) gives

$$\partial_t u + \frac{1}{\rho}\partial_x p = 0. \tag{B.1.1}$$

Combining (5.1.3d) and (5.1.3a) reveals that the mass fraction is constant in time:

$$\partial_t \beta = 0. \tag{B.1.2}$$

The equations

$$\partial_t \rho_1 + \frac{\rho_1}{\alpha_1}\partial_t \alpha_1 + \rho_1 \partial_x u = 0, \tag{B.1.3a}$$
$$\partial_t \rho_2 - \frac{\rho_2}{\alpha_2}\partial_t \alpha_1 + \rho_2 \partial_x u = 0, \tag{B.1.3b}$$

are directly obtained from (5.1.3d). Next, we write

$$\partial_t p = \left(\frac{\partial p}{\partial \rho_1}\right)_{s_1} \partial_t \rho_1 = c_1^2 \partial_t \rho_1, \tag{B.1.4a}$$
$$\partial_t p = \left(\frac{\partial p}{\partial \rho_2}\right)_{s_2} \partial_t \rho_2 = c_2^2 \partial_t \rho_2, \tag{B.1.4b}$$

and subsequently a substitution of (B.1.5) gives

$$\partial_t p = -\rho_1 c_1^2 \left(\frac{1}{\alpha_1} \partial_t \alpha_1 + \partial_x u \right), \tag{B.1.5a}$$

$$\partial_t p = -\rho_2 c_2^2 \left(-\frac{1}{\alpha_2} \partial_t \alpha_1 + \partial_x u \right). \tag{B.1.5b}$$

The primitive equations for the volume fraction and the pressure follow directly

$$\partial_t p + \rho c^2 \partial_x u = 0, \tag{B.1.6a}$$

$$\partial_t \alpha_1 + \phi \partial_x u = 0, \tag{B.1.6b}$$

where the mixture speed of sound obeys the Wood formula [35]:

$$\frac{1}{\rho c^2} = \frac{\alpha_1}{\rho_1 c_1^2} + \frac{\alpha_2}{\rho_2 c_2^2}. \tag{B.1.7}$$

Next, we derive the primitive equations of the entropies of the single phases, denoted as s_k, $k = 1, 2$. The EOS can be written in terms of the entropy as $s_k(p, \rho)$ see [1]. Furthermore, we state without proof (see [1] for the proof) the expression for the speed of sound $c^2 = -\partial_\rho s_k / \partial_p s_k$. Expanding the time derivative in thermodynamical variables gives

$$\partial_t s_k = \partial_p s_k \partial_t p + \partial_\rho s_k \partial_t \rho. \tag{B.1.8}$$

Substitution of the primitive equations for the density and the pressure gives

$$\partial_t s_k = -\rho \partial_x u \left(c^2 \partial_p s_k + \partial_\rho s_k \right) = 0. \tag{B.1.9}$$

B.2 Some thermodynamical relations

Here we derive some thermodynamical relations which are used in Section 7.2.
To find an equation for the entropy we use the Gibbs relation, which reads

$$T_k ds_k = de_k - \frac{p}{\rho_k^2} d\rho_k, \tag{B.2.1}$$

where T_k is the temperature of fluid k. Take the material derivative, $k = 1$, and multiply by $\alpha_1 \rho_1$ to find

$$\alpha_1 \rho_1 T_1 \frac{\mathrm{D}s_1}{\mathrm{D}t} = \alpha_1 \rho_1 \frac{\mathrm{D}e_1}{\mathrm{D}t} - \frac{\alpha_1 p}{\rho_1} \frac{\mathrm{D}\rho_1}{\mathrm{D}t}. \tag{B.2.2}$$

Similarly, for fluid 2 we get

$$\alpha_2 \rho_2 T_2 \frac{\mathrm{D}s_2}{\mathrm{D}t} = \alpha_2 \rho_2 \frac{\mathrm{D}e_2}{\mathrm{D}t} - \frac{\alpha_2 p}{\rho_2} \frac{\mathrm{D}\rho_2}{\mathrm{D}t}. \tag{B.2.3}$$

Substitution of (7.1.11), (7.1.13) and (7.1.14) gives the entropy equations

$$\alpha_1\rho_1 T_1 \frac{\mathrm{D}s_1}{\mathrm{D}t} = \tilde{\dot{W}}_T + p\frac{\mathrm{D}\alpha_1}{\mathrm{D}t} - \dot{m}\left[e_1 - \frac{1}{2}\mathbf{u}\cdot\mathbf{u} + \frac{p}{\rho_1}\right] \tag{B.2.4a}$$

$$\alpha_2\rho_2 T_2 \frac{\mathrm{D}s_2}{\mathrm{D}t} = -\tilde{\dot{W}}_T - p\frac{\mathrm{D}\alpha_1}{\mathrm{D}t} + \dot{m}\left[e_2 - \frac{1}{2}\mathbf{u}\cdot\mathbf{u} + \frac{p}{\rho_2}\right] \tag{B.2.4b}$$

Furthermore, we derive an alternative expression for the Grüneisen coefficient. Using Gibbs relation (B.2.1), we can deduce

$$T_k = \left(\frac{\partial e_k}{\partial s_k}\right)_{\rho_k}, \quad k = 1, 2. \tag{B.2.5}$$

Hence, we have

$$\left(\frac{\partial p}{\partial s_k}\right)_{\rho_k} = \left(\frac{\partial p}{\partial e_k}\right)_{\rho_k}\left(\frac{\partial e_k}{\partial s_k}\right)_{\rho_k} = \left(\frac{\partial p}{\partial e_k}\right)_{\rho_k} T_k, \quad k = 1, 2. \tag{B.2.6}$$

The Grüneisen coefficient can be written as

$$\Gamma_k = \frac{1}{\rho_k T_k}\left(\frac{\partial p}{\partial s_k}\right)_{\rho_k}, \quad k = 1, 2. \tag{B.2.7}$$

B.3 Equation thermodynamical rate-of-work term

In this Section we provide the derivation of Eq. (7.2.2). The pressure can be expressed as a function of two independent thermodynamical variables (EOS). For this we consider two options. The first one is to use entropy and density for the independent variables and to make use of the entropy equations derived in Section B.2. This means we use the EOS for both fluids as: $p = p(s_1, \rho_1), p = p(s_2, \rho_2)$. Take the total derivative of the pressure to find

$$\frac{\mathrm{D}p}{\mathrm{D}t} = \left(\frac{\partial p}{\partial \rho_1}\right)_{s_1}\frac{\mathrm{D}\rho_1}{\mathrm{D}t} + \left(\frac{\partial p}{\partial s_1}\right)_{\rho_1}\frac{\mathrm{D}s_1}{\mathrm{D}t} \tag{B.3.1a}$$

$$\frac{\mathrm{D}p}{\mathrm{D}t} = \left(\frac{\partial p}{\partial \rho_2}\right)_{s_2}\frac{\mathrm{D}\rho_2}{\mathrm{D}t} + \left(\frac{\partial p}{\partial s_2}\right)_{\rho_2}\frac{\mathrm{D}s_2}{\mathrm{D}t}. \tag{B.3.1b}$$

Substitution of (7.1.11), (7.1.26), (B.2.4) into (B.3.1a) gives

$$\begin{aligned}\frac{\mathrm{D}p}{\mathrm{D}t} = \; & c_1^2\left[-\frac{\rho_1}{\alpha_1}\frac{\mathrm{D}\alpha_1}{\mathrm{D}t} - \rho_1\nabla\cdot\mathbf{u} + \frac{\dot{m}}{\alpha_1}\right] \\ & + \left(\frac{\partial p}{\partial s_1}\right)_{\rho_1}\frac{1}{\alpha_1\rho_1 T_1}\left[\tilde{\dot{W}}_T + p\frac{\mathrm{D}\alpha_1}{\mathrm{D}t} - \dot{m}\left(e_1 - \tfrac{1}{2}\mathbf{u}\cdot\mathbf{u} + \frac{p}{\rho_1}\right)\right]\end{aligned} \tag{B.3.2}$$

Similarly, the substitution of (7.1.11), (7.1.26), (B.2.4) into (B.3.1b) yields

$$\begin{aligned}\frac{\mathrm{D}p}{\mathrm{D}t} = \; & c_2^2\left[\frac{\rho_2}{\alpha_2}\frac{\mathrm{D}\alpha_1}{\mathrm{D}t} - \rho_2\nabla\cdot\mathbf{u} - \frac{\dot{m}}{\alpha_2}\right] \\ & + \left(\frac{\partial p}{\partial s_2}\right)_{\rho_2}\frac{1}{\alpha_2\rho_2 T_2}\left[-\tilde{\dot{W}}_T - p\frac{\mathrm{D}\alpha_1}{\mathrm{D}t} + \dot{m}\left(e_2 - \frac{1}{2}\mathbf{u}\cdot\mathbf{u} + \frac{p}{\rho_2}\right)\right].\end{aligned} \tag{B.3.3}$$

By subtracting (B.3.3) from (B.3.2) we obtain an equation for the volume fraction α

$$\begin{aligned}
&\frac{\mathrm{D}\alpha}{\mathrm{D}t}\left[\frac{\rho_1 c_1^2}{\alpha_1}+\frac{\rho_2 c_2^2}{\alpha_2}-p\left(\frac{1}{\alpha_1\rho_1 T_1}\left(\frac{\partial p}{\partial s_1}\right)_{\rho_1}+\frac{1}{\alpha_2\rho_2 T_2}\left(\frac{\partial p}{\partial s_2}\right)_{\rho_2}\right)\right]\\
=\;&\left[\nabla\cdot\mathbf{u}\left(-\rho_1 c_1^2+\rho_2 c_2^2\right)+\dot{m}\left(\frac{c_1^2}{\alpha_1}+\frac{c_2^2}{\alpha_2}\right)\right.\\
&+\tilde{\dot{W}}_T\left(\frac{1}{\alpha_1\rho_1 T_1}\left(\frac{\partial p}{\partial s_1}\right)_{\rho_1}+\frac{1}{\alpha_2\rho_2 T_2}\left(\frac{\partial p}{\partial s_2}\right)_{\rho_2}\right)\\
&-\dot{m}\left(e_1-\frac{1}{2}\mathbf{u}\cdot\mathbf{u}+\frac{p}{\rho_1}\right)\frac{1}{\alpha_1\rho_1 T_1}\left(\frac{\partial p}{\partial s_1}\right)_{\rho_1}\\
&\left.-\dot{m}\left(e_2-\frac{1}{2}\mathbf{u}\cdot\mathbf{u}+\frac{p}{\rho_2}\right)\frac{1}{\alpha_2\rho_2 T_2}\left(\frac{\partial p}{\partial s_2}\right)_{\rho_2}\right].
\end{aligned}\tag{B.3.4}$$

By using (7.1.30), (7.1.32), (7.1.31) and (B.2.7), Eq. (B.3.4) simplifies to

$$\begin{aligned}
\frac{\mathrm{D}\alpha}{\mathrm{D}t}\left(\sigma-p\Gamma\right)=\;&\nabla\cdot\mathbf{u}\phi\sigma+\dot{m}\varsigma+\tilde{\dot{W}}_T\Gamma\\
&-\dot{m}\left(e_1-\frac{1}{2}\mathbf{u}\cdot\mathbf{u}+\frac{p}{\rho_1}\right)\frac{\Gamma_1}{\alpha_1}\\
&-\dot{m}\left(e_2-\frac{1}{2}\mathbf{u}\cdot\mathbf{u}+\frac{p}{\rho_2}\right)\frac{\Gamma_2}{\alpha_2},
\end{aligned}\tag{B.3.5}$$

with $\sigma,\varsigma,\Gamma_k$ defined in Chapter 7. Hence, we have obtained a relation between $\frac{\mathrm{D}\alpha}{\mathrm{D}t}$ and $\tilde{\dot{W}}_T$. Alternatively, the same relation can be found by expressing the pressure in terms of density and internal energy of both fluids, i.e. $p=p(e_1,\rho_1), p=p(e_2,\rho_2)$. Taking total derivatives and subsequently expanding into thermodynamical variables gives:

$$\left(\frac{\partial p}{\partial e_1}\right)_{\rho_1}\frac{\mathrm{D}e_1}{\mathrm{D}t}+\left(\frac{\partial p}{\partial \rho_1}\right)_{e_1}\frac{\mathrm{D}\rho_1}{\mathrm{D}t}=\left(\frac{\partial p}{\partial e_2}\right)_{\rho_2}\frac{\mathrm{D}e_2}{\mathrm{D}t}+\left(\frac{\partial p}{\partial \rho_2}\right)_{e_2}\frac{\mathrm{D}\rho_2}{\mathrm{D}t}.\tag{B.3.6}$$

Substituting of the primitive equations gives:

$$\begin{aligned}
\tilde{\dot{W}}_T&\left[\frac{1}{\alpha_1\rho_1}\left(\frac{\partial p}{\partial e_1}\right)_{\rho_1}+\frac{1}{\alpha_2\rho_2}\left(\frac{\partial p}{\partial e_2}\right)_{\rho_2}\right]=\\
&\frac{\mathrm{D}\alpha}{\mathrm{D}t}\left[\frac{\rho_1}{\alpha_1}\left(\frac{\partial p}{\partial \rho_1}\right)_{e_1}+\frac{\rho_2}{\alpha_2}\left(\frac{\partial p}{\partial \rho_2}\right)_{e_2}\right]\\
&+\left(\rho_1 c_1^2-\rho_2 c_2^2\right)\nabla\cdot\mathbf{u}\\
&+\frac{\dot{m}}{\alpha_1\rho_1}(e_1-\tfrac{1}{2}\mathbf{u}\cdot\mathbf{u})\left(\frac{\partial p}{\partial e_1}\right)_{\rho_1}+\frac{\dot{m}}{\alpha_2\rho_2}(e_2-\tfrac{1}{2}\mathbf{u}\cdot\mathbf{u})\left(\frac{\partial p}{\partial e_2}\right)_{\rho_2}\\
&-\frac{\dot{m}}{\alpha_1}\left(\frac{\partial p}{\partial \rho_1}\right)_{e_1}-\frac{\dot{m}}{\alpha_2}\left(\frac{\partial p}{\partial \rho_2}\right)_{e_2}.
\end{aligned}\tag{B.3.7}$$

By substituting (7.1.30), (7.1.29), (7.1.32) and (7.1.31) into (B.3.7), we arrive at Eq. (B.3.5).

C
Relaxation approach

In this Appendix we briefly discuss the idea of the obtaining a relaxed system [31].

C.1 Relaxed system

Consider the one-dimensional partial differential equation

$$\partial_t u + \partial_x f(u) = 0, \tag{C.1.1}$$

where $f = f(u)$ is a complicated nonlinear function. This nonlinear function makes the equation possibly difficult to solve. The idea is now to consider a larger but simpler system of equations. Therefore a so-called *surrogate parameter* v approximating the function f is introduced. This is the *relaxation approach*:

- Deal with larger but simpler system,
- Introduce new surrogate variable.

Let us determine the equation satisfied by the *surrogate parameter* v. We compute the derivatives:

$$\partial_t \left(f(u)\right) = \partial_u f \partial_t u = -\partial_u f \partial_x \left(f(u)\right) = -\left(\partial_u f\right)^2 \partial_x u, \tag{C.1.2}$$

which can be written as:

$$\partial_t \left(f(u)\right) + \left(\partial_u f\right)^2 \partial_x u = 0. \tag{C.1.3}$$

The Suliciu approximation of (C.1.1) reads

$$\begin{cases} \partial_t u + \partial_x v & = 0 \\ \partial_t v + a^2 \partial_x u & = \mathfrak{y}\left(f(u) - v\right). \end{cases} \tag{C.1.4}$$

The first equation in (C.1.4) is in the same form as the original PDE (C.1.1) with $v = f(u)$, where the second equation corresponds to (C.1.3). The parameter $\mathfrak{y}$ will be specified later. Here the parameter a approximates $\partial_u f$. A theoretical analysis reveals that a must satisfy the so-called *subcharacteristic condition*

$$a > \partial_u f \tag{C.1.5}$$

to have the necessary stability requirements. For more details we refer to [34, 23]. In practice [9], a value a_{LR} for each interface at time level n is chosen as

$$a_{LR} = H \max\left((\partial_u f)_L^n, (\partial_u f)_R^n\right), \tag{C.1.6}$$

where $L = j, LR = j + 1/2, R = j + 1$ and $H \geq 1$.

C.2 Numerical method

The numerical method is a **two step approach** consisting of the following steps:

- *evolution step*,
- *source step*.

In the evolution step we take $\mathfrak{y} = 0$, i.e.:

$$\begin{cases} \partial_t u + \partial_x v & = 0 \\ \partial_t v + a^2 \partial_x u & = 0, \end{cases} \tag{C.2.1}$$

and solve the functions $u^n, v^n = f(u^n)$ at time level n to intermediate time level $n + 1-$. Note that this system is a linear PDE and therefore easy to solve. Next, in the source step we take $\mathfrak{y} \to +\infty$ and solve

$$\begin{cases} \partial_t u & = 0 \\ \partial_t v & = \mathfrak{y}\left(f - v\right), \end{cases} \tag{C.2.2}$$

from intermediate time level $n + 1-$ to time level n: $u^{n+1} = u^{n+1-}, v^{n+1} = f(u^{n+1-})$.